

# **POLITECNICO DI TORINO**

Energy Department

Master's Degree in  
**Energy and Nuclear Engineering**



Master's Thesis

## **Modelling, Prototyping and Economic Analysis of a Membraneless Electrolyzer**

Supervisors:

Prof. Massimo Santarelli

Prof. Francesco Ciucci

Ing. Emanuele Quattrocchi

Candidate:

Alessandro Manzotti

Academic year 2019/2020



In collaboration with



香港科技大學  
THE HONG KONG  
UNIVERSITY OF SCIENCE  
AND TECHNOLOGY



DEPARTMENT OF MECHANICAL  
AND AEROSPACE ENGINEERING

---

THE HONG KONG UNIVERSITY OF  
SCIENCE AND TECHNOLOGY



DEPARTMENT OF  
**CHEMICAL AND  
BIOLOGICAL  
ENGINEERING**  
化學及生物工程學系

## **Abstract**

Electrolysis has long been the preferred way to produce clean hydrogen. Until now, it is performed in electrolyzers that use diaphragms (alkaline) or membranes (PEM and SOEC) to keep separated the areas of hydrogen and oxygen reaction. However, recently a new variant of electrolysis has emerged, which does not involve the use of physical separators. These are membraneless electrolyzers, where the only thing that keep separated hydrogen from oxygen inside the cell is the fluid dynamic forces generated by the design and operation of the cell. This has direct repercussions on the investment cost since a membrane or a diaphragm is eliminated. Those ones are elements most susceptible to load changes and variations in operating temperature. This variant of electrolyzers has been studied only for applications at low temperatures, in the range of alkaline and PEM electrolyzers.

Therefore, reducing the initial investment costs and increasing the versatility of the electrolyzer are two of the most important characteristics of this technology. Especially given that the initial investment costs of electrolyzers still remain one of the main issues to their large-scale use. In addition to the fact that the electrolyzers would be coupled to intermittent renewable energy sources, such as solar and wind, so the versatility is fundamental.

To study this technology, the first step was an analysis on the different types of membraneless electrolyzers present in the literature and then, a preliminary comparison was carried out based on the available data, to define which projects proved to be the most promising. Subsequently, a model was developed to obtain the flow rate and purity of the hydrogen produced, and the characterization of the cell with  $j$ - $V$  curves. In this way it was possible to evaluate the efficiencies of the studied plants and compare them. After comparing the types of membraneless electrolyzers selected, the one that showed the most promising prospects was chosen.

To validate the model data, a prototype was designed starting from the designs found in the literature and the versions used for the execution of the experimental tests were 3D printed. Tests of watertightness and operation of the circuits and subsequently, the electrochemical performance to obtain the polarization curves of the electrolyzer. Once the validation of the model data was performed, ways were also tried to evaluate the purity of hydrogen and the flow rates produced in the field.

The economic analysis was performed on the chosen design. Different scenarios and possible cases have been developed, including technology level, power supply, taxation and four locations have been selected (China, USA, Hong Kong and EU-27), in which to carry out the economic analysis of plants capable of producing from 500 to 1000 tons of hydrogen per year. With this study very

competitive prices were obtained, in a case the levelized cost of hydrogen evaluated was  $1.95 \frac{\text{USD}}{\text{kgH}_2}$ .

Once the analyzes were carried out to determine the economic performance of a plant for the production of hydrogen by applying electrolysis without membranes, and compared the results, a sensitivity analysis was carried out. This analysis, applied to various parameters impacting on economic analysis, was used to determine the main intervention strategies to further reduce production costs and thus increase the marketability of hydrogen.

## **Abstract (ita)**

L'elettrolisi è da molto tempo la strada preferenziale per produrre idrogeno pulito. Fino ad ora viene eseguita in elettrolizzatori che utilizzano diaframmi (alcalini) o membrane (PEM-SOEC) per separare le aree di reazione dell'idrogeno e dell'ossigeno, ma di recente è emersa una nuova tipologia che non comporta l'utilizzo di separatori fisici. Si tratta degli elettrolizzatori senza membrane, in cui l'unica cosa che separa l'idrogeno dall'ossigeno, all'interno della cella, sono le forze fluidodinamiche generate da come è stata progettata e da come viene controllata la cella stessa. Questo ha delle ricadute dirette sul costo dell'elettrolizzatore, dato che si elimina una membrana o un diaframma, togliendo uno degli elementi più suscettibili agli sbalzi di carico e alle variazioni di temperatura operativa. Questa variante di elettrolizzatori è stata studiata per ora, solo per applicazioni a basse temperature, nel range di elettrolizzatori alcalini e PEM.

Ridurre quindi i costi di investimento iniziale e aumentare la versatilità dell'elettrolizzatore sono due tra le più importanti caratteristiche di questa tecnologia. Soprattutto dato che i costi di investimento iniziale degli elettrolizzatori rimangono ancora uno dei maggiori problemi da risolvere per il loro utilizzo su vasta scala. Oltre al fatto che gli elettrolizzatori verrebbero accoppiati a fonti di energia rinnovabili intermittenti come solare ed eolico, perciò la versatilità è fondamentale.

Per studiare questa tecnologia si è partiti da un'analisi sulle diverse tipologie di elettrolizzatori senza membrane presenti in letteratura e quindi, si è svolto un preliminare confronto in base a quelli che erano i dati disponibili, per definire quali progetti si sono rivelati più promettenti. Successivamente è stato elaborato un modello per ricavare la portata e la purezza dell'idrogeno prodotto, e la caratterizzazione della cella con curve j-V. In questo modo si sono potute valutare le efficienze degli impianti studiati e confrontarli. Dopo aver confrontato le tipologie di elettrolizzatore senza membrana selezionate, si è scelta quella che ha mostrato le prospettive più promettenti.

Per validare i dati del modello, è stato progettato un prototipo a partire dai design presenti in letteratura e ne sono state stampate in 3D delle versioni usate per l'esecuzione delle prove sperimentali. Prove di tenuta stagna e funzionamento dei circuiti e successivamente, le performance elettrochimiche per ottenere le curve di polarizzazione dell'elettrolizzatore. Una volta riscontrata la validazione dei dati del modello si sono tentate anche delle strade per valutare sul campo la purezza dell'idrogeno e le portate prodotte.

Con il design prescelto si è passati alla analisi economica. Sono stati elaborati diversi scenari e casi possibili, tra livello della tecnologia, alimentazione, tassazione e sono stati selezionati quattro luoghi (Cina, USA, Hong Kong e UE-27), in cui eseguire l'analisi economica di impianti in grado di produrre dai 500 alle 1000 tonnellate di idrogeno all'anno. Arrivando ad ottenere anche dei costi

dell'idrogeno molto competitivi, in un caso anche di  $1.95 \frac{\text{USD}}{\text{kgH}_2}$ . Svolte le analisi per determinare le performance economiche di un impianto per la produzione di idrogeno mediante l'applicazione di elettrolisi senza membrane, e comparati i risultati, è stata svolta una analisi di sensibilità. Questa analisi, applicata a diversi parametri impattanti sull'analisi economica, è servita per determinare le principali strategie di intervento per ridurre ulteriormente i costi di produzione e così, aumentare la commerciabilità dell'idrogeno.

## **Acknowledgments**

Inizio ringraziando il professor Massimo Santarelli, mio professore e relatore al Politecnico di Torino, che mi ha dato l'opportunità di recarmi quasi dall'altra parte del mondo, alla Hong Kong University of Science and Technology, per svolgere questa tesi. I also thank Professor Francesco Ciucci my supervisor at HKUST and Ing. Emanuele Quattrocchi my co-supervisor, Tony, Alessio and Simona, my Italian lab-crew far from home, Stephen, Mei, Mohamed and all the other members of the research group, for having been supportive and friends during these 9 months abroad. Together you have made Hong Kong a great place to work and to explore, making it like a second home form me.

Poi ovviamente un enorme ringraziamento va alla mia famiglia mia madre e mio padre, sempre pronti a sostenermi, Edoardo il mio fratellone e Margherita, sorella che in qualche modo riesce ancora a sopportarmi. Ai miei nonni che sono e saranno sempre una grandissima fonte di ispirazione e guida per me e ovviamente, tutto il resto della famiglia. In questi anni di Politecnico, da tutti, mi sono sempre arrivati supporto e sostegno incondizionati oltre che fiducia e motivazione.

Continuo i ringraziamenti pensando agli amici che mi porto dietro dal liceo e con cui ho anche condiviso parte del mio percorso al Politecnico, per le grasse risate, gli importanti momenti di svago e amicizia durante questi anni. E come dimenticare i compagni che mi hanno aiutato a superare gli anni di Politecnico anche se in maniera un po' rocambolesca, tra sushi, gite, ciaspolate e altre innumerevoli avventure.

Ringrazio anche la comunità scout dell'Almese 1 in cui sono cresciuto, passando da semplice repartaro all'ingresso in comunità capi. È stato un onore percorrere una parte della mia strada con tutti voi, dai miei capi ai ragazzi del reparto con cui ho fatto servizio. Anche se in questi ultimi anni ho lasciato il servizio attivo, semel scout semper scout.

Infine, un sentito ringraziamento va alla squadra universitaria di canottaggio del CUS, in soli due anni ho acquisito una passione che porterò avanti per tutta la vita. È proprio grazie a questa squadra se ho deciso di andare a fare la mia tesi in Cina. Grazie per i momenti goliardici, gli allenamenti fino allo stremo e le fantastiche esperienze di gruppo, dalle gare in Cina, a Budapest, grazie UniversiTorì!

Tirando le somme di questo lungo cammino che è stato il Politecnico, le notti a studiare, le fitte e disastrose sessioni esami, mi rendo conto che senza aiuto non sarebbe stato possibile portare a termine questa impresa, grazie davvero a tutti.



## Contents

Abstract .....	IV
Abstract (ita) .....	VI
Acknowledgments.....	VIII
1 Introduction.....	1
2 Membraneless Electrolyzer Technology Overview.....	4
3 Methodology and Model.....	8
3.1 Physical model .....	8
3.1.1 Thermodynamics and Kinetics.....	8
3.1.3 System efficiency .....	12
3.1.4 Model computation .....	13
3.2 Economic Analysis.....	13
3.3 Costs accounting.....	14
3.3.1 Capital costs .....	14
3.3.2 Operating and maintenance costs.....	16
3.3.3 Cost of electricity .....	17
3.3.4 Plant size .....	17
3.3.5 Taxation and carbon tax.....	19
3.4 Products and gains.....	20
4 Experimental experiences.....	22
4.1 Fluid-dynamics simulations .....	23
4.2 Electrolyzer prototype designing.....	27
4.3 Gas separator design.....	33
4.4 Experimental setup .....	35
4.5 Testing.....	35
4.5.1 Electrolyzer polarization curve test.....	37
4.5.2 H <sub>2</sub> production and purity evaluation .....	40
5 Thermodynamic model results .....	43

5.1	Output H <sub>2</sub> Purity .....	43
5.2	Electrolyzer Efficiency .....	45
5.2.1	H <sub>2</sub> market specification .....	48
6	Economic analysis results .....	50
6.1	Net present value analysis .....	50
6.2	Carbon Tax .....	56
6.3	Sensitivity analysis .....	58
7	Conclusions .....	61
8	List of symbols and parameters .....	63
9	Appendix A .....	67
10	Appendix B .....	71
11	Appendix C .....	73
12	References .....	78

## Table of Figures

Figure 1 - Global demand of Hydrogen since 1975 [2] .....	1
Figure 2 - Global distribution of existing main refining, steelmaking and chemical cracking plants [2].....	2
Figure 3 - Hydrogen costs from renewable energy systems in the long term [2].....	3
Figure 4 –Schematics of the (a) flow-by, (b) flow-through and (c) buoyancy driven configurations.	4
Figure 5 - Production and energy cost of H <sub>2</sub> with different MEs.....	4
Figure 6 – HHV efficiency of various MEs .....	5
Figure 7 – Experimental current densities of various MEs.....	6
Figure 8 - General configuration of the electrolyzer system. ....	8
Figure 9 - Carbon Taxes in Operation, Scheduled, or under Consideration (as of February 2017) [50].....	20
Figure 10 - Divergent electrolyte flow through (DEFT™) scheme used as base for the prototype design [7].....	22
Figure 11 – Section of divergent electrolyte flow through (DEFT™) scheme used as base for the prototype design [7]. ....	22
Figure 12 - First original concept for the cell. ....	23
Figure 13 - Computational simulation of the fluid flow inside the cell of model 1.....	24
Figure 14 – Section on zy plane view of the velocity module of the fluid flow simulation of model 1 .....	24
Figure 15 - Model 1 cell grid mesh.....	25
Figure 16 - Flow rate value according to the degrees of freedom of the grid of the model .....	25
Figure 17 – Relative error of the grid independence analysis.....	26
Figure 18 -Fluid dynamic simulation results for model 2.....	26
Figure 19 - Model 3 fluid dynamic simulation results.....	27
Figure 20 - Prototype 1 .....	28
Figure 21 - Prototype 1 exploded view .....	28
Figure 22 - Prototype 2 .....	29
Figure 23 - Prototype 2 exploded view .....	29
Figure 24 - Prototype 3 exploded view .....	30
Figure 25 – 3D printed prototype; (a) view of the external side; (b) internal side; (c) assembled ....	30
Figure 26 - Prototype 4 exploded view .....	31
Figure 27 – Comparison of prototype 3 (left) and 4 (right) .....	32
Figure 28 - Prototype 5 electrode support.....	32

Figure 29 - Prototype 5 exploded view .....	33
Figure 30 - Gas separator .....	34
Figure 31 - Gas separator section.....	34
Figure 32 - Experimental setup .....	35
Figure 33 - Electrolysis experiment with alkaline electrolyte and Ni foam electrode.....	36
Figure 34 - electrode assembly with connected wires .....	36
Figure 35 - Electrolyzer polarization curves form experiments and the model results in dashed red line.....	37
Figure 36 - Electrodes after the j-V proves.....	38
Figure 37 - Comparison of j-V curves between Ni electrodes and Ni electrodes plus catalyst.....	39
Figure 38 Electrodes covered with catalyst after the prove .....	40
Figure 39 Detailed view of the H <sub>2</sub> gas separator.....	40
Figure 40 - Sample bag for the harvesting of H <sub>2</sub> .....	41
Figure 41 - Oxygen sensor used.....	42
Figure 42 - H <sub>2</sub> Purity at various temperatures for Re=1500 .....	43
Figure 43 - H <sub>2</sub> Purity at various current density at different flow rates for T=60°C .....	44
Figure 44 - H <sub>2</sub> Purity as a function of the current density at various temperatures for Re=1500.....	44
Figure 45 - HHV efficiency at different ASRΩ conditions, maintaining the same flow condition (Re=1500), temperature T=60°C and pressure 1 atm. ....	45
Figure 46 - Theoretical efficiency of the (a) FT and (b) FB design; the dashed red line indicates the maximum for each Re. ....	46
Figure 47 - Contour plots of the efficiency for the (c) FT and (d) FB.....	46
Figure 48 - Outlet H <sub>2</sub> purity maps for (e) FT and (f) FB.....	47
Figure 49 - Contour plots of the efficiency in operational range for the (c) FT and (d) FB.....	47
Figure 50 - Outlet H <sub>2</sub> purity maps in operational range for (e) FT and (f) FB.....	48
Figure 51 - Schematics of a passive recombiner for hydrogen purification .....	48
Figure 52 - NPV evolution for renewable connected plant of 1000 t/year size (18.38 MW), in (a) today scenario and (b) long-term scenario. ....	50
Figure 53 – (a) NPV comparison at 20 years. (b) Comparison between LCH, the industrial hydrogen price level has been highlighted in the plot with black dashed lines. ....	51
Figure 54 - LCH by component under the two scenarios: (a) 500 t/year, today stack cost and grid connected (worst scenario); (b) 1000 t/year, long-term stack cost and renewable connected (best scenario). ....	54

Figure 55 - Pie charts for the comparison of the LCH components for plant located in China, today scenario, 500 t/year: (a) grid connected; (b) renewable connected.....	55
Figure 56 - Pie charts for the comparison of the LCH components for plant located in China, long term scenario, 1000 t/year: (a) grid connected; (b) renewable connected. ....	55
Figure 57 - LCH components of ME plant in China.....	56
Figure 58 - NPV results in today stack scenario, 1000 t/year plant size and renewable coupled (a) with no carbon tax and (b) with strong carbon tax (350 USD/tonH2). ....	57
Figure 59 – Comparison of the NPV in different carbon tax scenarios, in today stack scenario. ....	58
Figure 60 - Sensitivity analysis results for plants located in China: LCH (a) and NPV (b) in today scenario, 500 t/year, grid coupling.....	59
Figure 61 - Sensitivity analysis results for plants located in China: LCH (a) and NPV (b) in today scenario, 1000 t/year, renewable coupling.....	59
Figure 62 - NPV comparison of the effect of capital cost for different location, considering today scenario, 1000 t/year plant size grid coupling (a) and renewable coupling (b). ....	59
Figure 63 - LCH composition for USA case.....	71
Figure 64 - LCH composition for HK case.....	71
Figure 65 - LCH composition for EU-27.....	72

## Table of Tables

Table 1 - Parameters and conditions used for the FB and FT systems. ....	7
Table 2 - Taxation rates and WACC values. ....	14
Table 3 – List and percentages for the capital cost cascade estimation, derived from [36]. ....	15
Table 4 - Stack cost taken from NERL report [35, 38].....	16
Table 5 - BoP cost taken from NERL report [35, 38].....	16
Table 6 - Prices of commodities .....	17
Table 7 -Subdivision of the LCH for the various components of the cost.....	53
Table 8 - Symbols .....	63
Table 9 - Parameters .....	66
Table 10 - Experimental results without catalyst.....	73
Table 11 - Experimental results with catalyst.....	76
Table 12 - Model results for the comparison with experimental results.....	77

# 1 Introduction

One of the most pressing threats to the future of humanity is climate change. Human influence on climate has been the dominant cause of observed warming since the mid-20th century. Induced warming reached approximately 1°C above pre-industrial levels in 2017, increasing at 0.2° per decade. [1]. To prevent irreversible climate change, most industrial sectors need to be decarbonized.

To solve this issue one of the possible ways is to look towards other energy carrier and other industrial commodities. Hydrogen has all the needed characteristics to be one of those items. It is already used in many industrial processes and its global demand has constantly risen for decades, see Figure 1. The issue with hydrogen is that is not available in nature on Earth, so it needs to be synthesized. The way in which I do this process affects the impact of the produced hydrogen on the environment. H<sub>2</sub> can be produced in a clean way, by mean of renewable energy sources. Green H<sub>2</sub> has risen interest worldwide, and especially in the European Union, due to the many green focuses and pushes given by European project and agenda, such as 2020 and 2030 climate & energy packages. The main hopes for hydrogen usage are for energy storage sector, and for decarbonization of processes in several industries, such as the steel industry and glass industry, also in the automotive sector, with the fuel cell vehicles [2], especially for long-range and heavy-duty applications in competition with electric vehicles. Nowadays hydrogen is massively used for industrial applications: more than 70 Mton of high purity hydrogen is consumed per year worldwide, primarily for oil refining and ammonia-based fertilizers [2]; in addition, other 45 Mton of low purity hydrogen are used for methanol production, iron steel production, and as synthesis gas, fuel or feedstock, see Figure 1.

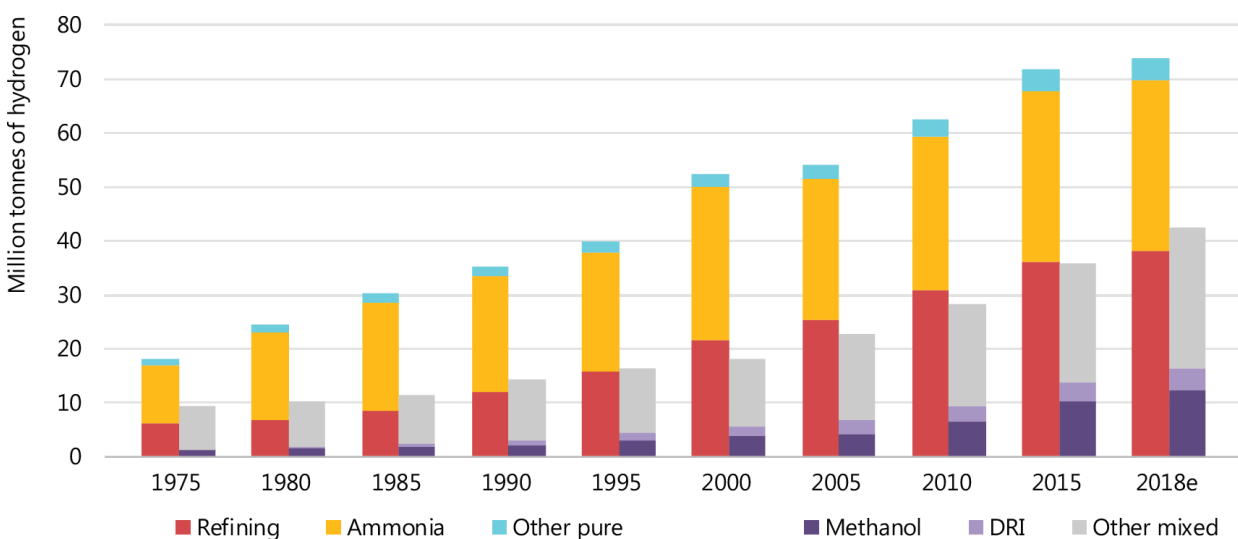


Figure 1 - Global demand of Hydrogen since 1975 [2]

The great importance of H<sub>2</sub> is witnessed by the fact that the hydrogen market value in 2019 was estimated of 117.49 billion USD [3].

However, nowadays almost all the hydrogen supplied at the industrial scale is produced starting from natural gas and coal. To give an order of magnitude of the impact of the present hydrogen production, according to IEA report, it is equivalent to the CO<sub>2</sub> emitted by Indonesia, and the United Kingdom combined [2].

The hydrogen demands is concentrated in industrial developed areas, as is possible to see in Figure 2: Central Europe, USA easter coast, China and India. In those regions are also available great amount of renewable energy, that guarantee cheaper hydrogen production cost, as is possible to see in Figure 3. So, the possibility to produce clean hydrogen directly near the main consuming area is a feasible way of action to try also to decarbonize the hydrogen production chain and other linked sector. While the energy usage of hydrogen is still very small, industrial hydrogen already has a massive market, and so, focus on this direction could accelerate the development of clean hydrogen production and subsequently to reduce the environmental impact of human activities.



Figure 2 - Global distribution of existing main refining, steelmaking and chemical cracking plants [2]

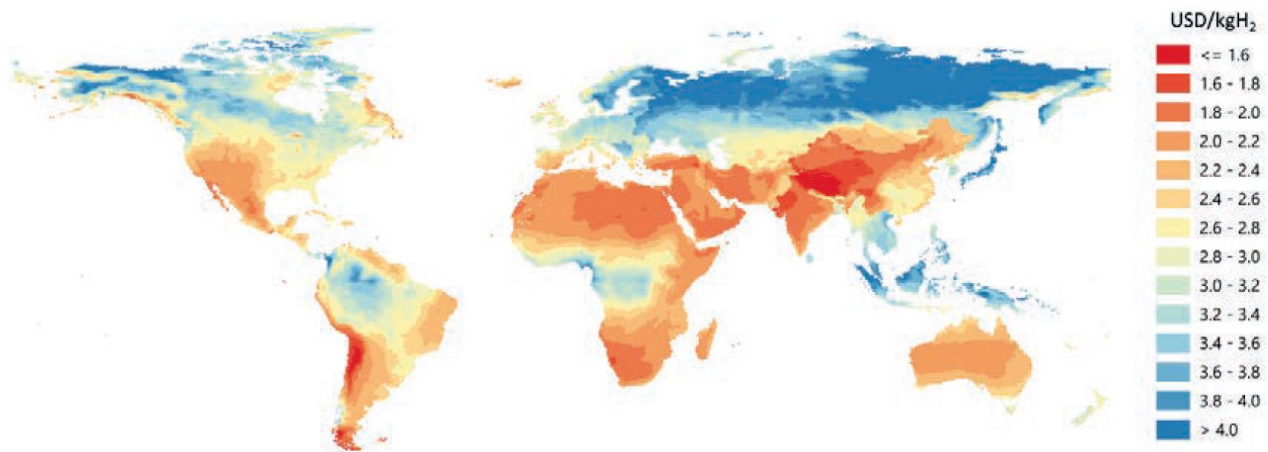


Figure 3 - Hydrogen costs from renewable energy systems in the long term [2]

An already established and promising way to produce clean hydrogen is through electrolysis coupled with renewable energy sources. The main technologies to perform electrolysis are alkaline water electrolysis, proton exchange membrane (PEM) and solid oxide electrolysis cell (SOEC). Nowadays, the most diffused electrolysis technology of commercial H<sub>2</sub> production plants is the alkaline water electrolysis [2]. This method requires an investment cost in the range of 1000-1200 €/kW [4]. However, these plants operate at low current density, so the main drawback is the low power density and the requirement of bigger plant to compete with a pollutant conventional H<sub>2</sub> production plant. A promising alternative to the existing electrolysis facilities could be membraneless electrolyzers, that have the potential to be cheaper than conventional ones (PEM and alkaline). In fact, they do not use a membrane or a diaphragm to keep the gases separated, but just fluid-dynamics, resulting in a simpler design. The absence of this component grants also a higher durability, since membranes are very sensitive to changes in operational conditions and load, they are also degradable components, that need substitution several times during plant lifetime. Another advantage of this technology is the possibility to be produced by 3D printing, making the first stages of prototyping, and testing easier and cheaper.

Membraneless electrolyzers could achieve high current density (2-4 A/cm<sup>2</sup>) and high outlet gas purity (> 95% at the outlet and > 99% after purification), as will be proved in this thesis.

The thesis will develop also, for the first time, a detailed economic assessment made for membraneless electrolyzers, and a comparison between different membraneless designs.

## 2 Membraneless Electrolyzer Technology Overview

An electrolyzer is an electrochemical device that uses electricity to split water into oxygen and hydrogen with the following overall reaction  $\text{H}_2\text{O} \rightarrow \frac{1}{2}\text{O}_2 + \text{H}_2$ . As outlined in the introduction, membraneless electrolyzers (MEs) separate the  $\text{O}_2$  and  $\text{H}_2$  gas streams through a fluid flow without the need of a physical barrier. MEs can be divided into two major categories “active” and “passive”. In an “active” ME, the fluid transport is driven by an external source (e.g. a pump) with the two configurations being the flow-by (FB) [5, 6] and flow-through (FT) [5, 7, 8]. Conversely, a “passive” ME uses natural buoyancy to operate [9, 10].

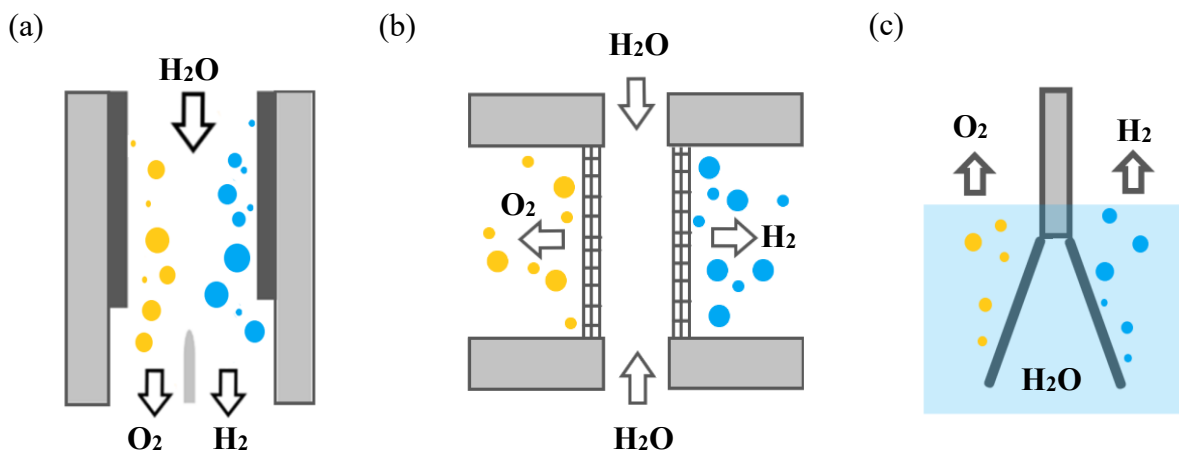


Figure 4 –Schematics of the (a) flow-by, (b) flow-through and (c) buoyancy driven configurations.

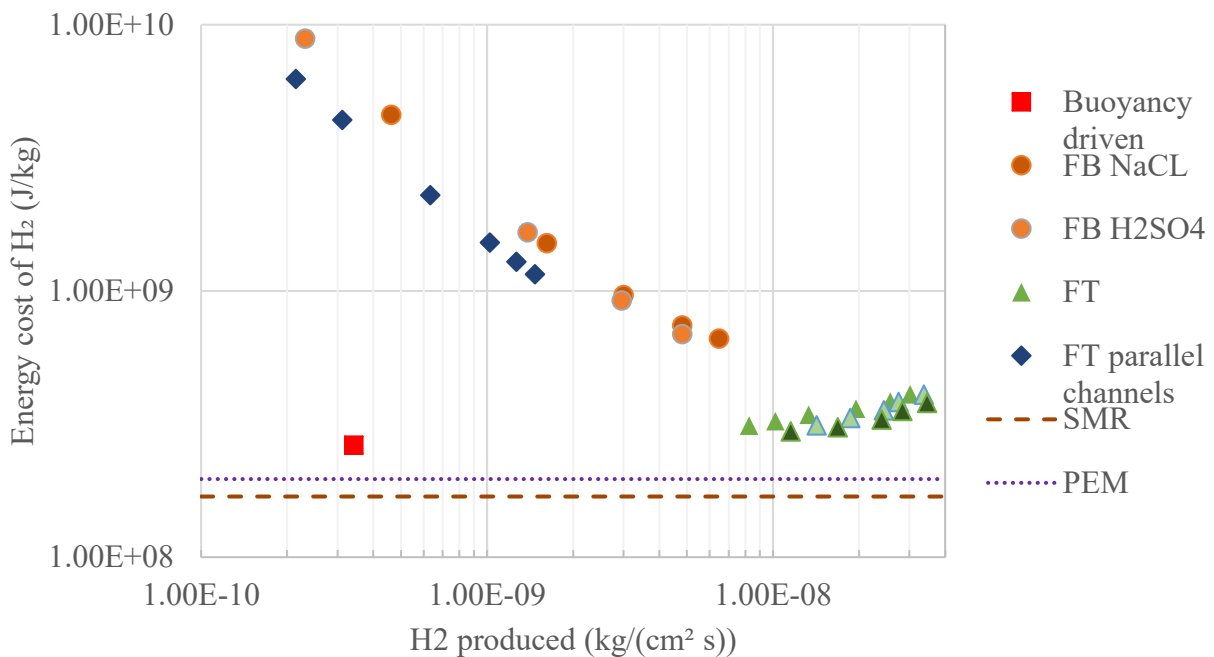


Figure 5 - Production and energy cost of H<sub>2</sub> with different MEs

By mean of the review of the literature about MEs [5–13], it was possible to summarize the experimental results of various designs. In Figure 5 are reported the specific energy consumption per kg of H<sub>2</sub>, the buoyancy driven and FT. The parallel channels FT is another configuration of FT typology, that has obliquus electrodes put in front of two parallel channel.

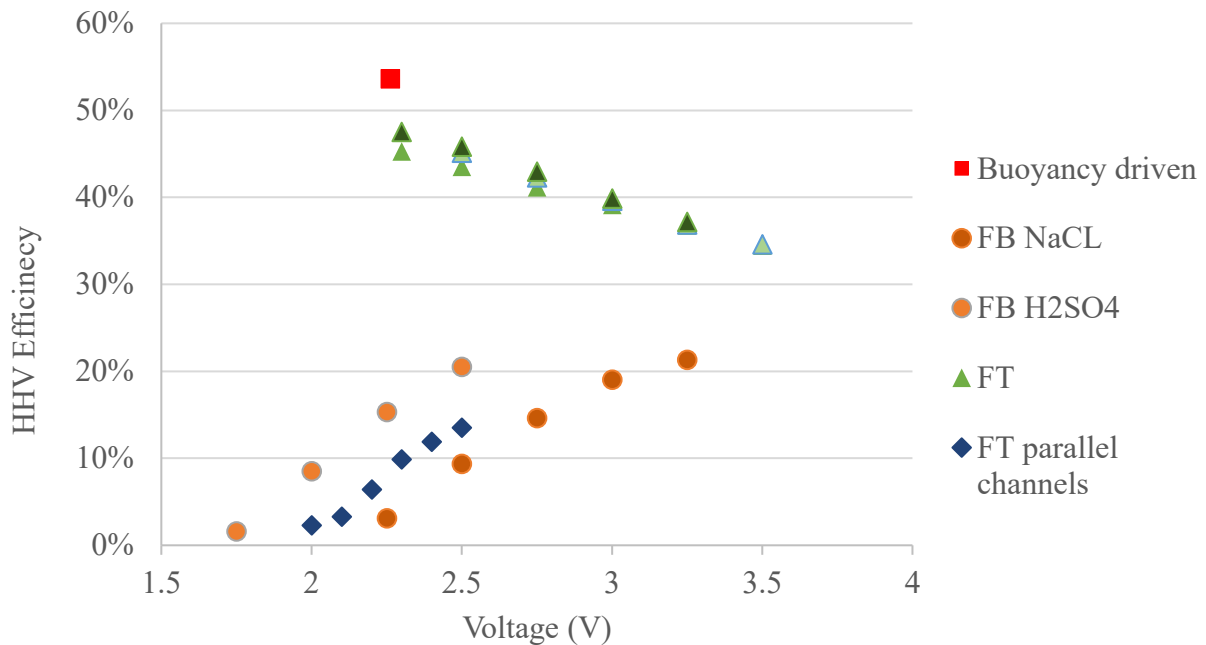


Figure 6 – HHV efficiency of various MEs

Considering also the electrolyzer efficiency (Figure 6), I can see how buoyancy driven has the highest, and FT-DEFT is right below it. The other configurations are at lower value less than 20%.

Lastly, I compared current density operational range for the reviewed MEs in Figure 7. FT has the highest values, while buoyancy driven design has the lowest. This implies that the production density for FT is the highest and so, the dimension and capital cost of a plant is lower. While for buoyancy driven bigger plants are required to produce the same amount of hydrogen than for the other designs.

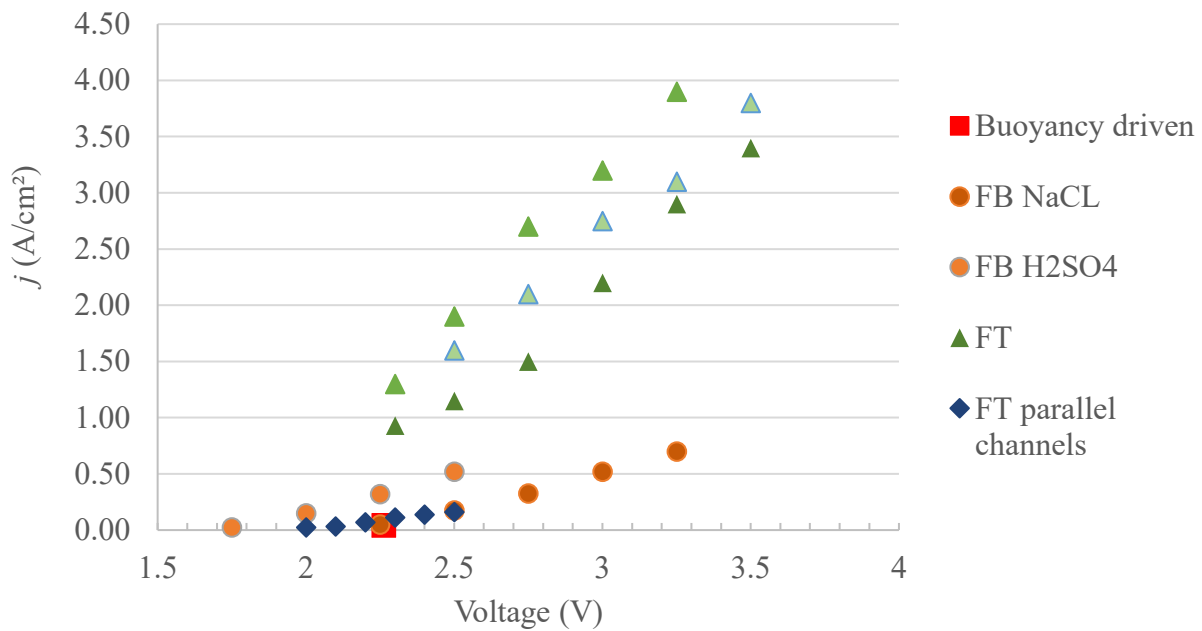


Figure 7 – Experimental current densities of various MEs

After having considered all the data, it has been made the choice to focus this study only on “active” MEs because they have shown the greatest promise in terms of operating current, that leads to a higher H<sub>2</sub> production density, purity, and energy efficiency.

In the electrolyzer, generated gases flow downstream where they are collected in two separate chambers. In FB the electrolyte flows beside the electrodes as shown in Figure 4 (a). To minimize gas mixing, the fluid flow needs to be laminar ( $Re < 2300$ ) [14]. In the FT design as shown in Figure 4 (b) the electrolyte directly flows through the meshed electrode carrying away the gas to the collection chambers. For the FT, flow laminarity is not strictly required, but electrode’s integrity can be compromised with too high flow rates, as it will be shown in the subsequent paragraphs.

In the literature overview [5–8, 11–13], it has been seen that FT projects have reached an advanced stage of considerable size, while FB devices are still in a less developed stage. Hydrox Holdings ltd. built a small scale H<sub>2</sub> production plant with a FT ME featuring ring-shaped electrodes with a 23 cm outer diameter [15]. For the FB design, the electrode and cell body need to be small, with the electrode area in the range of 1 cm<sup>2</sup> to ensure the laminarity of the fluid flow and a short mixing length, to keep the gas mixing as low as possible [6, 14]. As the flow for the FT design can be turbulent, the corresponding electrodes can be built significantly larger in size. As shown in Table 1, FT and FB designs are characterized by different operating current density range; while FT designs have shown to be able to reach 4 A/cm<sup>2</sup>, FB have been limited to 1 A/cm<sup>2</sup>. The different current density ranges

lead to a higher hydrogen production density for FT compared to the FB. For this analysis it has been chosen to set alkaline electrolyte also for FB design, to make a better and pair comparison

Table 1 - Parameters and conditions used for the FB and FT systems.

	<b>FB</b>	<b>FT</b>	<b>Unit</b>	<b>References</b>
Electrode gap	1-2.5	2.5-5	mm	[6, 7, 12, 13]
Electrode area	0.1-1	7-350	cm <sup>2</sup>	[6, 7, 12, 13]
Current density	0-0.7	0-4	A/cm <sup>2</sup>	[6, 7, 12, 13]
Electrolyte	30% KOH	30% KOH	kgKOH/kg <sub>electrolyte</sub>	[6, 7, 12, 13]
Electrodes	Ni foam plus Pt or NiO as catalyst	Ni foam plus Pt or NiO as catalyst	-	[6, 7, 12, 13]
Flow conditions	laminar	laminar/turbulent	-	[6, 13, 14]

### 3 Methodology and Model

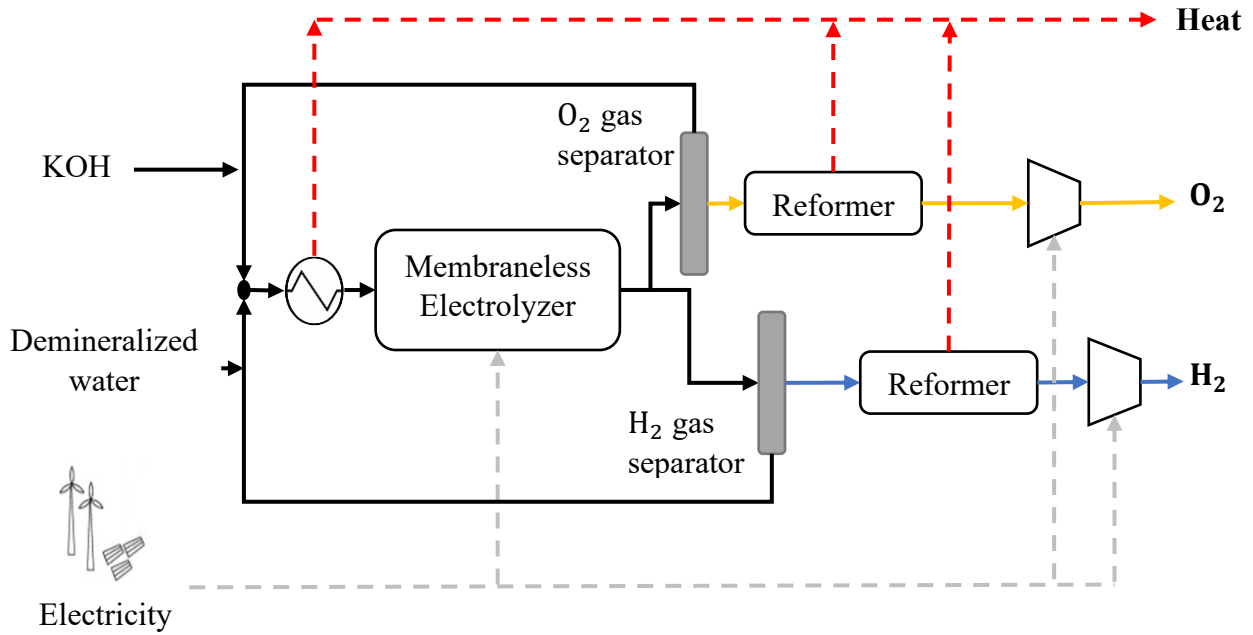


Figure 8 - General configuration of the electrolyzer system.

The system that I considered is constituted by the ME, gas separation and compression lines for both H<sub>2</sub> and O<sub>2</sub> and the heat recovery system, the plant is schematized in Figure 8.

Electricity, potassium hydroxide (KOH), as alkaline salt for the electrolyte, and de-ionized water are supplied as inputs and constitute the main operating cost in the ME plant. The main output is H<sub>2</sub>, and side products are oxygen and heat, as it can be noticed in Figure 8.

. For the electrolyzer model I made some assumptions: the electrolyzer cell is adiabatic; ii) ideal gas equation valid for the gas phase; iii) no leakages in the hydraulic circuit, so, no electrolyte losses; iv) complete symmetry in the cell and so, symmetric fluid pathways and distribution in the cell; v) all products (*i.e.* gaseous H<sub>2</sub> and O<sub>2</sub>) leave the system; vi) steady state operation.

#### 3.1 Physical model

##### 3.1.1 Thermodynamics and Kinetics

For alkaline electrolysis, the half reactions occurring at the anode and cathode, respectively, are



The reversible voltage  $E_0$  needed to split water molecules is given by [16]

$$E_0 = \frac{\Delta g_{\text{rxn}}}{2F} \quad (2)$$

where  $\Delta g_{\text{rxn}}$  and  $F$  are the Gibbs free energy of reaction and the Faraday's constant, respectively. At standard conditions (25 °C and 1 atm) the value of  $E_0$  is 1.23 V [16].  $E_0$  is the ideal value of the potential at which electrolysis takes place. The actual voltage  $V_{\text{cell}}$  needed to run an electrolytic cell can be considerably higher because of the following losses: 1) activations of the electrocatalytic reactions; 2) ohmic resistances; and 3) deviations of the concentration of reactants from their "bulk" values to the values at the reaction sites. Specifically,  $V_{\text{cell}}$  can be written as [16]

$$V_{\text{cell}} = E_0 + \eta_{\text{act}} + \eta_{\text{ohm}} + \eta_{\text{conc}} \quad (3)$$

where  $\eta_{\text{act}}$ ,  $\eta_{\text{ohm}}$ , and  $\eta_{\text{conc}}$  are activation, ohmic, and concentration overpotentials, respectively. Activation and concentration overpotential contributions must be considered for both anode and cathode, implying that  $\eta_{\text{act}} = \eta_{\text{act}}^{\text{anode}} + \eta_{\text{act}}^{\text{cathode}}$  and  $\eta_{\text{conc}} = \eta_{\text{conc}}^{\text{anode}} + \eta_{\text{conc}}^{\text{cathode}}$ . I must point out that  $\eta_{\text{conc}}$  will be neglected due to its very small contribution to  $V_{\text{cell}}$  in the considered operational range, as reported in the literature [6, 7, 16].

The use of Butler-Volmer equation for the charge transfer kinetic model [16, 17] allows us to write  $\eta_{\text{act}}$  as

$$\eta_{\text{act}} = \frac{RT}{2\alpha F} \ln \left( \frac{j}{j_0} \right) \quad (4)$$

where  $R$  is the ideal gas constant,  $T$  is the temperature,  $\alpha$  is the transfer coefficient (it is assumed  $\alpha = 0.5$ ),  $j$  is the current density (i.e. the current normalized with respect to the electrode cross sectional surface), and  $j_0$  is the exchange current density[16].

The  $\eta_{\text{ohm}}$  is computed as follows

$$\eta_{\text{ohmic}} = j \cdot \text{ASR}_{\Omega} \quad (5)$$

where  $\text{ASR}_{\Omega}$  ( $\Omega \cdot \text{cm}$ ) is the area specific resistance due to the ionic transport in the electrolyte and the electronic transport in the electrodes [16]. If the electrodes are a distance  $h$  apart and are characterized by a thickness  $t$ , I can write [16, 17]

$$\text{ASR}_{\Omega} = \rho_{\text{ely}} h + 2 \rho_{\text{elect}} t \quad (6)$$

where  $\rho_{\text{ely}}$  and  $\rho_{\text{elect}}$  are the electrolyte and electrode resistivities, respectively. Since  $\rho_{\text{ely}} \gg \rho_{\text{elect}}$  and  $t \approx h$ , the electrode contribution can be neglected. The  $\rho_{\text{ely}}$  depends on the concentration of salt in the electrolyte and on  $f$ , the volume fraction of the fluid occupied by bubbles. Specifically,  $\rho_{\text{ely}}$  can be written as  $\left( \text{for } f \leq \frac{2}{3} \right)$  [17, 18]

$$\rho_{\text{ely}} = \frac{\rho_0}{1 - \frac{3}{2}f} \quad (7)$$

where  $\rho_0$  is the bulk (or bubble-free) ionic resistivity of the electrolyte (which depends on the salt concentration [19]).

### 3.1.2 Outlet gas production and purity

The cell model that was used to evaluate the molar flow rates considers the production of the gas species through Faraday's law

$$\dot{n}_k = \frac{I}{z_k * F} * \eta_{\text{faradic}} \quad (8)$$

where  $\dot{n}_k$  is the molar flow rate of the gas  $k$  ( $\text{H}_2$  and  $\text{O}_2$ ) produced by the electrochemical reaction,  $z_k$  is the number of free electrons in the reaction (2 for  $\text{H}_2$  and 4 for  $\text{O}_2$ ) and  $\eta_{\text{faradic}}$  is the faradic efficiency of the reaction.

The  $\dot{n}_{\text{H}_2}$  obtained is not the outlet gas that goes out the electrolyzer, because the dissolution of the gas phases in the electrolyte and gas mixing have to be considered. So, the gas outlet stream from the electrolyzer are characterized by a molar flow rate and a purity.  $\text{H}_2$  and  $\text{O}_2$  purities in the output channels  $c$  (i.e., the outlet channels  $c = 1, 2$  for  $\text{H}_2$  and  $\text{O}_2$ , respectively) were computed as follows

$$\text{purity}_{\text{H}_2,c} = \frac{\dot{n}_{\text{H}_2,\text{gas,out},c}}{\dot{n}_{\text{H}_2,\text{gas,out},c} + \dot{n}_{\text{O}_2,\text{gas,out},c}} \quad (9a)$$

$$\text{purity}_{\text{O}_2,c} = \frac{\dot{n}_{\text{O}_2,\text{gas,out},c}}{\dot{n}_{\text{H}_2,\text{gas,out},c} + \dot{n}_{\text{O}_2,\text{gas,out},c}} \quad (9b)$$

where  $\dot{n}_{\text{H}_2,\text{gas,out},c}$  and  $\dot{n}_{\text{O}_2,\text{gas,out},c}$  are the output molar flow rate of the species in the corresponding channels evaluated with the model, constituted by algebraic equation of mass balance and ideal gas law for each channel, for the  $\text{H}_2$  channel (i.e.  $c = 1$ )

$$\dot{n}_{\text{H}_2} + 0.5 \dot{n}_{\text{H}_2,\text{liq,in},1} = \dot{n}_{\text{H}_2,\text{gas,out},1} + \dot{n}_{\text{H}_2,\text{liq,out},1} \quad (10)$$

$$0.5 \dot{n}_{\text{O}_2,\text{liq,in},1} = \dot{n}_{\text{O}_2,\text{gas,out},1} + \dot{n}_{\text{O}_2,\text{liq,out},1} \quad (11)$$

$$\dot{n}_{\text{O}_2,\text{gas,out},1} = \frac{p_{\text{O}_2} \text{Vol}}{RT} \quad (12)$$

where  $\dot{n}_{\text{H}_2,\text{liq,in},1}$  is the molar flow rate of  $\text{H}_2$  dissolved in the electrolyte that enter in the cell,  $\dot{n}_{\text{H}_2,\text{liq,out},1}$  is the molar flow rate of dissolved  $\text{H}_2$  in the liquid electrolyte that goes out from the cell, and  $\dot{n}_{\text{O}_2,\text{liq,in},1}$ ,  $\dot{n}_{\text{O}_2,\text{liq,out},1}$  are the dissolved molar flow rates of  $\text{O}_2$  that go in and out from the cell,  $p_{\text{O}_2}$  is the partial pressure of  $\text{O}_2$  and  $\text{Vol}$  is the volume of the gas phase. To determine the outlet flow rates of dissolved gases I know that  $\dot{n}_{k,\text{liq,out},c} = x_{e,k} \cdot \dot{n}_{\text{ely}}$ , where  $x_{e,k}$  is the molar fraction of the

dissolved gas  $k$  in the electrolyte in the considered channel, and  $\dot{n}_{\text{ely}}$  is the electrolyte molar flow rate. From Henry's law I compute the molar fraction of the gaseous species

$$p_k = H_k \cdot x_{e,k} \quad (13)$$

where  $p_k$  is the partial pressure of the species  $k$  in the gaseous phase.  $H_k$  is the Henry coefficient of the gas species  $k$ , and  $x_{e,k}$  is the molar concentration of the dissolved  $\text{H}_2$  and  $\text{O}_2$  in the electrolyte. Partial pressures are correlated by the relation with  $p$ , the total pressure of the electrolytic cell,  $p = \sum_{i=1}^2 p_k$ . Combining (11), (12) and (13) it was possible to evaluate  $x_{e,k}$  by mean of an analytical expression

$$x_{e,\text{O}_2} = \frac{0.5 \dot{n}_{\text{O}_2,\text{liq,in},1}}{\dot{n}_{\text{ely}} + H_{\text{O}_2} \text{Vol}/RT} \quad (14)$$

Knowing  $x_{e,\text{O}_2}$ , it was possible to compute the partial pressures of  $\text{H}_2$  and  $\text{O}_2$  and the rest of the parameters by substitution.

Henry coefficients  $H_k$  for  $\text{H}_2$  and  $\text{O}_2$  were evaluated considering the effect of the dissolved salt

$$H_k = 10H_k^0 K_k w \quad (15)$$

$H_k^0$  is the Henry's coefficient in water,  $K_k$  is the Setchenov constant, and  $w$  is the weight percentage of the salt in the electrolyte (value from 0 to 1).

$H_k^0$  was obtained from the Harvey equation [20]

$$\ln\left(\frac{H_k^0}{p_{\text{vap}}}\right) = \frac{A_1}{T_R} + \frac{B_1(1 - T_R)^{0.355}}{T_R} + C_1 T_R^{-0.41} \exp(1 - T_R) \quad (16)$$

where  $A_1$ ,  $B_1$  and  $C_1$ , are empirical parameters specific for every gas [20],  $T_R = T/T_c$  and  $T_c$  is the critical temperature of the species, and  $p_{\text{vap}}$  is the vapor pressure of water, that value can be estimated from the Antoine equation [21]

$$\ln\left(\frac{p_{\text{vap}}}{\text{kPa}}\right) = A_2 - \frac{B_2}{\frac{T - 273.15}{K} + C_2} \quad (17)$$

where  $A_2$ ,  $B_2$  and  $C_2$  are empirical parameters for every substance, in our case water [21].

Lastly to consider the effect of the KOH electrolyte on the dissolution of product gases, I used the Setchenov relation [22, 23]

$$\log_{10}\left(\frac{x_{0,k}}{x_{e,k}}\right) = K_k w \quad (18)$$

where  $x_{0,k}$  is the concentration of the dissolved gas in pure water, while  $x_{e,k}$  is the concentration in the electrolyte,  $K_{H_2} = 3.14$  and  $K_{O_2} = 3.66$  for a water solution with 30% of KOH [8] for both gas species in the electrolyte.

I checked if the diffusion processes taking place in the area between the two electrodes could affect the purities of the gases, using Fick's Law, considering the max gradient of concentration obtained by the model and the length of the chamber. I obtained  $H_2$  currents of  $10^{-12}$  mol/s (from the  $H_2$  and  $O_2$  outlet channels). Therefore, diffusion processes were neglected.

### 3.1.3 System efficiency

I used the higher heating value (HHV) to define the efficiency of the electrolyzer,  $\eta_{HHV}$ , namely

$$\eta_{HHV} = \frac{\dot{n}_{H_2 \text{ gas out}} \mathcal{M}_{H_2} HHV_{H_2}}{P_{el} + P_{\text{pump}}} \quad (19)$$

where  $\mathcal{M}_{H_2}$  is the molecular mass of hydrogen,  $HHV_{H_2}$  is the higher heating value of hydrogen ( $HHV_{H_2} = 1.41 \cdot 10^8 \text{ J/kg}$  [5]),  $P_{el}$  is the electric power directly used by the cell, and  $P_{\text{pump}}$  is the pumping power needed to circulate the fluid in the hydraulic circuit. The  $P_{\text{cell}}$  is given by

$$P_{\text{cell}} = I_{\text{cell}} V_{\text{cell}} \quad (20)$$

where  $I_{\text{cell}}$  is the total cell electric current. The  $P_{\text{pump}}$  is calculated as

$$P_{\text{pump}} = \frac{\dot{m}_{\text{ely}} H_{\text{tot}} g}{\eta_{\text{pump}}} \quad (21)$$

where  $\dot{m}_{\text{ely}}$  is the electrolyte flow rate,  $H_{\text{tot}}$  is the head of the hydraulic circuit,  $g$  is the acceleration of gravity, and  $\eta_{\text{pump}}$  is the hydraulic efficiency of the pump.  $H_{\text{tot}}$  is computed as

$$H_{\text{tot}} = H_{\text{dist}} + H_{\text{minor}} + H_{\text{dev}} \quad (22)$$

where  $H_{\text{dist}}$ ,  $H_{\text{minor}}$ , and  $H_{\text{dev}}$  are the sum of all pipe, minor, and device head losses, respectively.

Pipe losses defined as  $H_{\text{dist}} = f_{\text{dist}} \frac{L_{\text{tube}}}{D_{\text{tube}}} \cdot \frac{v^2}{2g}$ , where  $L_{\text{tube}}$  is the length of the tubes,  $D_{\text{tube}}$  is the diameter of the tube,  $v$  is the speed of the fluid flow in the pipes, and  $f_{\text{dist}}$  is the loss factor (for a laminar flow  $f_{\text{dist}} = \frac{64}{\text{Re}}$  and in turbulent flow I apply Colebrook equation [24]). Minor losses  $H_{\text{minor}} = k_{\text{conc}} \frac{N_{\text{minor}} v^2}{2g}$ , where  $k_{\text{conc}}$  is the loss factor for the discontinuities or curves in the circuit and  $N_{\text{conc}}$  is the number of minor losses considered. A generic hydraulic circuit was guessed for this part of the analysis, 2 m of tubes with 10 mm of diameter and six generic hydraulic discontinuity for minor losses.

### 3.1.4 Model computation

I used a semi-0D model, where the electrolyzer operation is described by a series of algebraic equation reported in 3.1 section. The simulation was implemented in Matlab using the current density as input value to solve the problem  $N$  times until a certain tolerance was reached ( $1 \cdot 10^{-8}$ ) between the mass balances of inlet and outlet, considering a current density range between  $0.04 \text{ A/cm}^2$  and  $3.5 \text{ A/cm}^2$ .

The used base Matlab code can be found in **Appendix A**.

### 3.2 Economic Analysis

This analysis follows the net present value (NPV) method [25], which is an investment planning approach to evaluate project profitability and estimate the break-even period, i.e. the time  $t^*$  for which  $NPV(t^*) = 0$ . In other words,  $t^*$  denotes the time at which the investment recovered its initial value, and the plant starts to be profitable. The NPV is defined as the difference between the present value of cash inflows and outflows (*i.e.* net cash inflow) over the lifetime of the plant. The present value of cash flows are evaluated considering an appropriate discount rate, that takes into account interest rates and financial parameters [4, 25–28]

$$NPV(n) = -I + \sum_{n=1}^N \frac{B(n)}{(1+i)^n} \quad (23)$$

where  $I$  is the initial investment, the index  $n$  denotes the year (after the initial investment),  $B(n)$  is the net cash flow at year  $n$ , and  $\frac{1}{(1+i)^n}$  is the depreciation factor characterized by an average discount rate  $i$ .

The levelized cost of hydrogen (LCH), defined as the specific price of hydrogen that allows breaking even financially, was also estimated. The LCH allowed comparing  $\text{H}_2$  costs of different size plants and from technologies and see if the produced commodity is compatible on the market [4, 29–32]. LCH is defined as

$$LCH(n) = \frac{I + \sum_{n=1}^N \frac{c(n)}{(1+i)^n}}{\sum_{n=1}^N \frac{\dot{m}_{\text{H}_2}}{(1+i)^n}} \quad (24)$$

where  $c(n)$  is the total operating cost of the plant at year  $n$ , and  $\dot{m}_{\text{H}_2}$  is yearly mass of hydrogen produced by the plant, according to the plant size.

The weighted average cost of capital (WACC) is used in the evaluation of NPV in (23) and LCH in (24), as it includes interest rate, the financial characteristics (corporate tax rate, cost of debt, inflation rate *etc.*). The WACC is defined as [25]

$$\text{WACC} = \frac{e}{e+d} e_r + \frac{d}{e+d} d_i (1 - C_{\text{tax}}) \quad (25)$$

where  $e$  is equity,  $d$  is debt,  $e_r$  equity rate of return,  $d_i$  debt interest rate, and  $C_{\text{tax}}$  is the corporate tax rate. The WACC values were taken from “WACC Expert” [33, 34]. The corresponding values are reported in Table 2.

Table 2 - Taxation rates and WACC values.

<b>Economic and financial parameters</b>		
Corporate tax rate		
China	25%	[33]
USA	40%	[33]
HK	16.5%	[33]
UE-27	30.0%	[34]
WACC		
China	7%	[33]
USA	6%	[33]
HK	6.8%	[33]
UE-27	4.0%	[34]

To perform the analysis, I selected four separate entities: the European Union (27 countries), China, the USA, and Hong Kong. Each location has its specific financial and market characteristics (such as electricity price, taxation rate *etc.*), impacting the economic performance of the hydrogen production plant.

### 3.3 Costs accounting

It has been found that the factors that determine the cost of an electrolysis plant include the size of the plant, geographical location, power source, market conditions, and taxation [4, 29, 30, 35]. A detailed analysis of how these factors influence the capital and operating costs is presented below.

#### 3.3.1 Capital costs

I estimated the initial capital costs following the method of National Energy Technology Laboratory (NETL) [36, 37]. This approach permits to compute the capital cost from the initial machinery and labor cost, in a rigorous and easy way, that takes into account all the phase and requirement of an energy project with a cascade series of correlation factors. as shown in Table 3.

Table 3 – List and percentages for the capital cost cascade estimation, derived from [36].

<b>Levels of capital cost</b>	
Bare erected cost (BEC)	Machinery and labor
Engineering, procurement, and construction cost (EPCC)	109% of the BEC
Process and project contingencies (TPC)	135% of the EPCC
Overnight costs (TOC)	120% of the TPC
Interest and escalation (TASC)	110% of the TOC

The bare erected cost (BEC) includes: 1) costs for machinery; 2) stack; 3) balance of plant (BoP), and 4) labor needed to build the plant. The stack cost and BoP are described in detail in the next paragraph. Engineering, procurement, and construction cost (EPCC). The total plant cost (TPC) includes: 1) process contingencies; and 2) project contingency costs. That are linked to the maturity of the technology, such as unexpected problems during the construction that were not foreseen at the design stage of the project (e.g. detailed layout of the plant, ancillary materials, organization etc.). Total overnight cost (TOC) includes other owner’s costs, such as: 1) bureaucracy; 2) finance; and 3) pre-production. Lastly, I obtain the investment capital of the plant as total as spent capital (TASC), that includes: 1) inflation; and 2) escalation of goods prices. To gain TASC I start from stack, purifiers, compressors and BoP cost, that constitute the BEC, than I use the factor listed in Table 3, to obtain the TASC, that is used as an initial investment  $I$  in (23) and (24).

The BEC is composed by stack cost and balance of plant (BoP) cost. The stack cost is related to the electrolyzer itself, cell, sealant, circuits etc., while BoP takes into account all the other machineries need to make the plant works, such as compressors, piping, water managing system etc.

Regarding the stack cost, after having consulted the analysis of National Renewable Energy Laboratory (NREL) [35, 38], three scenarios were selected: 1) “today” with a production of just some units per year; 2) “medium-term” with 50 units/year (5 years horizon), and 3) “long-term” with 1000 units/year (10-20 years horizon). For reference, a stack for a 200 kW plant costs 460 USD/kW, while in a large scale production (long-term scenario), the stack cost may decrease to 51 USD/kW [35, 38], this is due to the scale production and the improvement in the process and technology.

Table 4 - Stack cost taken from NERL report [35, 38]

STACK						
Stack part	Today scenario		Mid-term scenario		Long-term scenario	
	Plant size		Plant size		Plant size	
	200 kW	1000 kW	200 kW	1000 kW	200 kW	1000 kW
Frame/ seal (USD)	75	16	17	4	3	2
Electrodes (USD)	100	35	50	20	25	15
Bipolar plates (USD)	140	37	40	15	15	11
Assembly (USD)	85	23	20	7	2	2
BoS (13% of tot) (USD)	60	17	19	7	7	4
Specific cost [USD/kW]	460	128	146	53	51	34

The BoP cost was estimated using the stack costs method mentioned above. Moreover, being the BoP linked to mature technologies (*i.e.* pumps, pipes *etc.*), I assumed that this cost would not change in the near future, because they are well established and wide used technologies. However, it should be noted that the power-specific cost of the BoP decreases with plant size. As shown in Table 5, if the plant power increases from 50 kW to 10 GW the power-specific costs will decrease from 2400 USD/kW to 300 USD/kW.

Table 5 - BoP cost taken from NERL report [35, 38]

BALANCE OF PLANT								
System	Plant size							
	50 kW	100 kW	200 kW	500 kW	1000 kW	2000 kW	5000 kW	10000 kW
Power supplies (kUSD)	23.3	27.9	44.6	132.6	198.6	336.1	734.8	1 405.5
Deionized water (kUSD)	26.4	30.9	48.8	57.1	87.1	149.6	275.1	511.2
Gas processing (kUSD)	24.2	28.2	36.4	57.3	83.9	143.4	267.4	478.1
Cooling (kUSD)	17.2	17.5	17.5	21.4	28.7	38.4	59.4	81.0
Miscellaneous (kUSD)	6.0	6.0	6.0	6.0	6.0	6.0	6.0	6.0
Total cost (kUSD)	121.3	138.7	189.6	331.7	488.1	816.9	1 610.1	2 959.8
Specific cost (kUSD/kW)	2.4	1.4	0.9	0.7	0.5	0.4	0.3	0.3

### 3.3.2 Operating and maintenance costs

Operation and maintenance costs (O&M) include employees' wages, ordinary maintenance cost and inputs streams (e.g. H<sub>2</sub>O, KOH) excluding electricity and extraordinary maintenance (e.g. component

replacement). Following [29], I conservatively assumed the annual O&M costs to be 5% of the TASC. I also assumed that the electrolyzer stack and the gas purification system are replaced every 10 [4] and 5 [39] years, respectively. Other parts of the plant, such as pumps and piping, have a lifetime longer than 20 years, implying that ordinary maintenance is sufficient, of course excluding accidents and extraordinary events.

### 3.3.3 Cost of electricity

I considered two electrical power sources, namely, “grid” and “renewables”. In “grid” configuration the electricity is provided by the electrical grid, it is a constant supply, but generally expensive. In contrast, in “renewables” configuration, the power supply is provided by renewable energy sources, such as photovoltaic or wind turbines, they are cheaper but intermittent., The cost of grid electricity depends on location, while renewable are set fundamentally constant [5], as shown in Table 6. I used the capacity factor (CF) to consider the different availability of the power sources. It is defined as annual hours of operation divided by total hours of the year. I set CF=90% for the grid-connected plant<sup>1</sup> [5], and CF=40% for the renewable coupled plant [5]. The latter value is smaller as it takes into account power supply discontinuities typical of renewables.

Table 6 - Prices of commodities

<b>Market parameters</b>		
	value	reference
Electricity prices (USD/kWh)		
China	0.08	[40]
USA	0.06	[41]
HK	0.14	[42]
UE-27	0.08	[43]
Renewable	0.03	[5]
Natural gas price (USD/kWh)		
China	0.03	[44]
USA	0.01	[45]
HK	0.13	[46]
UE-27	0.07	[43]
Oxygen price (USD/kg)		
all locations	0.05	[47]
Hydrogen price (USD/kg)		
all locations	1.60-5.70	[48]

### 3.3.4 Plant size

<sup>1</sup> Plants need stops for maintenance, periodical checks etc. It is usually assumed about 8000 operative hours/year.

I chose two plant sizes able to produce 500 and 1000  $\text{ton}_{\text{H}_2}/\text{year}$ , respectively. To test the impact of scale variation on the economic output of a medium and a big size plant, in the range of plant cost data available from NREL [35, 38]. The power source and the electrolyzer performances determine the power consumption of the plant. Since the  $\text{H}_2$  production is fixed, lower CF requires a larger plant, which is more expensive. According to the capital cost analysis, the difference in capital cost between the grid-connected and the renewable-connected increases with the  $\text{H}_2$  production rate. Comparing the 500 and 1000  $\text{ton}_{\text{H}_2}/\text{year}$  sizes, the renewable-connected plants result 110% more expensive than the grid-connected plants for the 500  $\text{ton}_{\text{H}_2}/\text{year}$  size, while the 1000  $\text{ton}_{\text{H}_2}/\text{year}$  plant is 102% more expensive.

### 3.3.5 Taxation and carbon tax

The taxation on the profits generated by H<sub>2</sub> and the other commodities selling was computed with the corporate taxation rate proper of the location of the plant. Corporate tax rates, according to the country, are reported in Table 2 with the WACC values.

To mitigate climate change, several organizations have suggested taxing the emissions of carbon dioxide, such as the United Nations (UN) and the European Union (EU). Some countries has already implemented it, as is possible to see in Figure 9. The carbon tax aims to reduce carbon emission by increasing the production cost of H<sub>2</sub> using conventional technologies such as steam methane reforming (SMR) and coal gasification (CG). It should point out that SMR and CG provide nearly 95% of the current H<sub>2</sub> production [2]. According to Mehmeti and coworkers, 12 tons and 18-24 tons of CO<sub>2</sub> from SMR and CG are emitted respectively for every kg of H<sub>2</sub> produced [49]. I considered three carbon tax scenarios for the analysis: the first is with no carbon tax enforced, the second is moderate and the third has a strong carbon tax policy. The moderate carbon tax value was set to  $135 \frac{\text{USD}}{\text{tonCO}_2}$ , which is similar to the carbon tax already implemented in some countries, such in Sweden  $\left(132 \frac{\text{USD}}{\text{tonCO}_2}\right)$  [50]. The strong carbon tax was set to  $350 \frac{\text{USD}}{\text{tonCO}_2}$  [50], which has been advocated by the World Bank to tackle the global climate change. I must point out that UN report suggest carbon tax till  $5500 \frac{\text{USD}}{\text{tonCO}_2}$  [51].

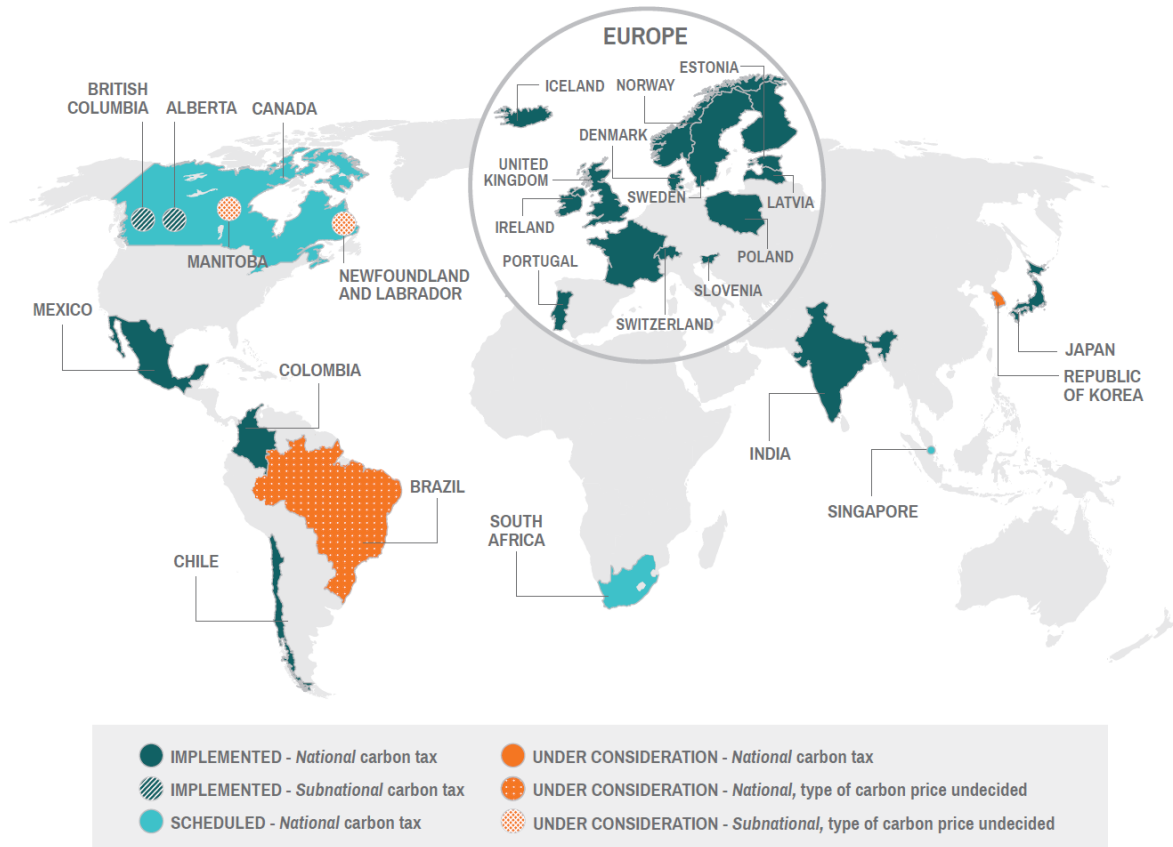


Figure 9 - Carbon Taxes in Operation, Scheduled, or under Consideration (as of February 2017) [50]

### 3.4 Products and gains

The plant studied produces hydrogen, oxygen and recovers heat at low temperature (50-60 °C). Outlet stream of H<sub>2</sub> is assumed to be compressed at 200 bar and purified till purity >99.9% [39]. The hydrogen market for industrial usage has a range of prices in the range between  $1.3 \frac{\text{USD}}{\text{kgH}_2}$  and  $5.7 \frac{\text{USD}}{\text{kgH}_2}$  [48]. Then, I estimated the price of H<sub>2</sub> considering the carbon tax scenarios, that leads to higher H<sub>2</sub> market prices respect the no carbon tax scenario.

Since the electrolyzer usually operates at 60°C, the temperature difference between the system and ambient can be exploited to produce hot water through a heat exchanger. This commodity could be useful for producing domestic hot water, providing heat in industrial low enthalpy processes, laundry, greenhouses heating, etc. Recovering and using such heat could result in reduced need and consumption of natural gas for the same purpose, reducing CO<sub>2</sub> emissions and selling it, it has a positive economic impact on the plant economic balance.

Lastly, oxygen can also be utilized in many situations from health care to steel industry and it has almost the same price worldwide, near 40 USD/ton, even if it is cheap it has a positive contribution on the final balance [47]. Especially considering the present pandemic situation in which oxygen for

medical treatments is required more than before, this represent another important contribution to the society.

## 4 Experimental experiences

Part of this work was also to build a prototype with the aim of verify the theoretical result of the model with a real electrolyzer. After having checked all various MEs design in Section 2, I focused on FT to design a little prototype, to make this, I used massively Gillespie's *et all* works [7, 12, 13, 52] in a process of reverse engineering.

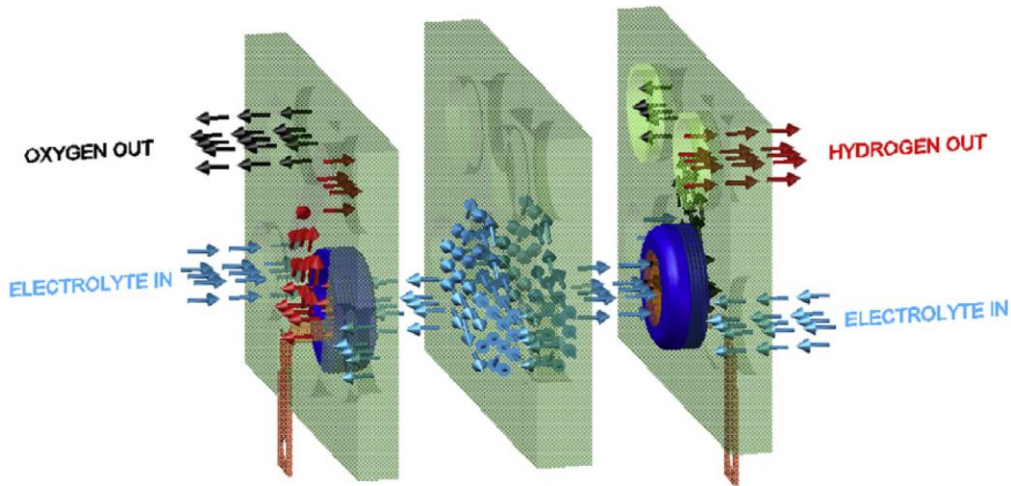


Figure 10 - Divergent electrolyte flow through (DEFT™) scheme used as base for the prototype design [7].

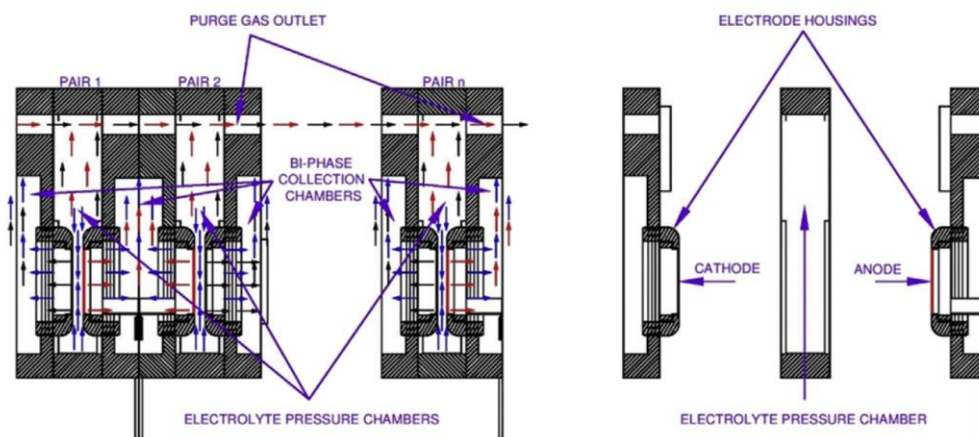


Figure 11 – Section of divergent electrolyte flow through (DEFT™) scheme used as base for the prototype design [7].

In those works, the experimental setups reported are already in an advanced stage, in terms of stacks and little pilot plants. My work focused on creating a one cell electrolyzer, as first step.

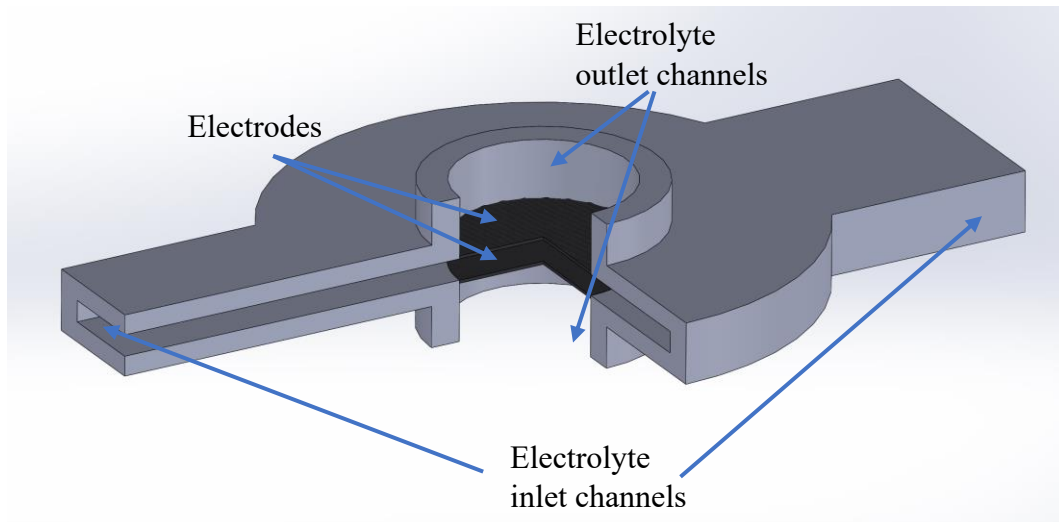


Figure 12 - First original concept for the cell.

The first concepts were very basic, focusing only on the fundamental design principle I was able to take from the literature. SolidWorks™ program was used in the entire prototyping process.

#### 4.1 Fluid-dynamics simulations

This first design was used in a fluid dynamic computational simulation to try to understand the behavior of the fluid inside the chamber, by means of COMSOL Multiphysics™, the first results are reported in Figure 13 and Figure 14. In these figures are reported the streamlines of the flow and the module of the fluid velocity. To simplify the computation, I considered only half of the cell, cutting with a plane parallel to the electrodes at half the electrode's gap. It would have been possible to simplify further the computational domain considering only one eighth of the cell, but to better visualize the results I chose to run the simulations on half-cell. Fortunately, this decision did not affect so much the computational time.

The program was set with laminar fluid flow equation for the empty part, with electrolyte properties (at this stage water), and with Brinkman equations for porous materials for the electrode.

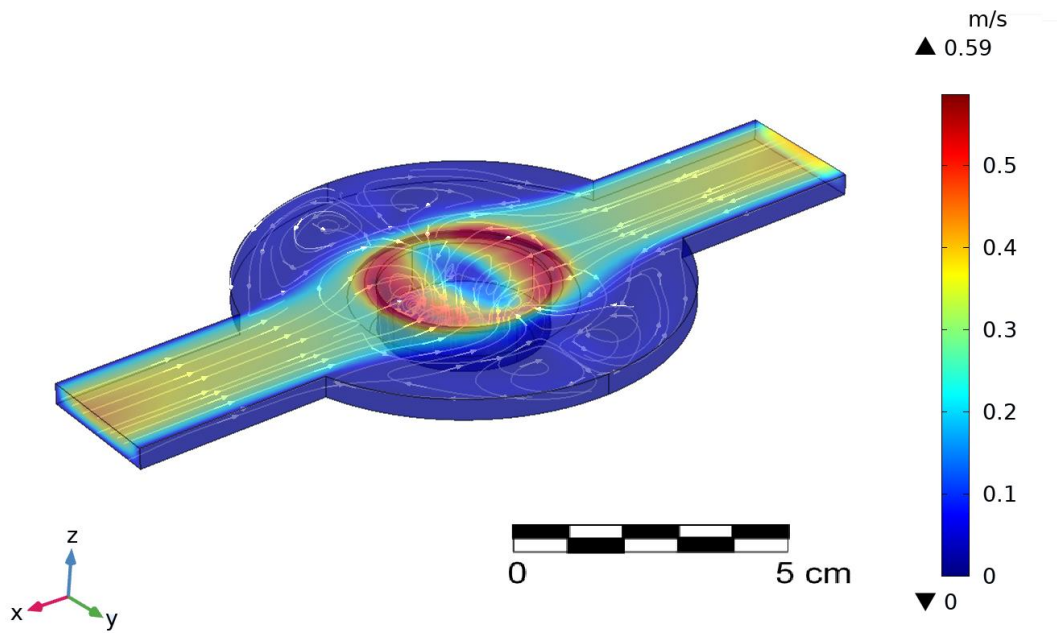


Figure 13 - Computational simulation of the fluid flow inside the cell of model 1.

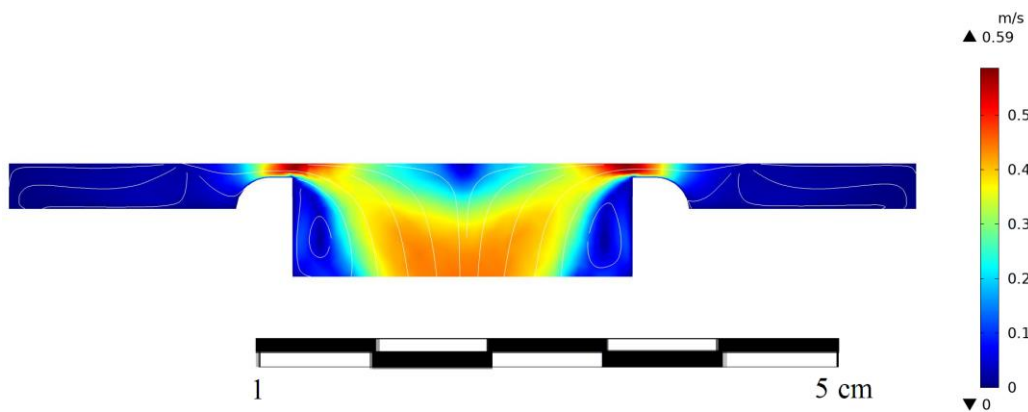


Figure 14 – Section on zy plane view of the velocity module of the fluid flow simulation of model 1.

To check the value to the results obtained, a small grid independence analysis was performed. On the outlet flow rate obtained in the model, respect to the analytical value expected from the geometry and the initial conditions, in [7] is reported the value of the suggested mean velocity on the electrode face, the flow rate in the cell, for this configuration, was evaluated as  $5E-5 \text{ m}^3/\text{s}$ .

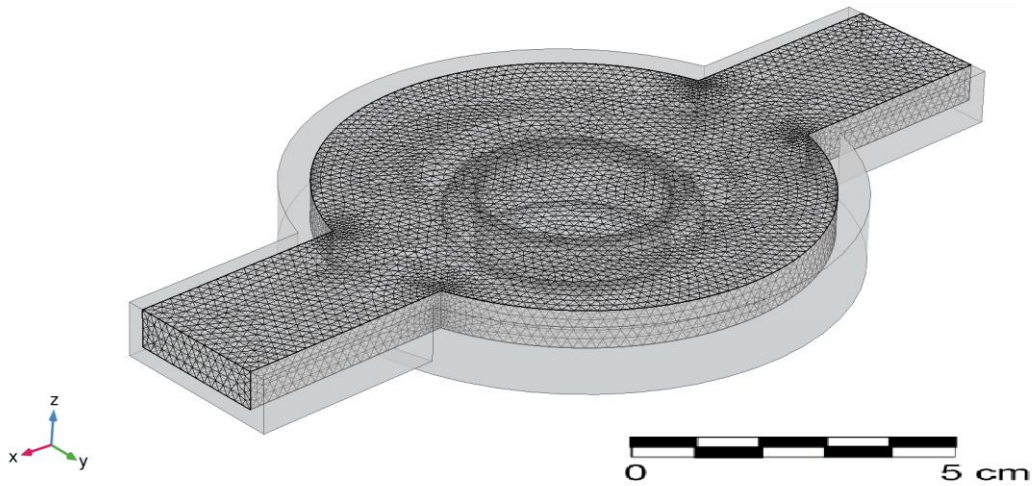


Figure 15 - Model 1 cell grid mesh.

The grid mesh was set taking into account particular regions near discontinuity in the geometry with finer mesh elements, than in the rest of the grid. This leads to reduce computational weight but, without neglecting hot points in the computation.

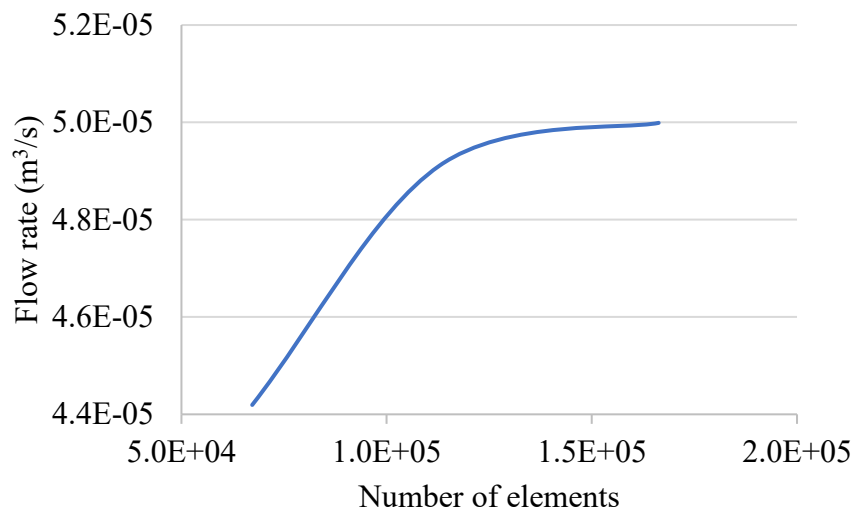


Figure 16 - Flow rate value according to the degrees of freedom of the grid of the model.

The flow rate value tends to converge to the analytical value, and already near  $1.5 \cdot 10^5$  grid elements. From the point of view of relative error, the results of the simulation reach relative error in the range of almost  $1E-4$ , that was taken as enough precise, see Figure 17.

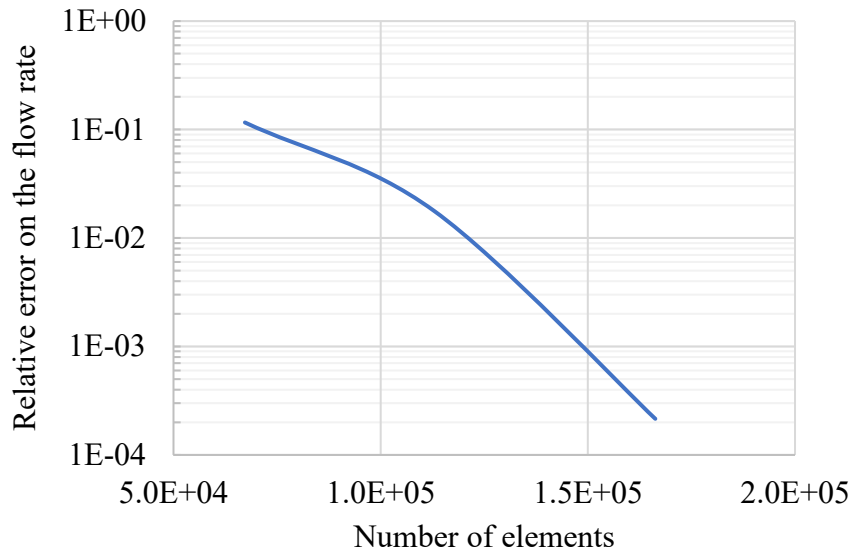


Figure 17 – Relative error of the grid independence analysis.

Considering the grid independence analysis results, the further simulations were performed considering as first try value of further sensitivity analysis, but a proper sensitivity check has been made for every geometry, since that changes with the development of the project.

After the first model, in order to improve the flow distribution and reduce inert areas, it was designed the 2 model electrolyzer, see Figure 18.

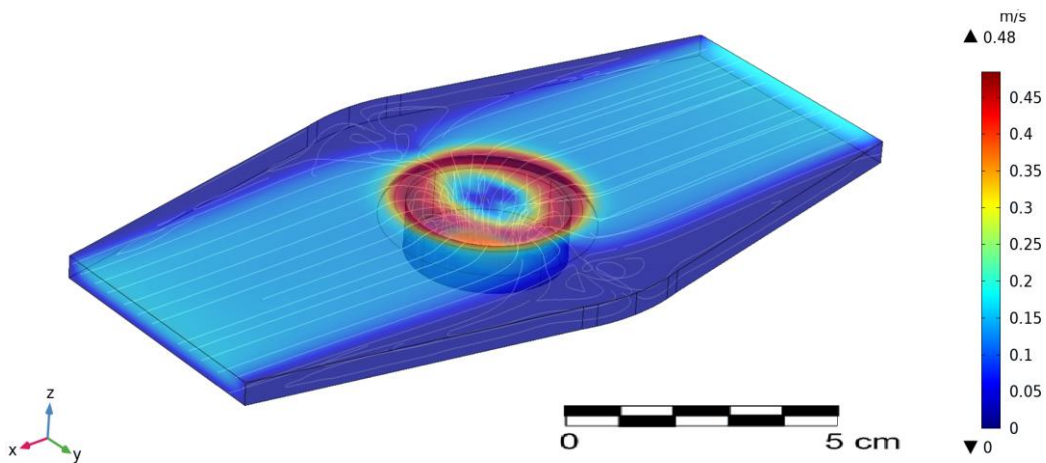


Figure 18 -Fluid dynamic simulation results for model 2.

Further attempts later, finally the last cell model was designed, here reported as model 3. Considering the next prototyping phase, the diameter of the electrodes is reduced from 3 cm, of the previous models, to 1 cm.

The average velocity at the electrode face, that is the only information that I had from previous work, reached near 0.075 m/s, as recommended in [7] to avoid gas meniscus and the bad electrolyte distribution along the electrode mesh.

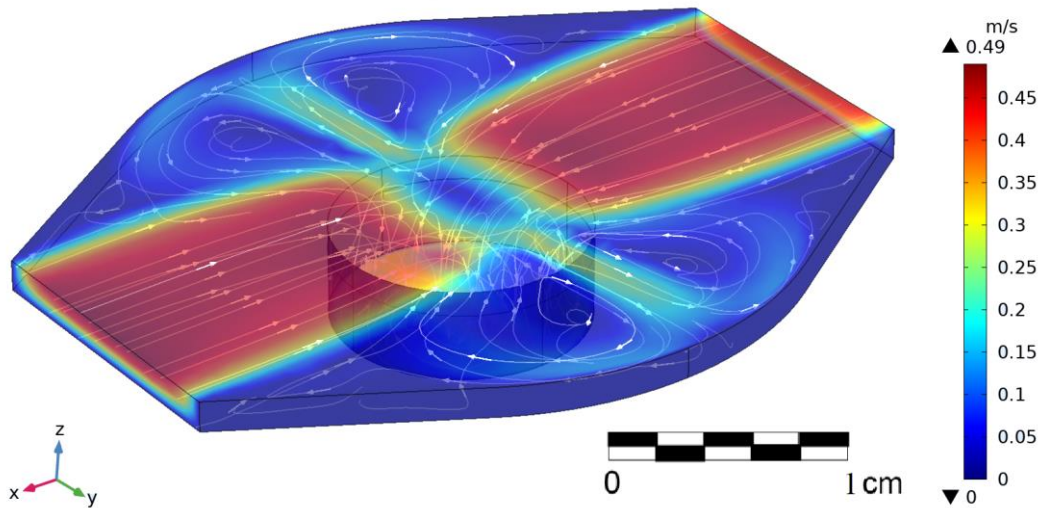


Figure 19 - Model 3 fluid dynamic simulation results.

This fluid dynamic analysis had only the aim to have a qualitative look on the internal behavior of the electrolyzer cell, because a detailed and rigorous fluid flow optimization would have required a specific work, and that will be one of the recommendations for future work on this technology.

## 4.2 Electrolyzer prototype designing

From the fluid dynamic study, a first prototype design was attempted, this prototype had still the old electrode diameter of 3 cm. The cell body is composed by two identical parts, that are kept in position by 4 screws. There is a transition from the rectangular central chamber to the two circular inlet channels, to make possible to join the pipes of the hydraulic circuit of the electrolyte, see Figure 20. This first attempt is till raw, simple design and without gaskets.

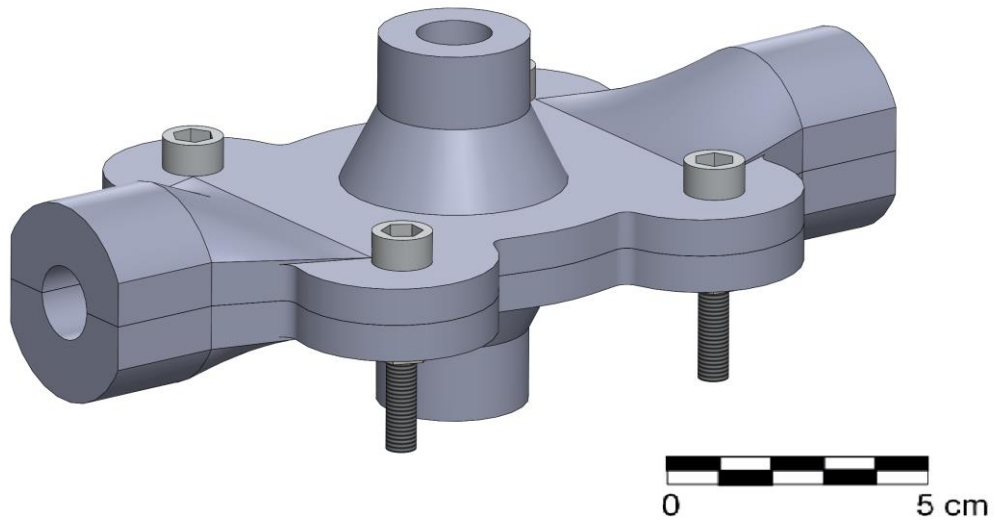


Figure 20 - Prototype 1.

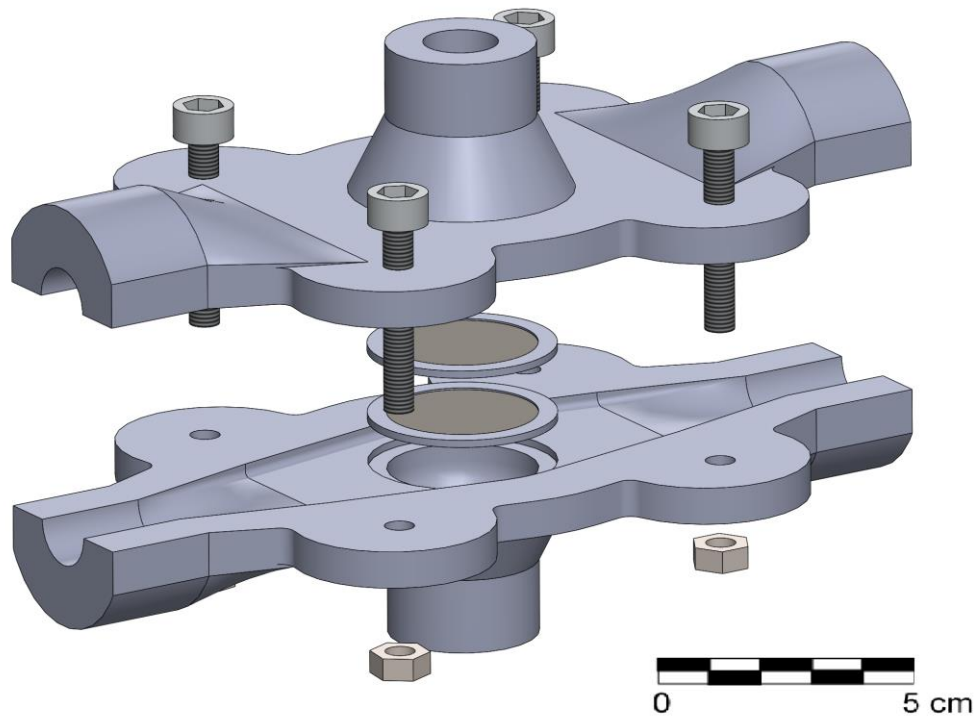


Figure 21 - Prototype 1 exploded view.

In the second prototype from the structure of 2 identical half-cell body part, it has come to a cup structure, as is possible to see in Figure 22 and Figure 23. This configuration has the advantage that the coupling surface is much shorter, and it can be covered with a simple circular gasket. In this prototype I started also to design an electrode support, here constituted by two rings of support, one for each electrode, and a series of little lines of materials, to keep the electrode separated at the

designed distance, the imposed electrode's gap. The cup has also supportive ribs to enforce the structure and distribute better the pressure of the screws.

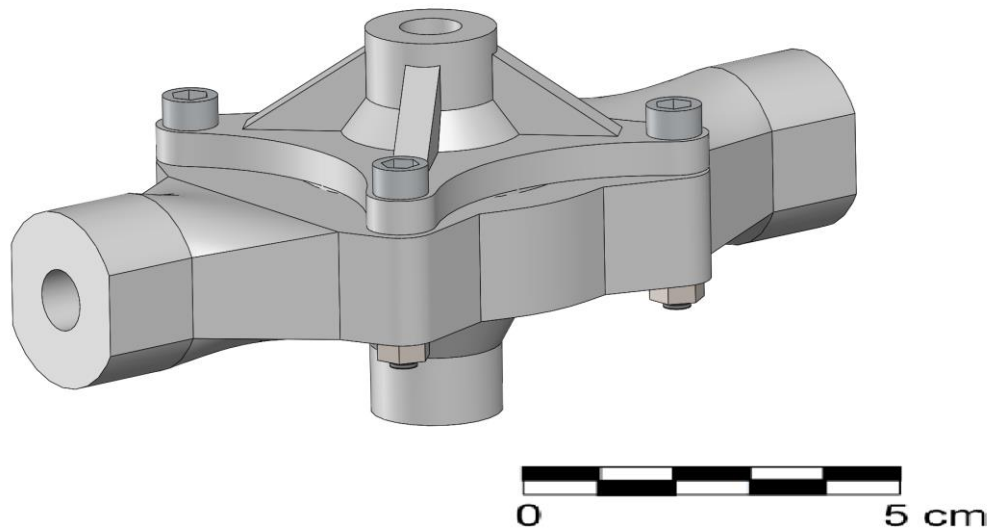


Figure 22 - Prototype 2.

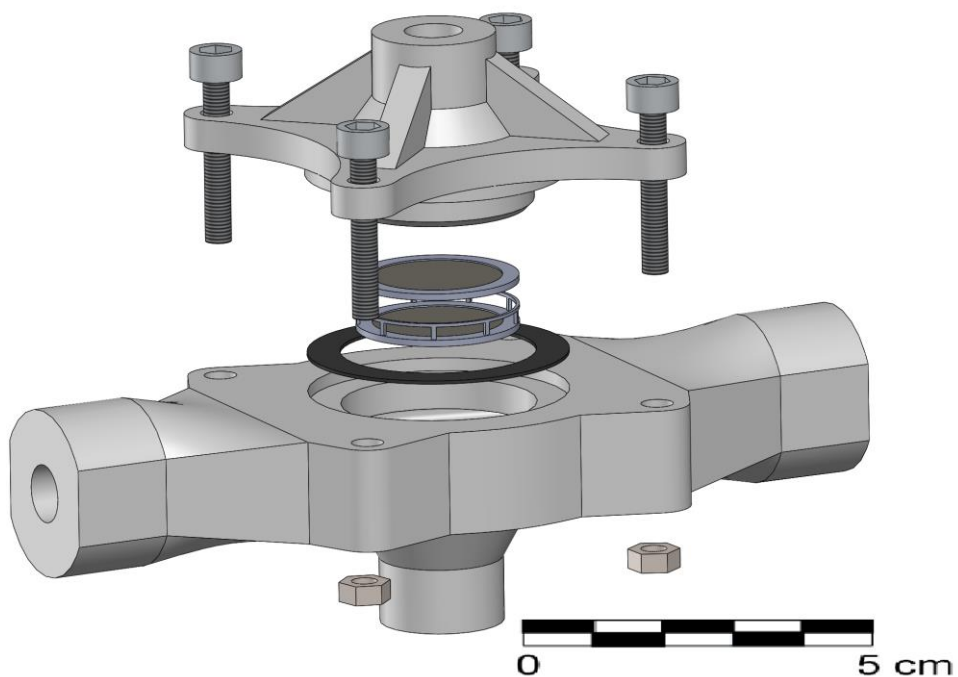


Figure 23 - Prototype 2 exploded view.

In the next stage of design, the entire electrolyzer was reduced in dimension, in order to save material. From this stage on, all the prototype were designed with the chosen electrode diameter of 1 cm. The electrode support has changed structure, it is more massive and compact. This prototype was the first to be 3D-printed.

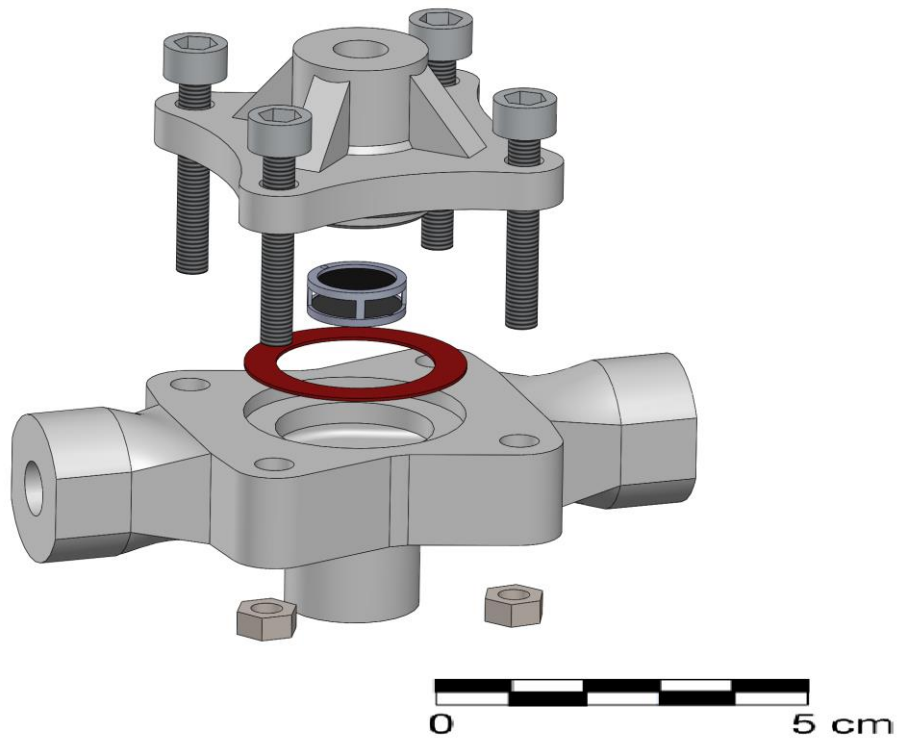


Figure 24 - Prototype 3 exploded view.

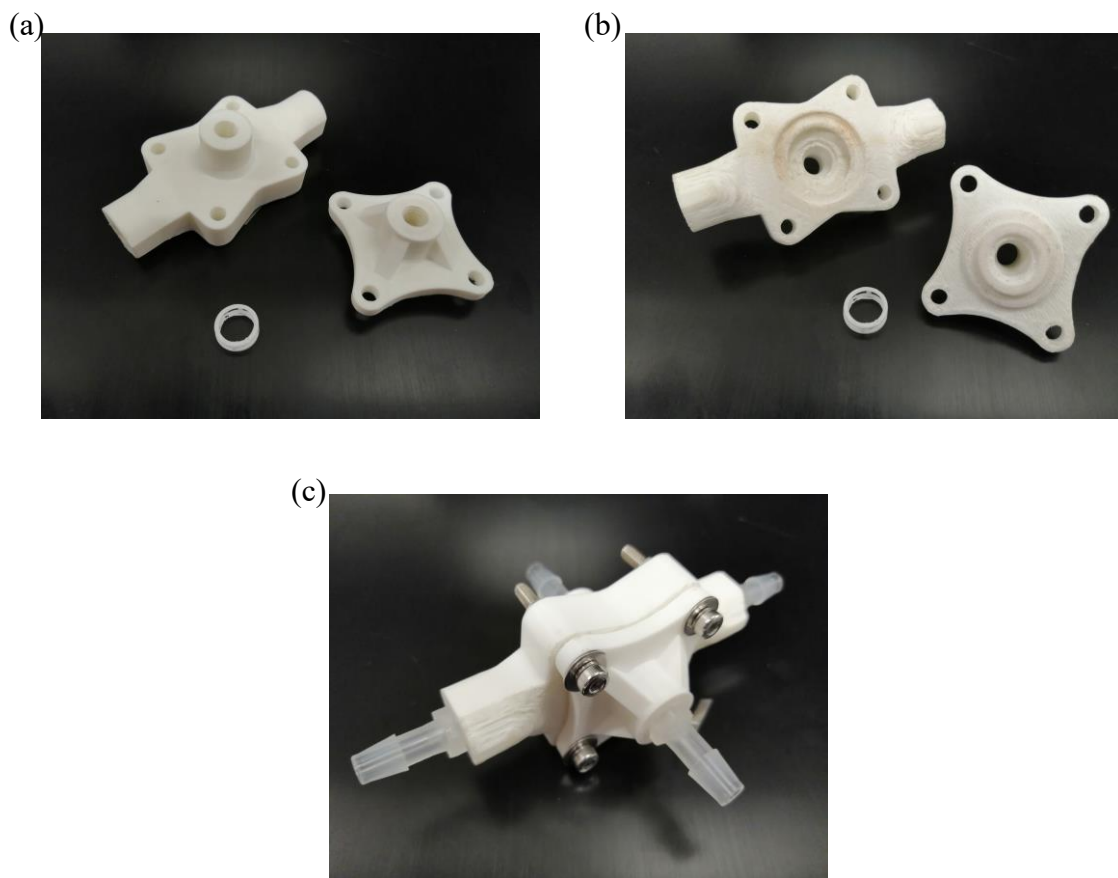


Figure 25 – 3D printed prototype; (a) view of the external side; (b) internal side; (c) assembled.

This prototype was printed in Acrylonitrile butadiene styrene (ABS), material resistant the KOH, with a FDM 3D printer. The inlet and outlet channels were mechanically threaded, to make them couplable with the piping junctions, as is possible to see in Figure 25 (c). Unfortunately, this first printing was not of high quality in the internal faces, due to the production process and the resolution of the printer. This electrolyzer was tested to prove its watertight, but the experiment gave negative results. That bad result led to prototype 4, Figure 26.

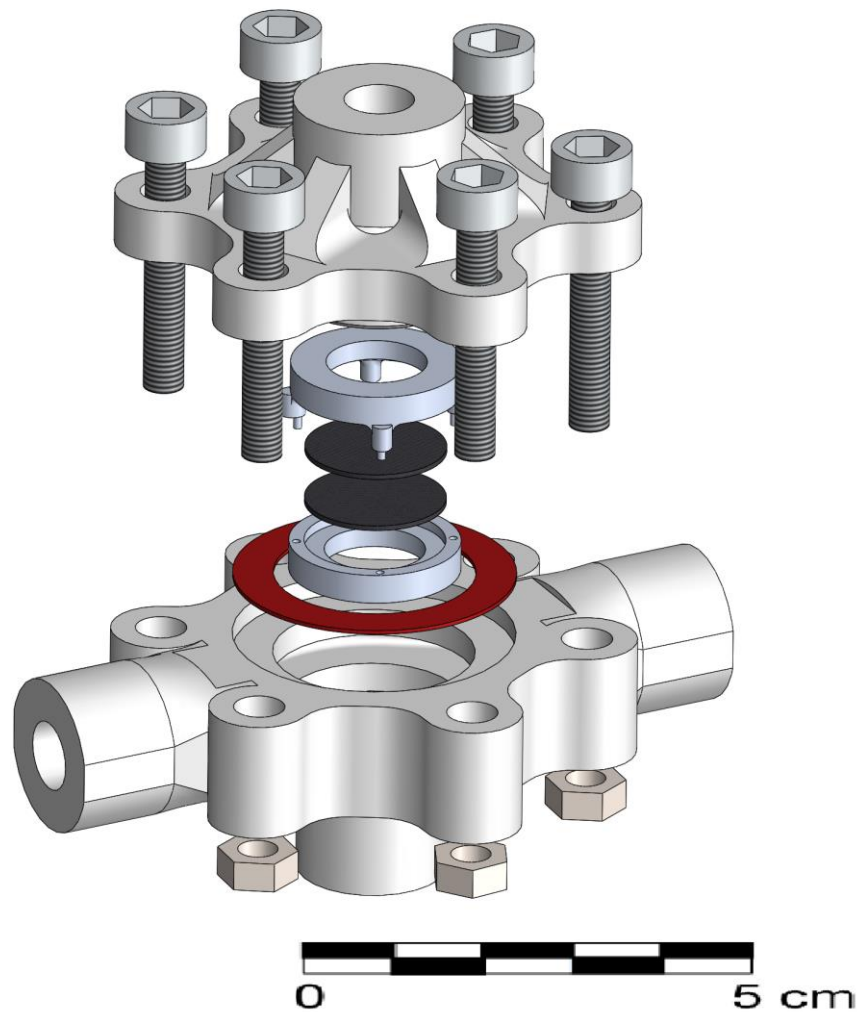


Figure 26 - Prototype 4 exploded view.

This prototype has six coupling screws in hexagonal distribution around the central chamber. The prototype was printed with a different material than the previous one, resin (Connex350). The texture and the quality were better (see Figure 27) and the electrolyzer was proved to have no leakages. Also, the electrode support structure has changed, it is made of two assemblable parts, with space for the electrodes, in order to glue them.

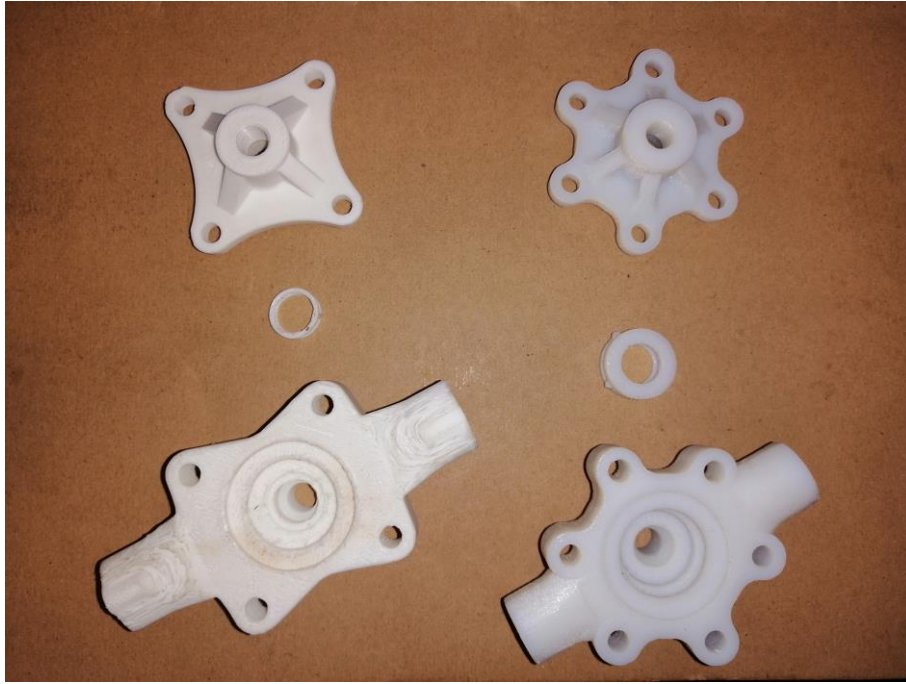


Figure 27 – Comparison of prototype 3 (left) and 4 (right).

The last prototype was designed, to improve the electrolyte support and made it able to keep in position the electrodes just mechanically, see Figure 28.



Figure 28 - Prototype 5 electrode support.

The new support has little material parts that block the electrode in a sort of carpentry joint.

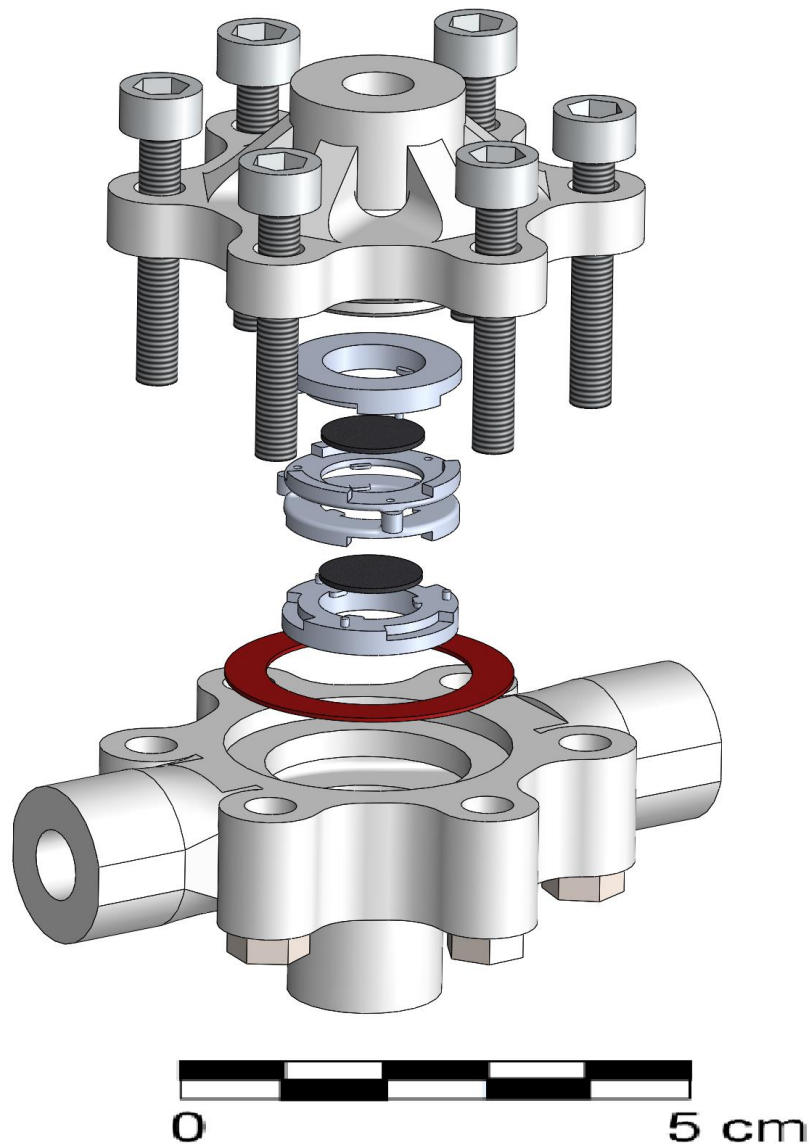


Figure 29 - Prototype 5 exploded view.

The prototype 5 is the design that was used to the electrolyzer test.

### 4.3 Gas separator design

The gas separator was the last part to be designed and realized for the experimental setup. It was 3D-printed as the electrolyzer with the same resin. It was designed to let the gas accumulate in the top of the internal chamber, with a security pipe, that in case of a too large amount of gas inside the chamber, will just let the gas go out, see

Figure 30 and Figure 31. The open top, make possible the refill of the entire circuit, keeping the hydrogen always isolated from the external environment.

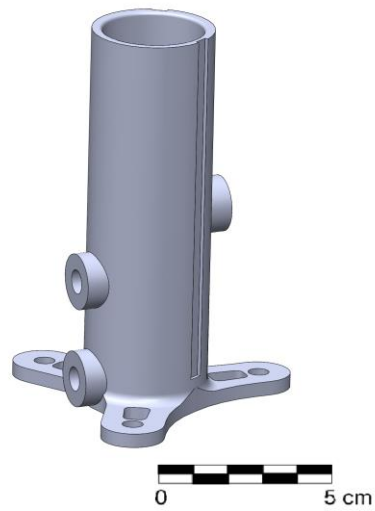


Figure 30 - Gas separator

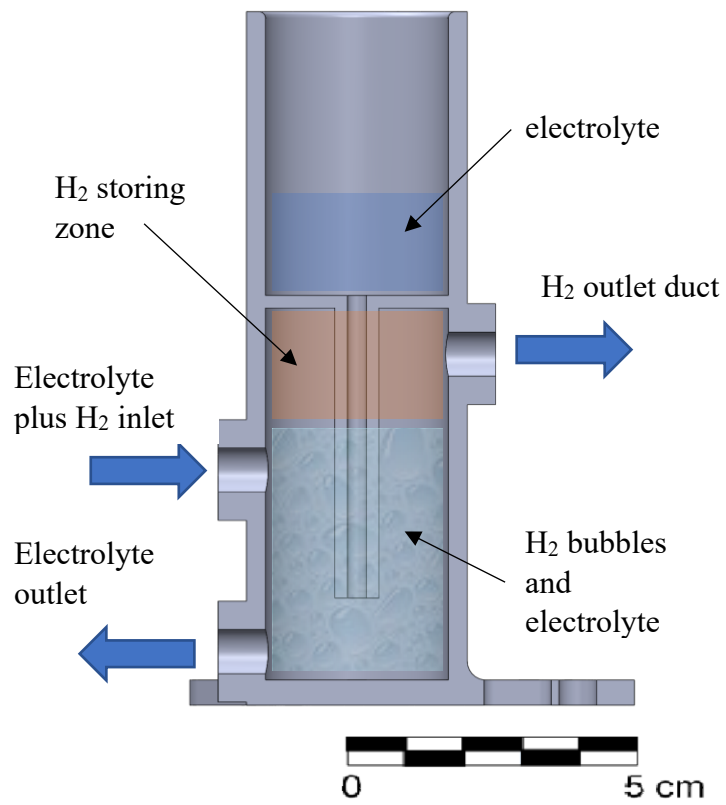


Figure 31 - Gas separator section.

## 4.4 Experimental setup

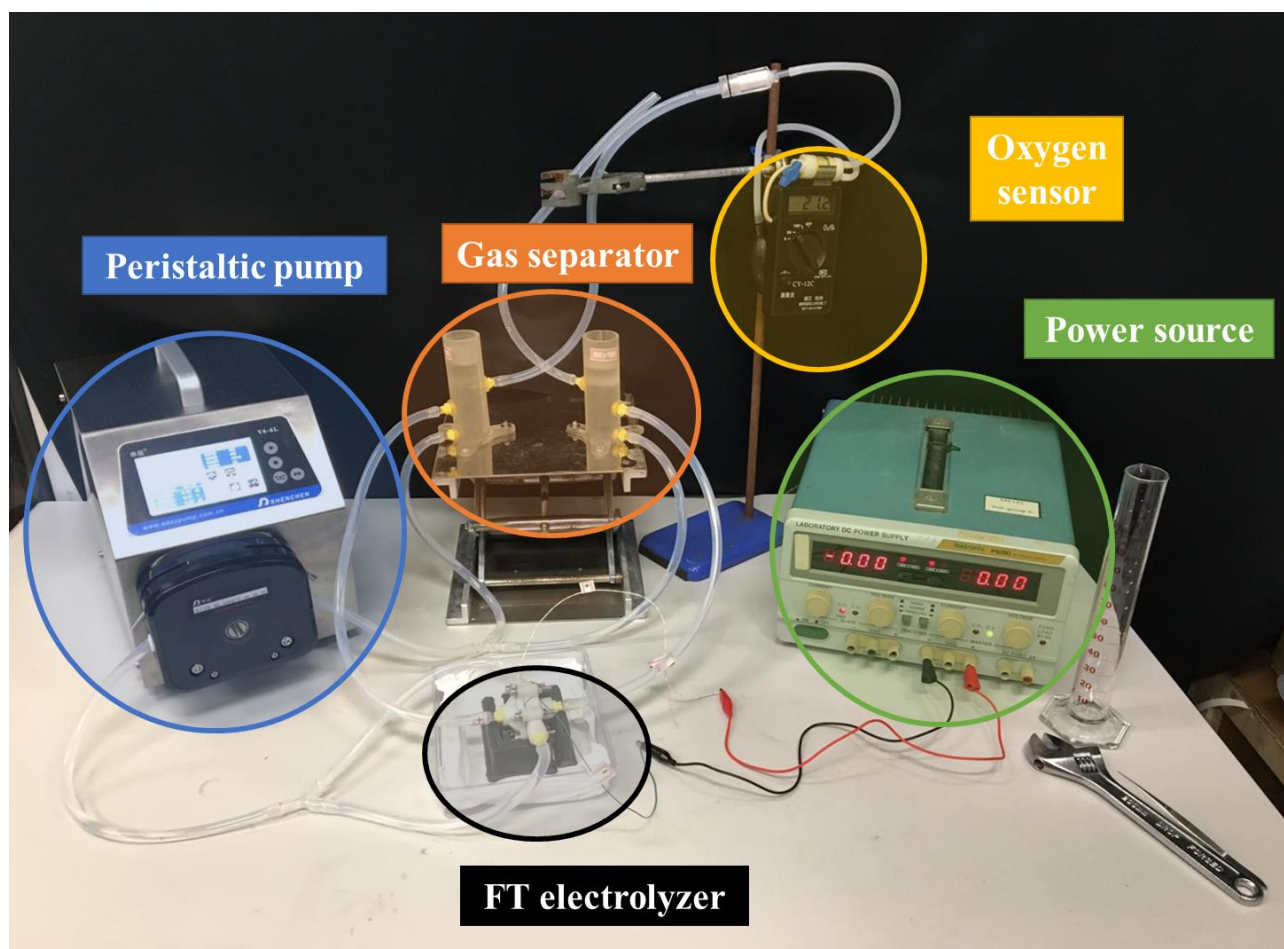


Figure 32 - Experimental setup.

After having printed the electrolyzer and the two gas separator (one for  $O_2$  and one for  $H_2$ ), it was possible to assemble the complete electrolyzer system. A peristaltic pump provides the pumping force for the electrolyte. Pump model No: V6-6L from Baoding Shenchen Precision Pump Co. Ltd. The main characteristic of this type of pump is that the pump does not come in contact with the fluid, that in this case is corrosive. This guarantees us from eventual depletion of the pumping device. The entire tubing is made of silicon tubes of 6 mm of inner diameter, that are flexible to guarantee the correct operation of the peristaltic pump and easy junction and versatility of the circuit. Also, this material is KOH resistant. There is the power source, that is a simple laboratory DC power supply. Then there is the Oxygen sensor, to test the  $O_2$  pollutant concentration in the  $H_2$  stream.

## 4.5 Testing

The first thing to test was if the electrodes, assembled in the electrode support structure were able to perform electrolysis and to resist to the alkaline environment. As electrode was used Ni foam papers, that were welded with tin to with the power wires. For the first trial it was used a 50 mL of water with

2.63 g of NaOH to reach a 30% wt solution as electrolyte (0.206 S/cm). The electrodes and the 3D-printed support operated well and performed electrolysis in the testing baker, see Figure 33. Then it was used KOH, that with higher ionic conductivity (1.088 S/cm) was able to reach higher current density and so, to produce more H<sub>2</sub>. This first test was performed with prototype 4 electrode assembly, with simple glue to fix the electrodes on the support. With NaOH the glue seemed to resist, but in KOH it dissolved. This led to the prototype 5 evolution in electrode assembly design.

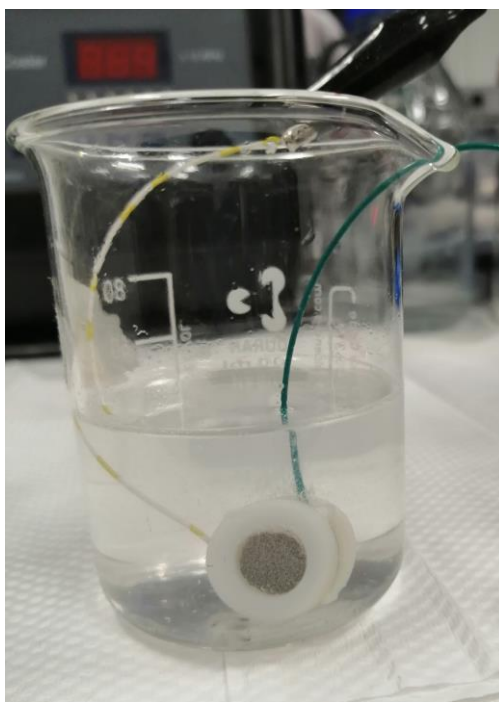


Figure 33 - Electrolysis experiment with alkaline electrolyte and Ni foam electrode.

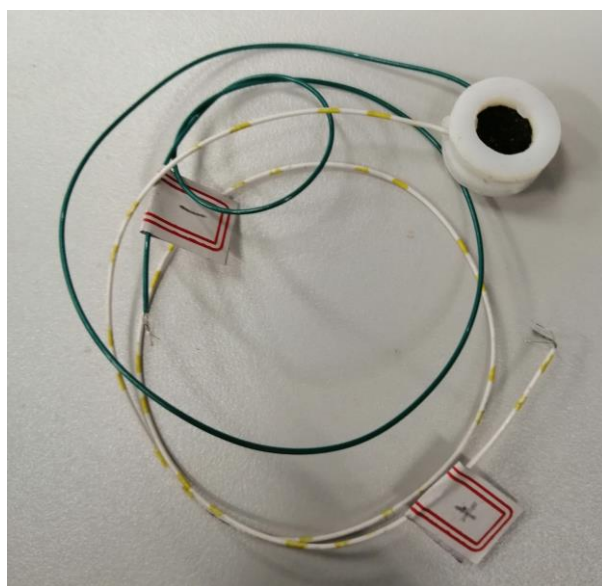


Figure 34 – Electrode's assembly with connected wires.

### 4.5.1 Electrolyzer polarization curve test

At last I performed the electrolyzer testing, with all the experimental facility put in position. Was performed a j-V characterization of the electrolyzer at different flow rate.

A water solution 0.1 M of KOH was used as electrolyte, with  $\sigma = 0.0241$  S/cm [53]. The decision to reduce the amount of KOH was made to reduce the salt used during the experiment (the model data were changed accordingly). To fill and operate the entire circuit was necessary 200 mL of electrolyte, to obtain this volume of solution were used 200 mL of water and 1.12 g of KOH. The flow rate range tested went from 300 mL/min to 1200 mL/min with interval of 100 mL/min. the range limit was chosen according to the pump operational limits. Two Ni foam electrodes welded with Cu lab testing wires were connected to the power source. The single electrode-wire part had an ohmic resistance of  $0.35 \Omega$ . Three series of data were recorded in every flow rate prove, so that it was possible to compute mean value and standard deviation.

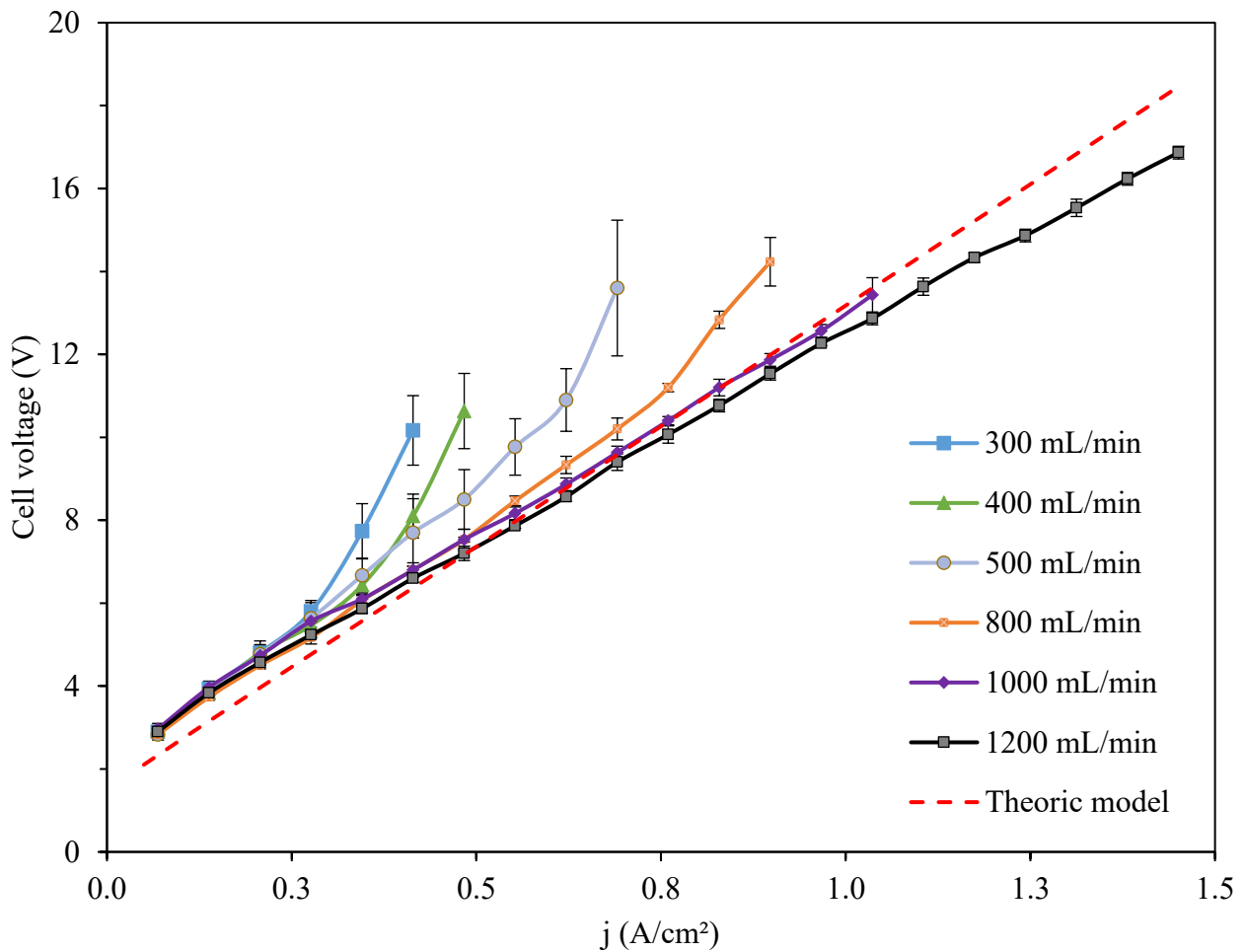


Figure 35 - Electrolyzer polarization curves from experiments and the model results in dashed red line.

During the tests, it was found out, as expected, that at every flow rate, there was a point in which the voltage starts to diverge. This is due to the accumulation of gas in the volume of the reaction, in the electrode central chamber. Higher is the flow rate, higher is the gas that can be dragged from the electrodes. So, the point from which the voltage starts to diverge moves towards higher current density and so to higher H<sub>2</sub> production volume. The model developed in this work does not consider the gas accumulation inside the cell, as is possible to see in Figure 35. In the figure is reported only one line for the model results, this was made because in the considered range of current densities the model results vary very little and can be represented with only one line, to make the plot more clear. When the voltage starts to diverge also the standard deviation grows, since in the moment of taking the measure, the tester showed a wide range of value changing rapidly. So, due to the high random behavior of the bubbles inside the cell in those conditions the cell voltage was not constant.

Comparing the experimental data with the model results it was possible to see a good match in the linear part of the j-V curves, the part in which are dominant the ohmic losses. The little gap in the first points at 0.05 A/cm<sup>2</sup> was maybe due to the fact that the activation overvoltages depended on  $j_0$  values, that was not computed specifically for this experiment, but it was taken from the literature for generic Ni electrodes in KOH electrolyte [54] [55]. The mismatch for 1200 mL/min may be linked to different factors, the directly observed one is the deposition of a layer of NiO on the negative electrode due to galvanic effect, that could have improved the performance of the cell, as NiO is a catalyst in the water electrolysis reaction [12], see Figure 36. Where is possible to see that one electrode had become black, due to the NiO deposition.

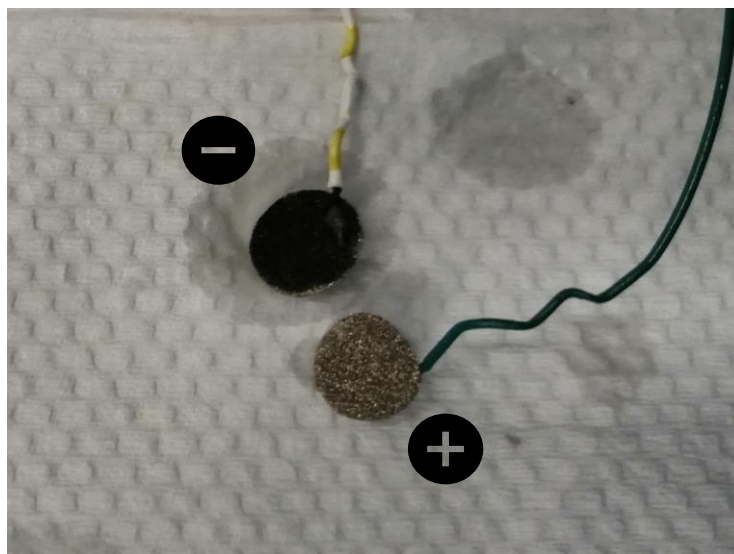


Figure 36 - Electrodes after the j-V probes.

After the first j-V prove on the electrolyzer, another one was made adding specific catalyst on the electrodes, in order to see improved performances. On positive electrode for OER was used MoS<sub>2</sub>/SCO, a compound of MoS<sub>2</sub> with perovskite SrCoO<sub>2.5</sub>, that was gently provided by Ing. Curcio [56]. On negative electrode for HER was used 20% Pt/C the catalyst was applied using drop deposition method. The reached voltages were little smaller than in the case without catalyst, see Figure 37. Unfortunately, after just one series of test the performance were seen deteriorated to similar level of electrode without catalyst.

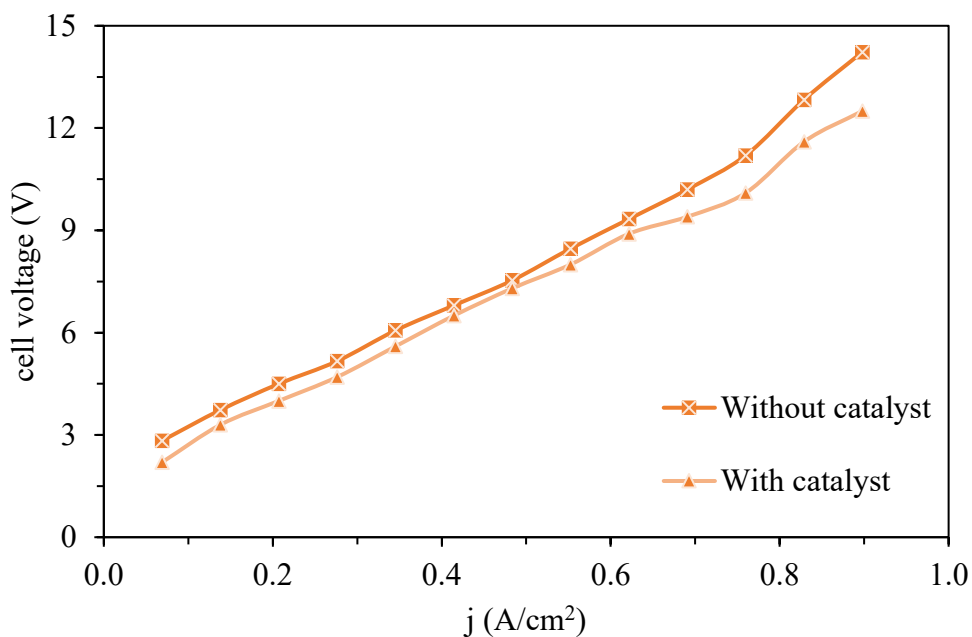


Figure 37 - Comparison of j-V curves between Ni electrodes and Ni electrodes plus catalyst at 800 mL/min.

So, after the first series of measures the electrolyzer were disassembled and looking at the electrodes showed the reason for the drop in the performance. The high flow rates, higher than 800 mL/min have removed the catalyst from the electrodes, as is possible to see in Figure 38. The positive electrodes shows clear signs of the catalyst removal (the catalyst was black colored), while negative electrodes seems intact, but is reasonable to think that it looks like this just because during the reaction while the catalyst was removed by the flowing electrolyte, a new layer of NiO formed.

To avoid this issue with the catalyst integrity, it was suggested to try to make the catalyst grow directly on the electrode, but for a lack of time, this process was not used. That will surely be part of future research on this field. All the data from the experimental experiences are reported in **Appendix C**.

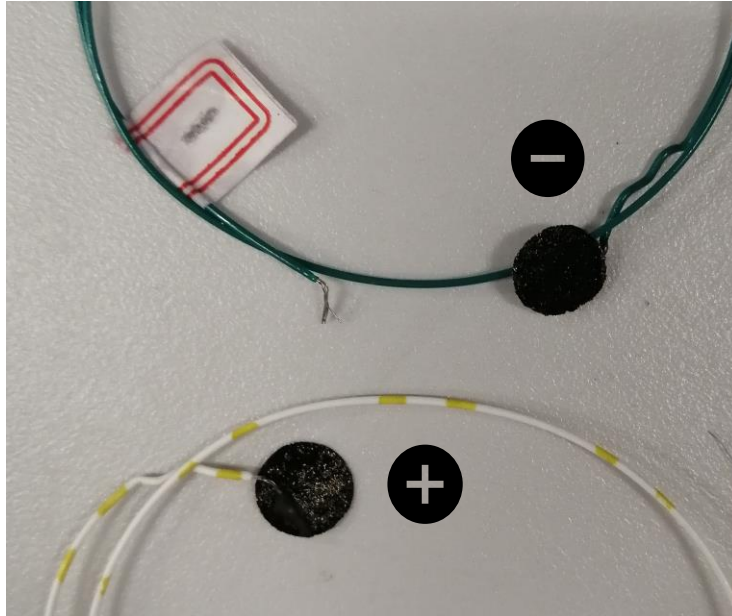


Figure 38 - Electrodes covered with catalyst after the prove.

#### 4.5.2 H<sub>2</sub> production and purity evaluation

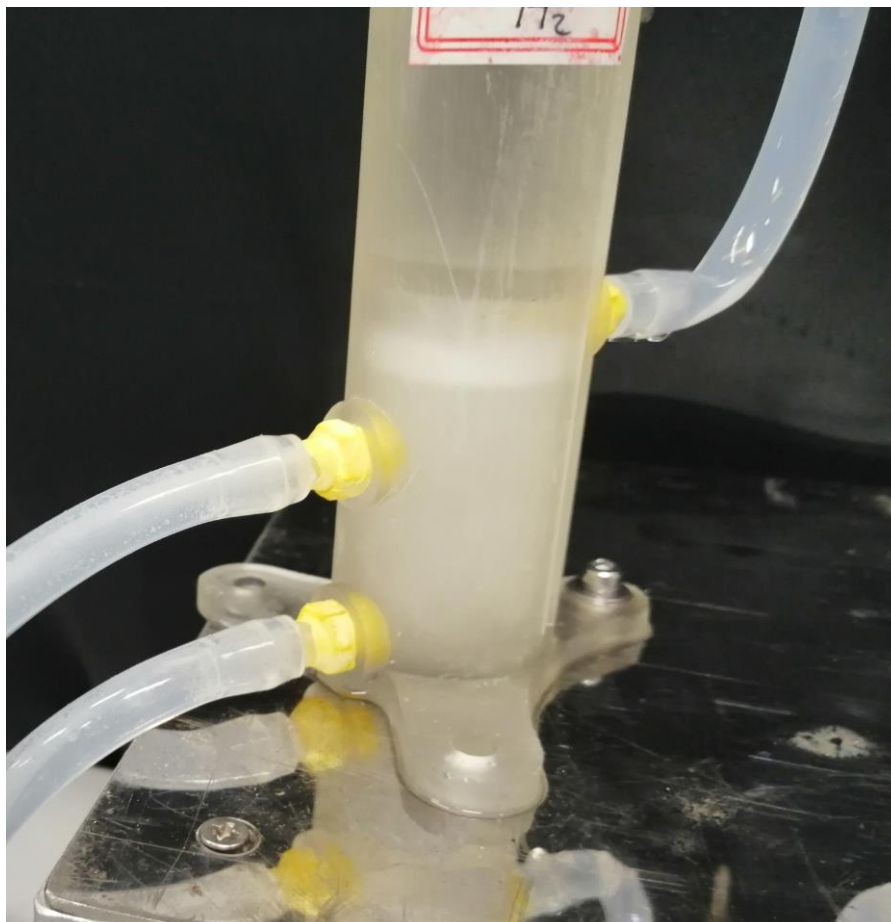


Figure 39 - Detailed view of the H<sub>2</sub> gas separator.

To manage the production and try to analyze the produced, own designed gas separators were used. Looking at Figure 39, it was possible to see the gas accumulating in the upper part of the collection chamber, there was also some electrolyte foam and the presence of many little bubbles made electrolyte volume looks white. Gas sample bag were used to collect the produced gas in attempt to evaluate the H<sub>2</sub> production volume and purity, see Figure 40.

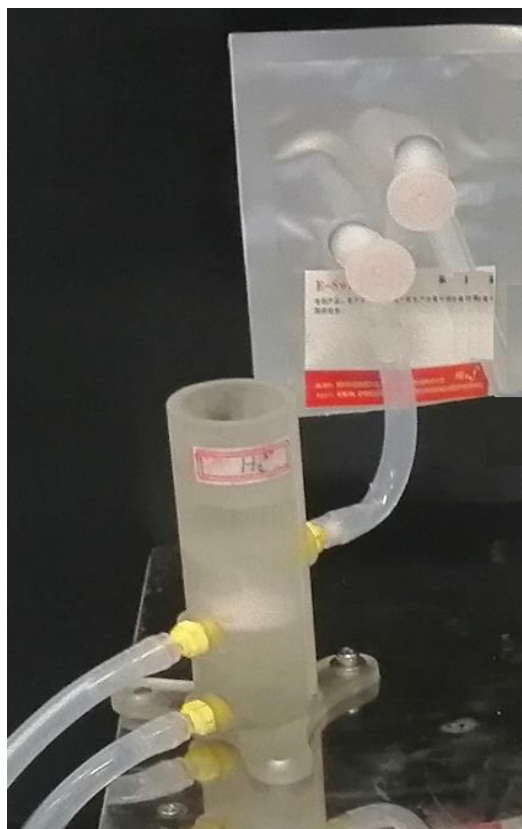


Figure 40 - Sample bag for the harvesting of H<sub>2</sub>

The bag was purged several times with the gas produced to be reasonably sure that the samples collected was effectively the produced gas. Various sampling was made to evaluate the mass of gas produced, checking for some time periods the amount of gas collected in the bag, but no consistent measure was successfully made. This led us to consider other methods to evaluate the production rate in future works.

Then, to try to evaluate the purity of the gas, not having a gas chromatographer suitable to measure the pollutant levels of O<sub>2</sub> in H<sub>2</sub> stream in an exact way, it was used an oxygen sensor, see Figure 41. This sensor was coupled with the gas separator directly on the gas outlet duct. This method did not work, unlucky. After more than an hour of operation no sensible changing on the display of the device was visible, even after many purges of the connection tubes between the device and the gas separator. Maybe leaving the electrolyzer work for 24 hours could have solved the problem, but I was not

allowed to let the device works for so much time in the lab, that was not designed for hydrogen production.



Figure 41 - Oxygen sensor used

## 5 Thermodynamic model results

This chapter presents the results of the thermodynamic and the economic analysis. First, I analyze the purity of the produced gas and the efficiency of the electrolyzer working at different conditions. With this model, I investigated how the design and operational conditions affect the purity of the products and the electrolyzer efficiency. Then I compared the performance of FT and FB electrolyzers.

### 5.1 Output H<sub>2</sub> Purity

The purity of the output H<sub>2</sub> is affected by several factors including temperature, current density and the electrolyzer geometry (considered as function of Re<sup>2</sup>). An increase of the operative temperature and/or current density leads to higher purity, see Figure 42 and Figure 43. In fact, the solubility of the H<sub>2</sub> in the electrolyte decreases as the temperature increases[22, 57]. Moreover, the results in Figure 43 suggest that at low current densities, most of the H<sub>2</sub> produced is less than the one stored dissolved in the electrolyte (especially for  $j < 0.35$  A/cm<sup>2</sup>) reducing the purity of the products. This phenomenon is even enhanced at high Re condition, see Figure 44, with more circulating electrolyte and so, a bigger capacity of dissolving the gases.

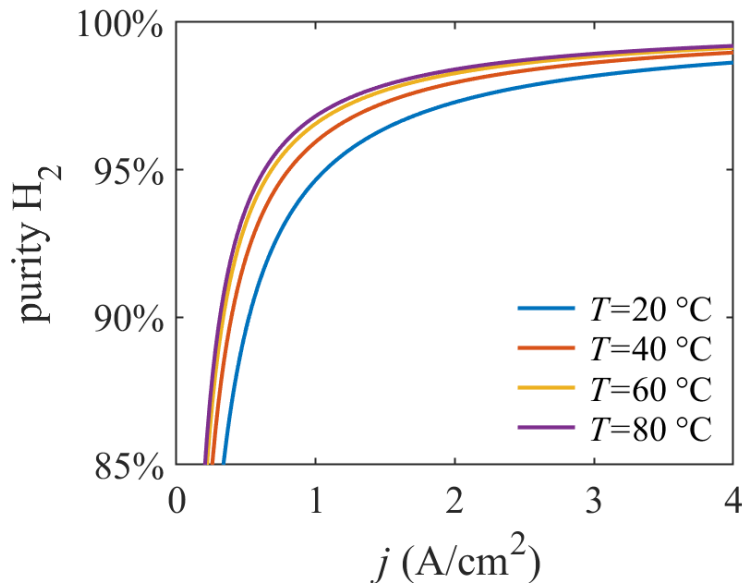


Figure 42 - H<sub>2</sub> Purity at various temperatures for Re=1500

---

<sup>2</sup> Re is Reynolds' number, an adimensional parameter used to characterize flow condition defined  $Re = \frac{v \rho D}{\mu}$  where  $v, \rho, \mu$  and  $D$  are fluid velocity, fluid density, characteristic length and fluid viscosity, respectively.

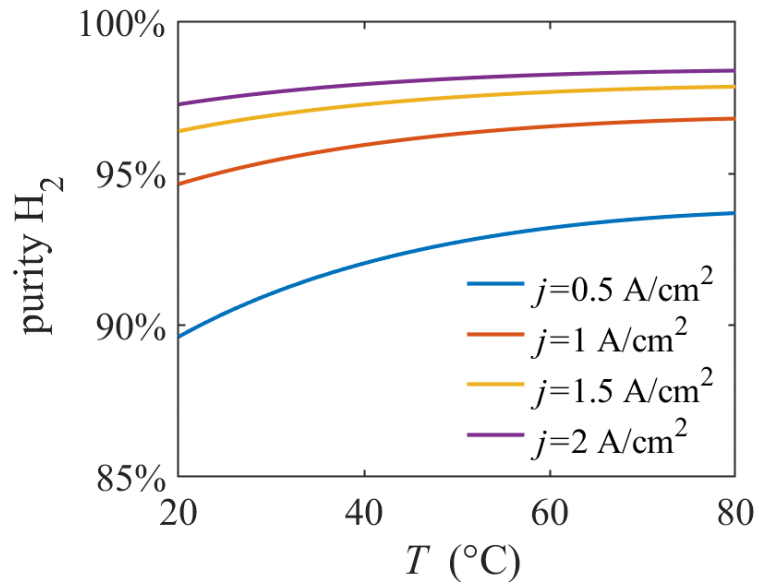


Figure 43 - H<sub>2</sub> Purity at various current density at different flow rates for T=60°C

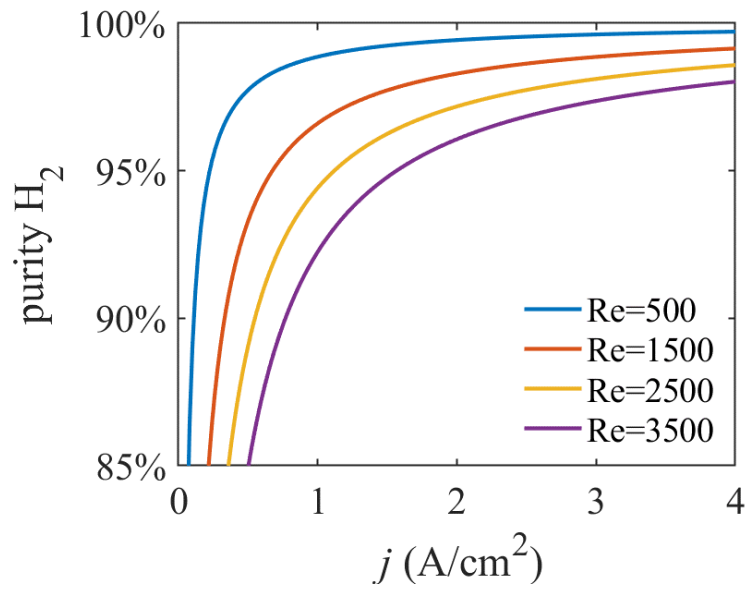


Figure 44 - H<sub>2</sub> Purity as a function of the current density at various temperatures for Re=1500

## 5.2 Electrolyzer Efficiency

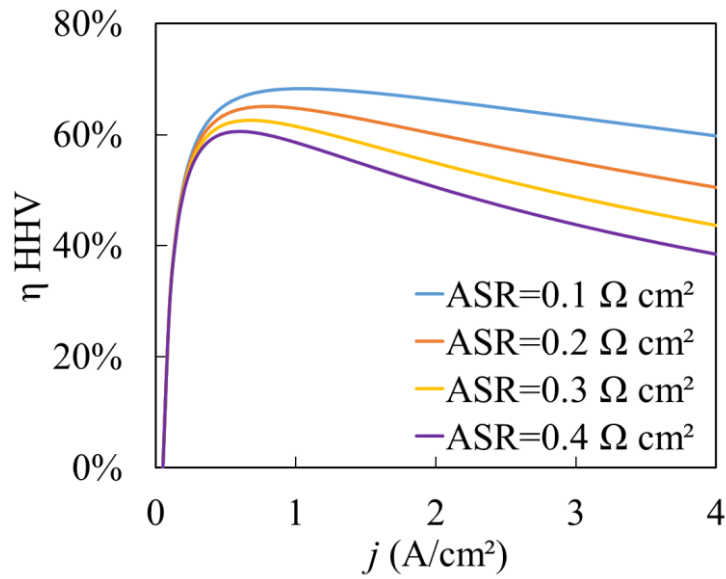


Figure 45 - HHV efficiency at different  $ASR_{\Omega}$  conditions, maintaining the same flow condition ( $Re=1500$ ), temperature  $T=60^{\circ}C$  and pressure 1 atm.

The efficiency of the electrolyzer improves as the  $ASR_{\Omega}$  decreases, see Figure 45. The two main parameters affecting the  $ASR_{\Omega}$  are the electrodes gap and the electrolyte conductivity. Unfortunately, to guarantee a good flow distribution along the electrodes and to reduce gas mixing, there is a lower limit for the electrodes gap. According to the literature, an electrode gap of at least 2.5 mm is optimal in experiments [7, 12, 13]. Likewise, to balance the corrosion effect of the electrolyte and the ionic conductivity for alkaline electrolyzers, 30 wt% (6.7 M) of KOH is used like a standard [4, 7, 8, 12, 13]. Under these conditions, the corresponding electrical conductivity is  $\sigma = 1.09$  S/cm [53].

FT and FB membraneless electrolyzer designs are compared in Figure 46. The evaluation was performed considering a constant electrode gap of 2.5 mm and electrolyte concentration of 30% wt of KOH. In this case, the efficiency is affected only by the gas volume fraction, which is linked to the flow rate, in terms of the ratio between the electrolyte and gas volumetric flow rates. Increasing the current density implies larger  $H_2$  production; at low flow rate the products cannot be readily evacuated, and the volume fraction of gas is high in the reaction zone between the electrodes. So, the  $ASR_{\Omega}$  increases as the flow rate decreases, causing the reduction in efficiency. It should be noted that to reach the maximum efficiency at different current densities are required different flow rate, there is not a unique optimum configuration, depends on the production rate that it is wanted for the plant.

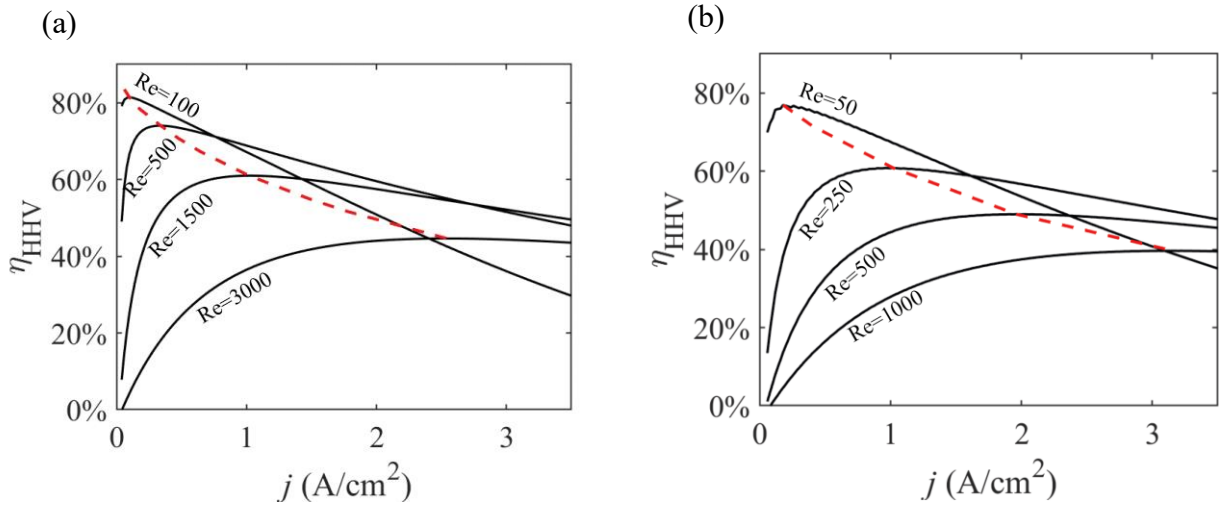


Figure 46 - Theoretical efficiency of the (a) FT and (b) FB design; the dashed red line indicates the maximum for each Re.

The panels (a) and (b) of Figure 46 show the  $\eta_{HHV}$  of the electrolyzer as a function of the Re for the FT and FB designs, respectively. The efficiency of the FB design is more sensitive to Re. For example, the HHV efficiency drops from 78% to 38% if Re increases from 50 to 1000. In contrast, the HHV efficiency of the FT design only drops from 82% to 72%, in the range from 100 to 1000 Re.

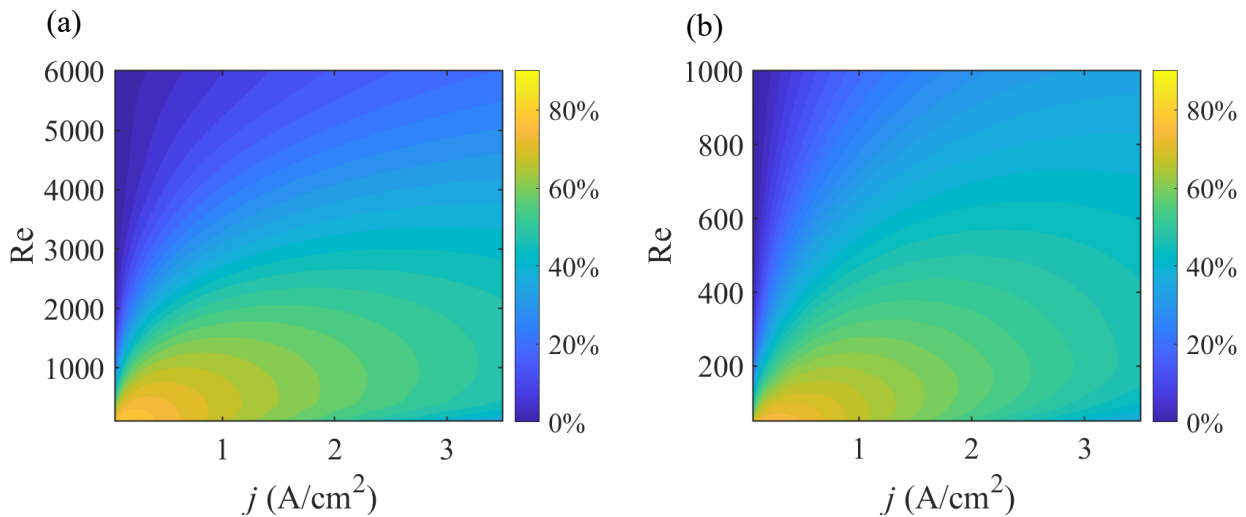


Figure 47 - Contour plots of the efficiency for the (c) FT and (d) FB.

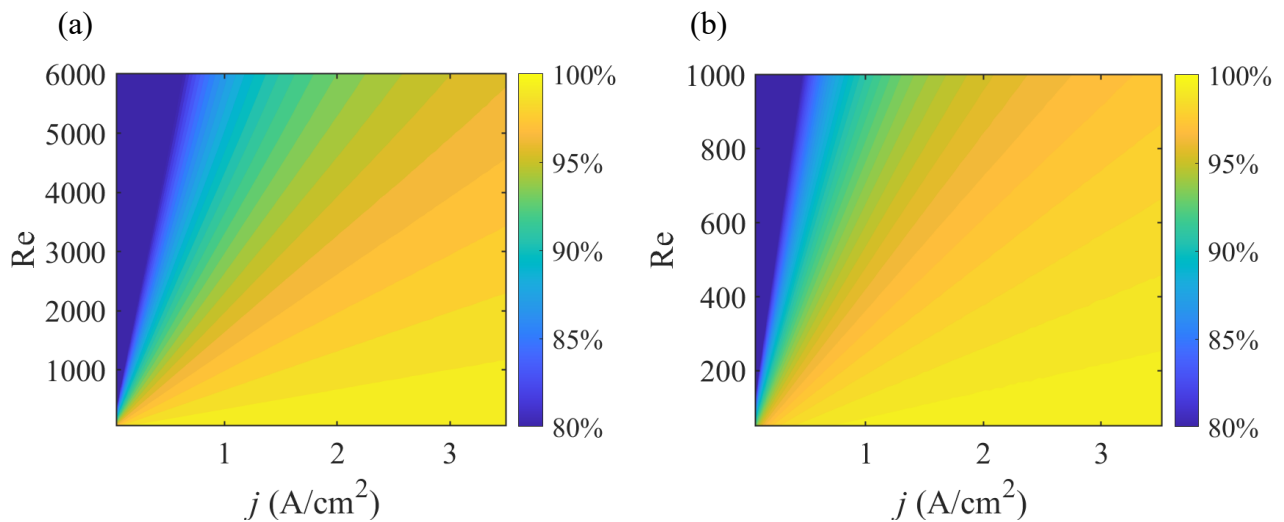


Figure 48 - Outlet H<sub>2</sub> purity maps for (e) FT and (f) FB.

As shown in Figure 47 (a), the FT design has an efficiency above 60%, for  $Re \leq 2500$ . In contrast, the efficiency of the FB electrolyzer drops below 60% if  $Re \geq 400$ , see Figure 47 (b). While the H<sub>2</sub> purity plots in Figure 48 (a) for FT and Figure 48 (b) for FB, appear to be similar, the operational conditions considered is totally different: high purity in the FB design is allowed in a narrower interval of Re number compared to FT.

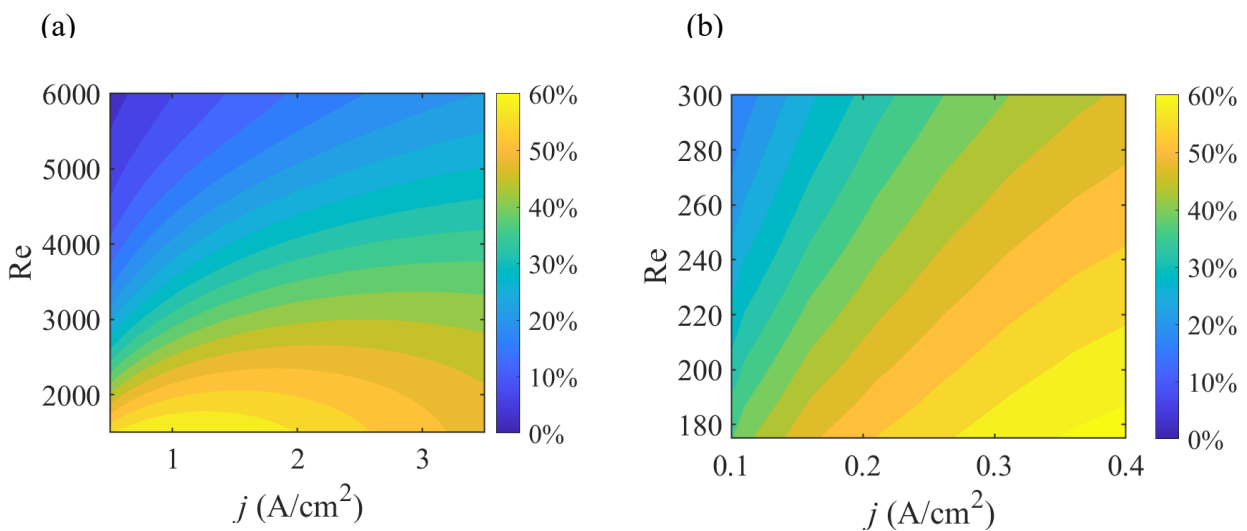


Figure 49 - Contour plots of the efficiency in operational range for the (c) FT and (d) FB.

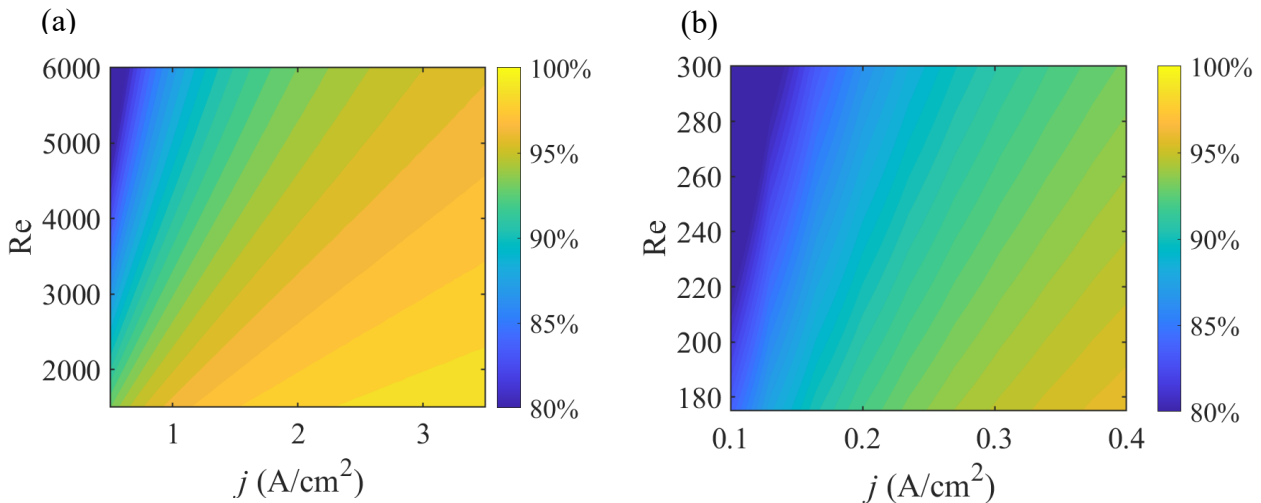


Figure 50 - Outlet H<sub>2</sub> purity maps in operational range for (e) FT and (f) FB.

The efficiency and purity plots are presented in the operational range of the respective device,  $1500 < Re < 6000$  and  $0.5 < j < 3.5 \text{ A/cm}^2$  for the FT design [7, 12, 13] in Figure 49;  $180 < Re < 300$  and  $0.1 < j < 0.4 \text{ A/cm}^2$  for the FB one [6] in Figure 50. The FT design has been chosen for the experimental study and for the techno-economic analysis, after having considered the higher efficiency, higher purity and a wider operating range compared to the FB.

### 5.2.1 H<sub>2</sub> market specification

To sell H<sub>2</sub> in the market, a purity above 99% is typically required, so after the electrolyzer (that produce ~95% pure H<sub>2</sub>) a purification stage is needed. Various technologies are available for downstream purification, such as pressure swing adsorption (PSA), palladium membranes, adsorption, and catalytic recombination [58].

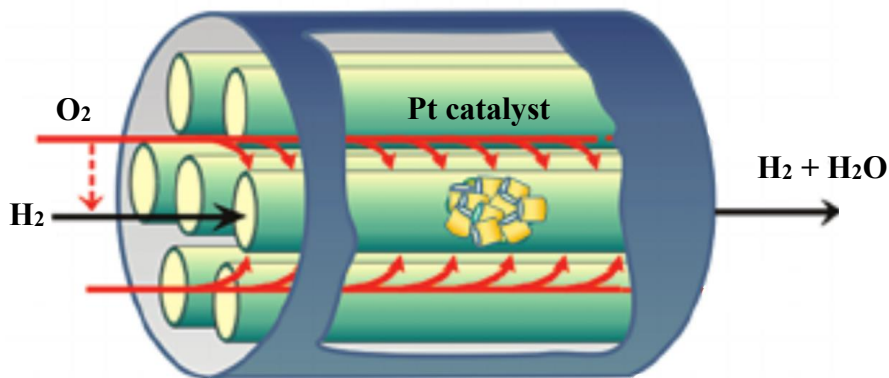


Figure 51 - Schematics of a passive recombiner for hydrogen purification.

Passive catalytic recombination is economically favorable because it does not consume energy. In this process, Pt is used as a catalyst to recombine  $O_2$  and  $H_2$  into a water molecule in a spontaneous exothermic reaction, see Figure 51. It can achieve the purity requirement by reducing the  $O_2$  pollutants to ppm levels [39]. It is also compact and easy to maintain because of its simple design [39].

## 6 Economic analysis results

### 6.1 Net present value analysis

NPV and LCH results are shown for the two selected plant sizes (500 and 1000 ton<sub>H<sub>2</sub></sub>/year); today, medium-term and long-term stack market scenarios; the four selected locations, China, USA, HK and EU-27; grid and renewables power source, and two carbon tax levels. Lastly, sensitivity analysis is reported to establish the impact of the main economic parameters on the final economic output.

The NPV depends strongly on the electrolyzer plant location, as according to the country, there are different taxation levels, electricity prices, etc. (see Figure 52 (a) in the “today” scenario). A plant located in HK has a break-even period of approximately 4 years resulting in an end-of-life profit much higher than the initial investment. At the end of life, the plant NPV results are 27.67 Million-USD in HK, 22.64 in EU-27, 11.68 in China, and 6.46 in the USA.

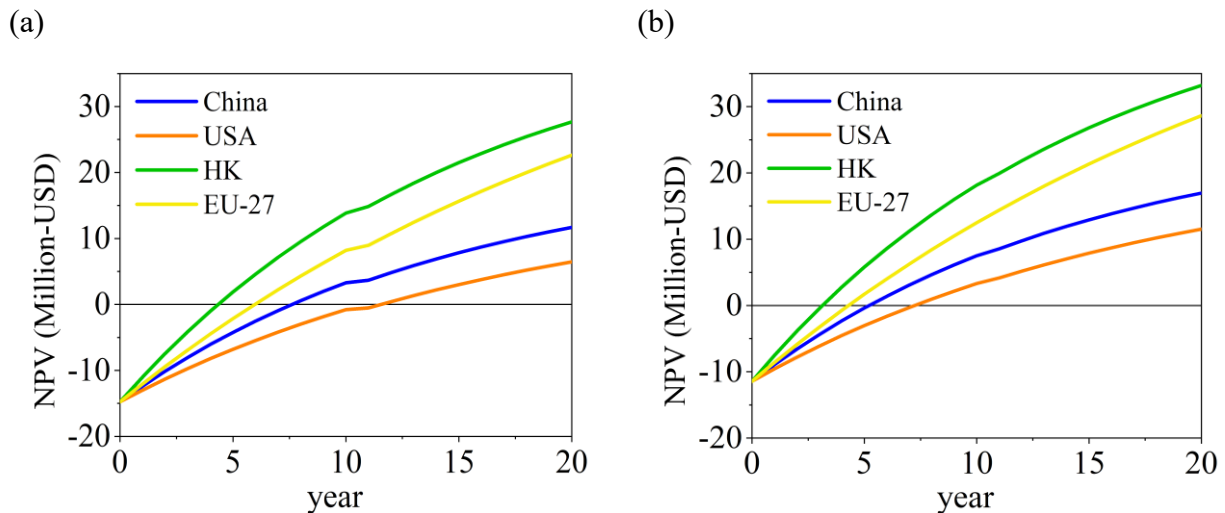


Figure 52 - NPV evolution for renewable connected plant of 1000 t/year size (18.38 MW), in (a) today scenario and (b) long-term scenario.

Figure 52 (b) shows the “long-term” scenario. Compared to the “today” scenario, initial capital, and stack replacement costs after 10 years of operation are much lower. I note that the better economic performance of the HK and EU-27 plants are due to the local higher price of natural gas, see Table 6.

The recovered heat can be sold at a higher price, which guarantees higher earnings compared to other locations.

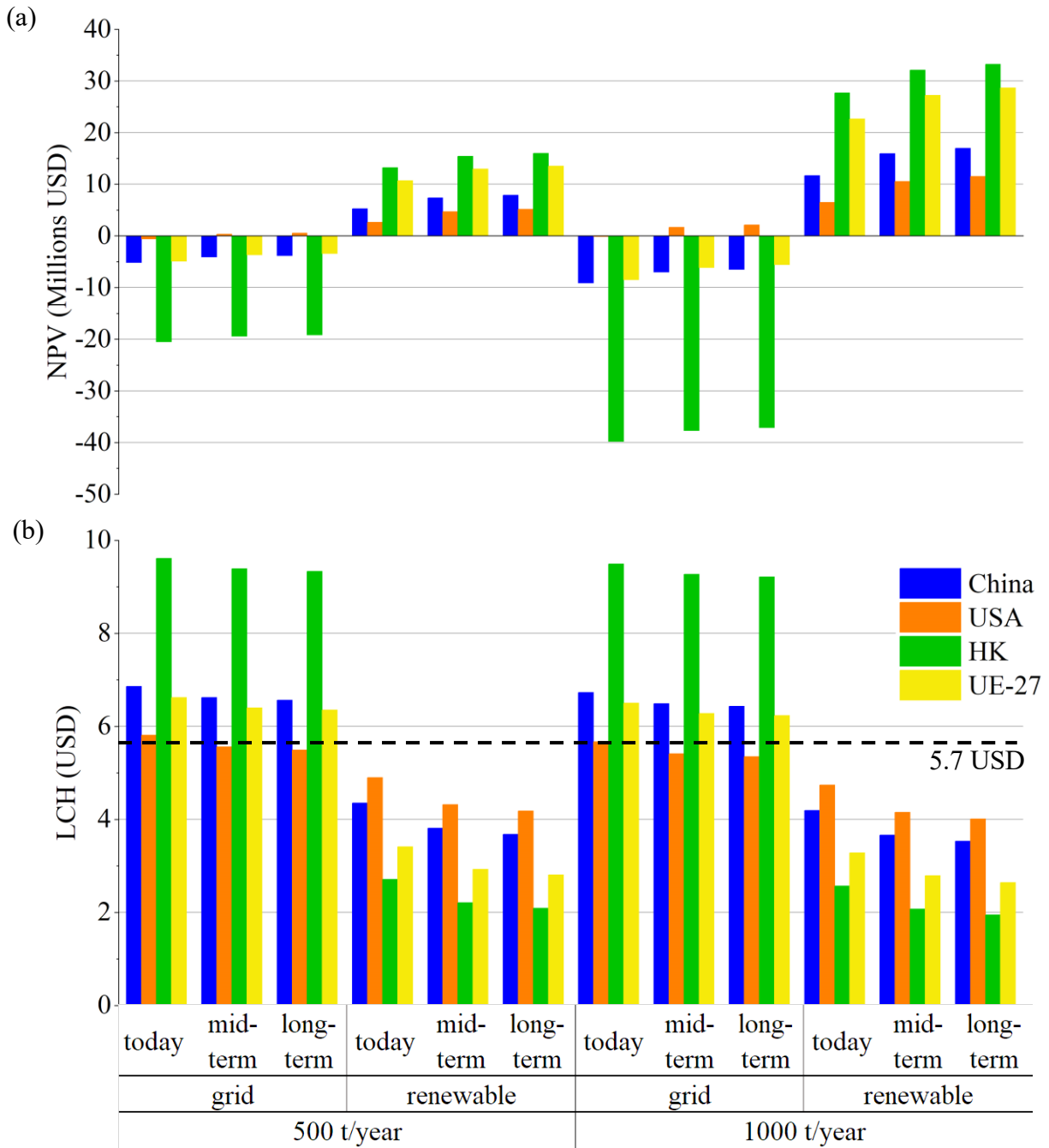


Figure 53 – (a) NPV comparison at 20 years. (b) Comparison between LCH, the industrial hydrogen price level has been highlighted in the plot with black dashed lines.

For a complete comparison, the results for all the cases and scenarios are reported in

Figure 53. Renewable coupled plants have better economic return than grid coupled, as it is possible to see in

Figure 53 (a), from which I can derive a general behavior that for renewable plant the increasing of size increases the profit and the economic feasibility, while for grid-connected plant smaller sizes

should be preferred. LCH decreases while the size of the plant increases, under the same conditions of power source and country, as I reasonably expected, as is possible to see in

Figure 53 (b). The LCHs evaluated are in between  $2.34 \frac{\text{USD}}{\text{kgH}_2}$  and  $9.87 \frac{\text{USD}}{\text{kgH}_2}$  depending on the combination of parameters. Considering hydrogen prices nowadays, as shown in Table 6, all the cases with a renewables coupling configuration have a LCH within the range of hydrogen market price, which is under  $5.7 \frac{\text{USD}}{\text{kgH}_2}$ .

The NPVs at year 20 show the return of investment of the electrolyzer plant. In Figure 53 (a) I report the highest hydrogen price among those illustrated in Table 6 (*i. e.*  $5.7 \frac{\text{USD}}{\text{kgH}_2}$ ). The grid-powered plants are not economically sustainable because of the higher electricity cost compared to renewables. Despite the higher capital cost (due to smaller CF), renewable-powered plants show a good economic return, especially if I consider 1000 t/year plant size.

US plants have the best performance in grid coupling but the worst in renewable coupling. The good result in the grid coupling is due to the lowest electricity price. Simultaneously, the bad performance with renewables is caused by a combination of high taxation rate and low heat value in the USA regarding the other locations. For HK, I have the opposite situation, worst economic output in grid coupling, but best with renewables. This is due to the highest grid electricity price that affects the grid coupled plant. In the renewable configuration, the low tax rate and high heat value guarantee the best economic output between the analyzed cases.

I further analyze the LCH, by evaluating the impact of each component: electricity, operation and maintenance, stack, the balance of plant, other capital costs (financial and contingencies), and taxes. All the data are summarized in Table 7, where heat and O<sub>2</sub> are negative components in LCH because they are profitable by-products and reduce the final LCH. The best and worst cases are shown in Figure 54 (a) and (b), respectively. For all locations, I present the best (*i. e.* 1000 t/year, renewable coupling, and long-term stack scenario) and worst scenario (500 t/year grid coupling and today stack scenario). In all the locations, it is evident that a larger plant size positively impacts the share of capital cost and electricity cost. By comparing the value of LCH, I am able to perform a general comparison between various cases, as shown in Figure 54, where it is also clear the contribution of selling the heat and oxygen as by-products on reducing the LCH.

Table 7 -Subdivision of the LCH for the various components of the cost.

Levelized cost of hydrogen composition (USD)														
location	price component	500 t/year						1000 t/year						
		grid			renewable			grid			renewable			
		today	mid-term	long-term	today	mid-term	long-term	today	mid-term	long-term	today	mid-term	long-term	
China	electricity	6.15	6.15	6.15	2.20	2.20	2.20	6.15	6.15	6.15	2.20	2.20	2.20	
	O&M	0.39	0.33	0.31	0.78	0.65	0.61	0.35	0.29	0.28	0.74	0.61	0.57	
	stack	0.10	0.04	0.03	0.23	0.10	0.06	0.10	0.04	0.03	0.23	0.10	0.06	
	BoP	0.17	0.17	0.17	0.31	0.31	0.31	0.14	0.14	0.14	0.27	0.27	0.27	
	other capex	0.19	0.16	0.15	0.38	0.31	0.30	0.17	0.14	0.13	0.36	0.29	0.28	
	taxes	0.57	0.48	0.45	1.16	0.95	0.91	0.52	0.43	0.41	1.09	0.90	0.85	
	heat and O <sub>2</sub>	-0.71	-0.71	-0.71	-0.71	-0.71	-0.71	-0.71	-0.71	-0.71	-0.71	-0.71	-0.71	-0.71
	LCH	6.86	6.62	6.56	4.35	3.81	3.68	6.73	6.49	6.43	4.19	3.66	3.53	
USA	Electricity	4.68	4.68	4.68	2.20	2.20	2.20	4.68	4.68	4.68	2.20	2.20	2.20	
	O&M	0.39	0.33	0.31	0.78	0.65	0.61	0.35	0.29	0.28	0.74	0.61	0.57	
	Stack	0.10	0.04	0.03	0.23	0.10	0.06	0.10	0.04	0.03	0.23	0.10	0.06	
	BoP	0.17	0.17	0.17	0.31	0.31	0.31	0.14	0.14	0.14	0.27	0.27	0.27	
	other capex	0.19	0.16	0.15	0.38	0.31	0.30	0.17	0.14	0.13	0.36	0.29	0.28	
	Taxes	0.70	0.60	0.56	1.42	1.18	1.12	0.64	0.53	0.51	1.36	1.10	1.05	
	heat and O <sub>2</sub>	-0.42	-0.42	-0.42	-0.42	-0.42	-0.42	-0.42	-0.42	-0.42	-0.42	-0.42	-0.42	-0.42
	LCH	5.81	5.56	5.49	4.90	4.32	4.18	5.67	5.41	5.35	4.74	4.15	4.01	
HK	Electricity	10.43	10.43	10.43	2.20	2.20	2.20	10.43	10.43	10.43	2.20	2.20	2.20	
	O&M	0.39	0.33	0.31	0.78	0.65	0.61	0.35	0.29	0.28	0.74	0.61	0.57	
	Stack	0.10	0.04	0.03	0.23	0.10	0.06	0.10	0.04	0.03	0.23	0.10	0.06	
	BoP	0.17	0.17	0.17	0.31	0.31	0.31	0.14	0.14	0.14	0.27	0.27	0.27	
	other capex	0.19	0.16	0.15	0.38	0.31	0.30	0.17	0.14	0.13	0.36	0.29	0.28	
	taxes	0.46	0.39	0.37	0.94	0.78	0.74	0.43	0.36	0.33	0.90	0.73	0.70	
	heat and O <sub>2</sub>	-2.13	-2.13	-2.13	-2.13	-2.13	-2.13	-2.13	-2.13	-2.13	-2.13	-2.13	-2.13	-2.13
	LCH	9.61	9.39	9.33	2.71	2.21	2.09	9.49	9.27	9.21	2.57	2.07	1.95	
EU-27	electricity	6.69	6.69	6.69	2.20	2.20	2.20	6.69	6.69	6.69	2.20	2.20	2.20	
	O&M	0.39	0.33	0.31	0.78	0.65	0.61	0.35	0.29	0.28	0.74	0.61	0.57	
	stack	0.10	0.04	0.03	0.23	0.10	0.06	0.10	0.04	0.03	0.23	0.10	0.06	
	BoP	0.17	0.17	0.17	0.31	0.31	0.31	0.14	0.14	0.14	0.27	0.27	0.27	
	other capex	0.19	0.16	0.15	0.38	0.31	0.30	0.17	0.14	0.13	0.36	0.29	0.28	
	taxes	0.42	0.35	0.34	0.85	0.71	0.67	0.38	0.31	0.30	0.81	0.66	0.59	
	heat and O <sub>2</sub>	-1.34	-1.34	-1.34	-1.34	-1.34	-1.34	-1.34	-1.34	-1.34	-1.34	-1.34	-1.34	-1.34
	LCH	6.62	6.40	6.35	3.41	2.93	2.81	6.50	6.28	6.23	3.28	2.79	2.64	

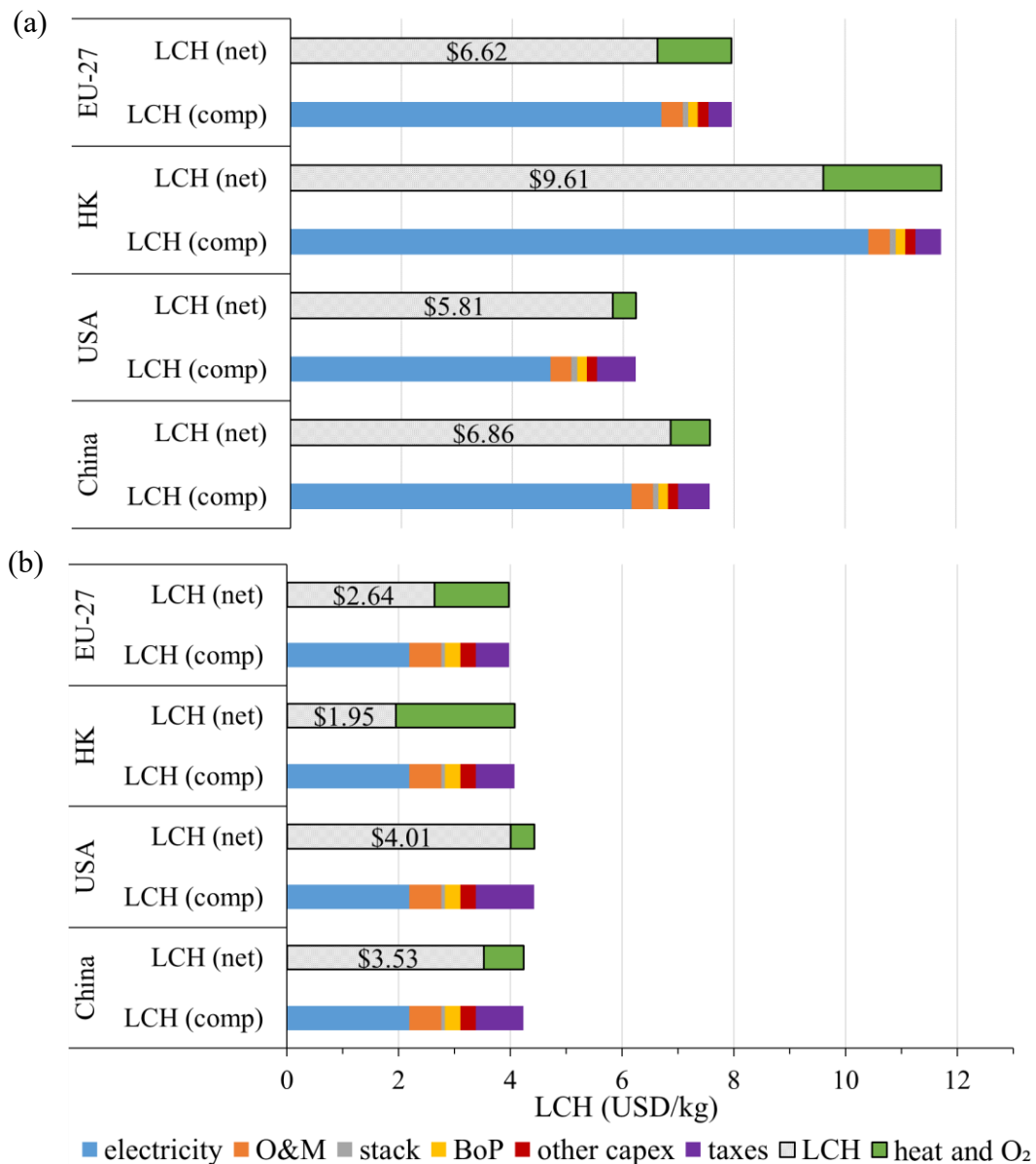


Figure 54 - LCH by component under the two scenarios: (a) 500 t/year, today stack cost and grid connected (worst scenario); (b) 1000 t/year, long-term stack cost and renewable connected (best scenario).

Focusing on China case, I compare the grid and renewable plants for the different plant sizes. For the grid connected plant, looking at Figure 55 (a) Figure 56 (a), the impact of capital cost on LCH is 14% with 500 t/year size, but only 7% in the case of 1000 t/year size. Due to the higher price of electricity from the grid, the LCH is expected to be much higher in a grid-connected configuration than a renewable coupled plant. A similar analysis for the renewable plants regarding the LCH is reported

in Figure 55 - Pie charts for the comparison of the LCH components for plant located in China, today scenario, 500 t/year: (a) grid connected; (b) renewable connected(b) Figure 56 (b).

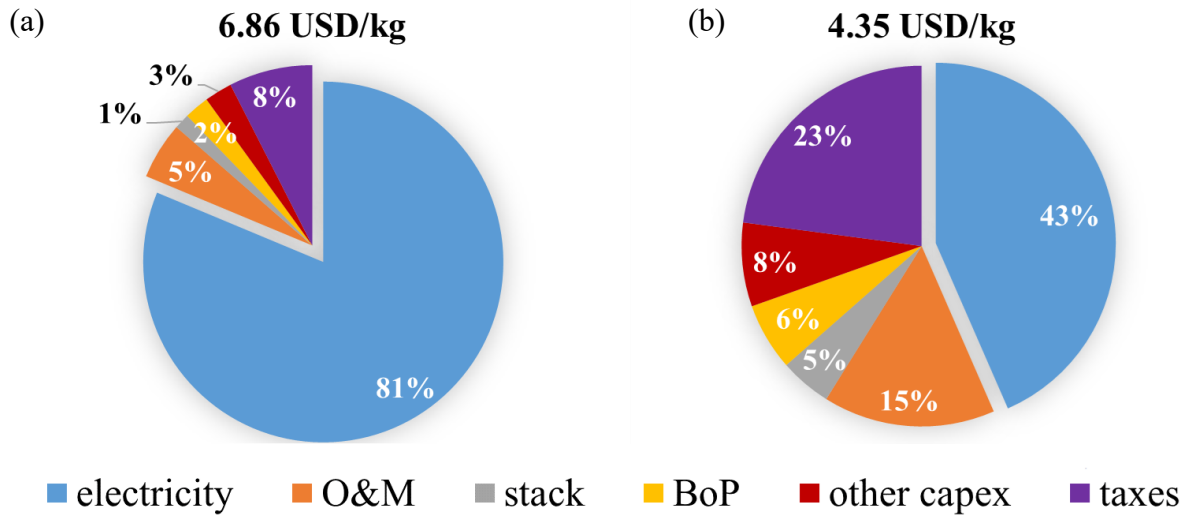


Figure 55 - Pie charts for the comparison of the LCH components for plant located in China, today scenario, 500 t/year: (a) grid connected; (b) renewable connected.

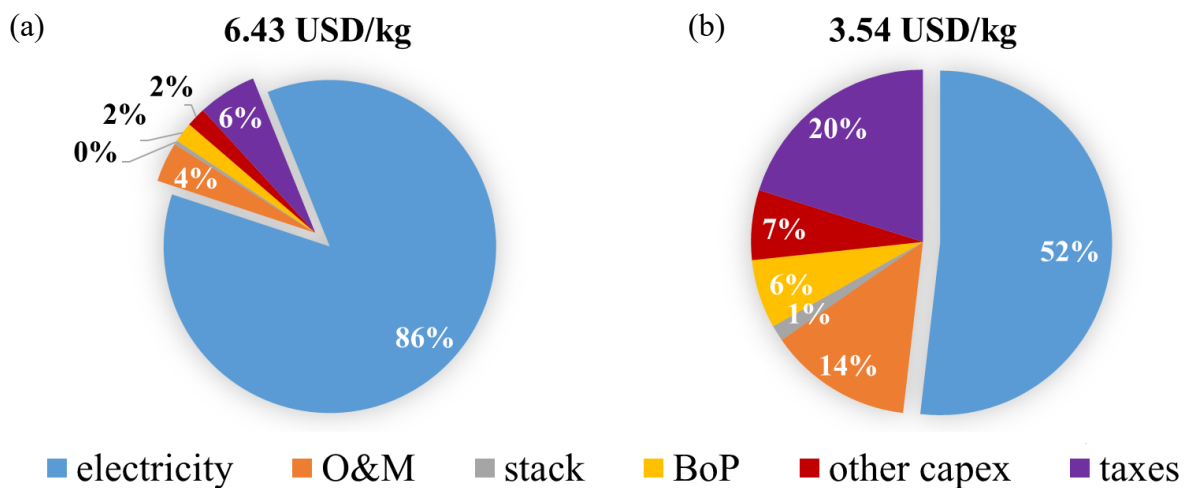


Figure 56 - Pie charts for the comparison of the LCH components for plant located in China, long term scenario, 1000 t/year: (a) grid connected; (b) renewable connected.

For a wider comparison of all the scenarios in the Chinese case, it has been presented the LCH composition in Figure 57. Where I can see the effect of the evolution in the stack technology, as for any series of today, mid-term and long term scenario, the total LCH reduces, by mean of the reduction in capital cost and in operating cost. The lower investment is also linked to lower taxes.

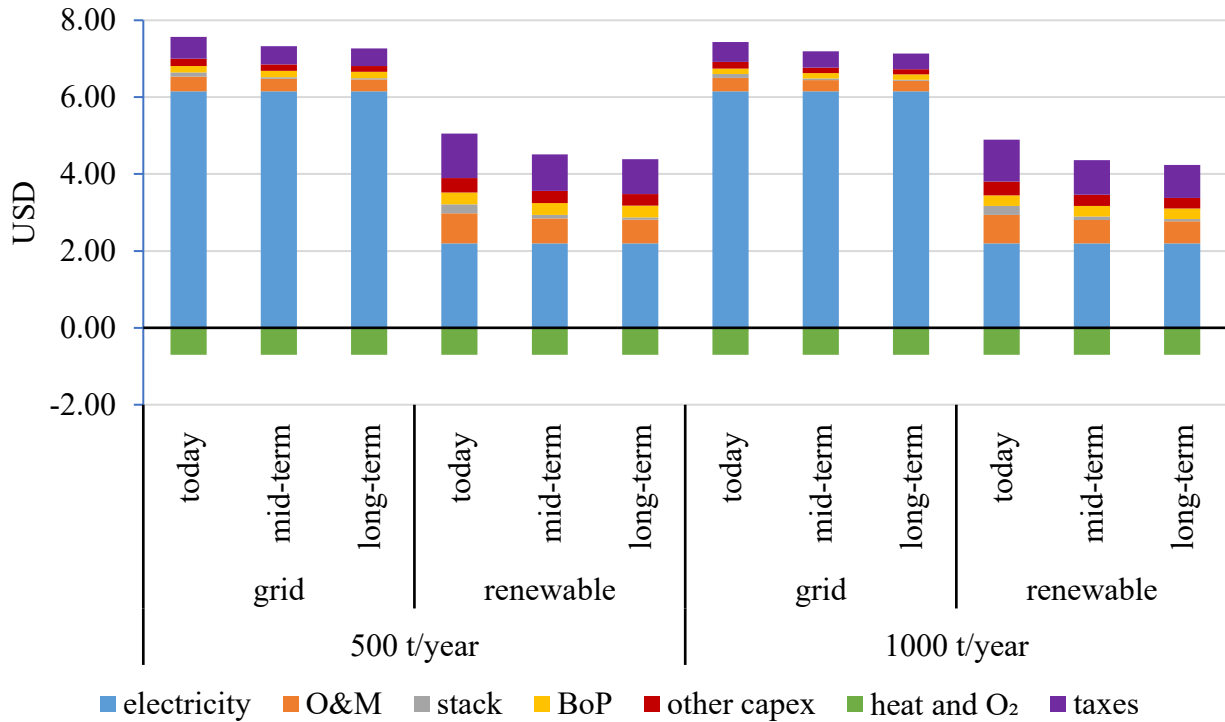


Figure 57 - LCH components of ME plant in China.

For the other locations, the plots of the LCH composition are in **Appendix B**.

## 6.2 Carbon Tax

The adoption of a carbon tax could financially impact the existing H<sub>2</sub> production technologies associated with carbon emission. The results presented in this section regard only renewable coupled plant, since carrying out electrolysis from grid coupled source produces approximately  $30 \frac{\text{kg}_{\text{CO}_2}}{\text{kg}_{\text{H}_2}}$  [49], resulting in higher emissions than SMR or CG. As a result, the electrolysis powered by a grid source is considered a polluting process.

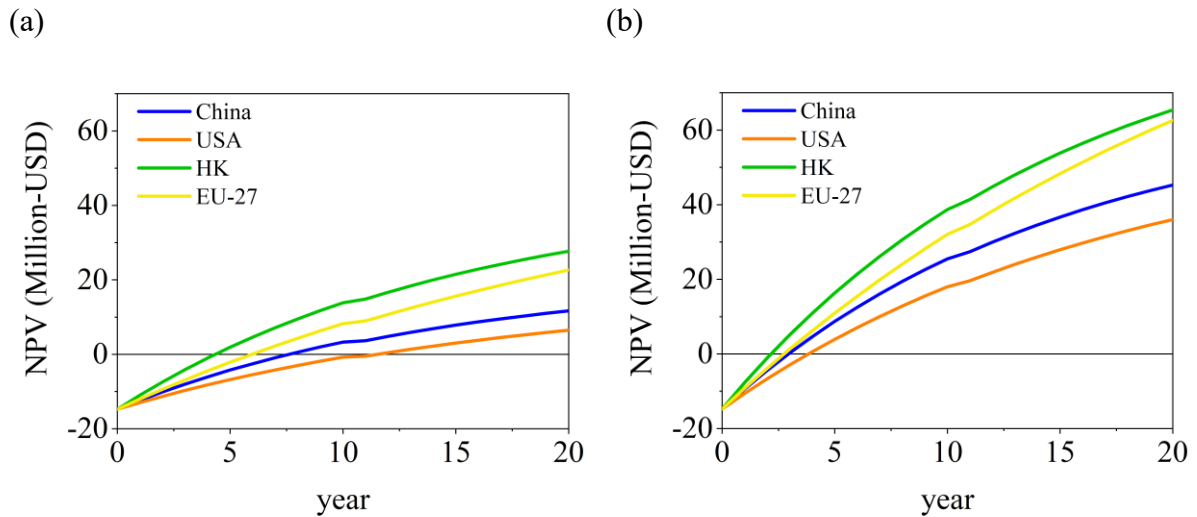


Figure 58 - NPV results in today stack scenario, 1000 t/year plant size and renewable coupled (a) with no carbon tax and (b) with strong carbon tax (350 USD/ton<sub>H<sub>2</sub></sub>).

In Figure 58 the results of NPV analysis with different levels of carbon taxes are reported. I can see the massive return of investment in the case of the 1000 t/year plant size. The carbon tax increases the price of hydrogen generated from SMR to  $7.3 \frac{\text{USD}}{\text{kg}_{\text{H}_2}}$  in the medium and to  $9.9 \frac{\text{USD}}{\text{kg}_{\text{H}_2}}$  in the strong carbon tax scenario. The higher revenues due to the higher hydrogen price increases the electrolyzer profits, see Figure 58, where in the case of strong carbon tax Figure 58 (b) the payback-time is between 3 and 4 years in HK and around 5 years in USA. The financial impact by adopting different level of carbon taxes on NPV is summarized in Figure 59. Figure 10 shows that increase in level of carbon tax could be financially favorable to the final NPV.

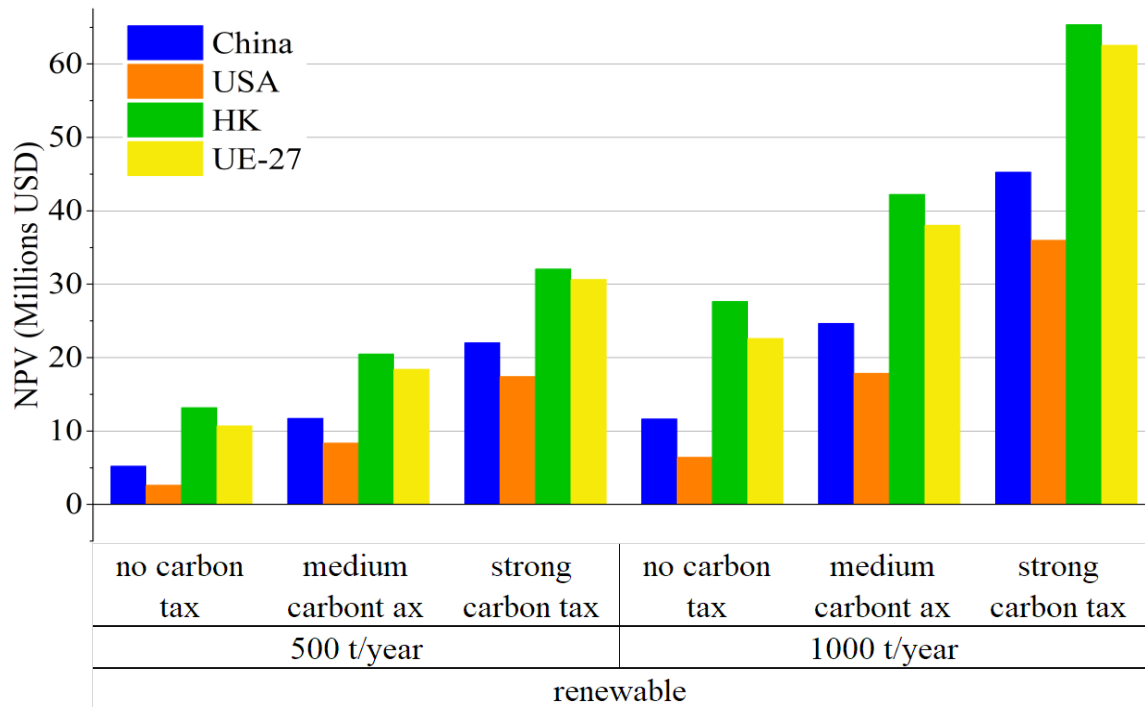


Figure 59 – Comparison of the NPV in different carbon tax scenarios, in today stack scenario.

The NPV results are presented according to the level of a carbon tax. If a higher carbon tax is adopted, there is a general improvement in the return of investment.

### 6.3 Sensitivity analysis

I performed a sensitivity analysis on LCH and NPV, considering hydrogen price, taxation rate, natural gas price, electricity cost, and capital cost as a parameter of interest. The sensitivity of the LCH and NPV to the various parameters has a linear behavior for both grid and renewable plants for all parameters.

In the grid coupled configurations, LCH has the highest sensitivity to the price of electricity. Then, capital cost, with little sensitivity and natural gas price, and taxation rate with almost a negligible sensitivity, as shown in Figure 60 (a). This behavior is due to the high electricity prices from the grid coupling. However, high CF result in smaller plant powers for the same production, explaining the reduced impact of capital cost on the final LCH. For the NPV, impact hierarchy of the parameter is similar to the addition of the hydrogen price, which has a massive influence on the final NPV. For the cases that do not generate profits, the taxation does not affect the economic Bop, so, also in the sensitivity analysis, the variation of taxation level don't affect the NPV, see Figure 60 (b), this behavior has been registered for every case that do not generate profits.

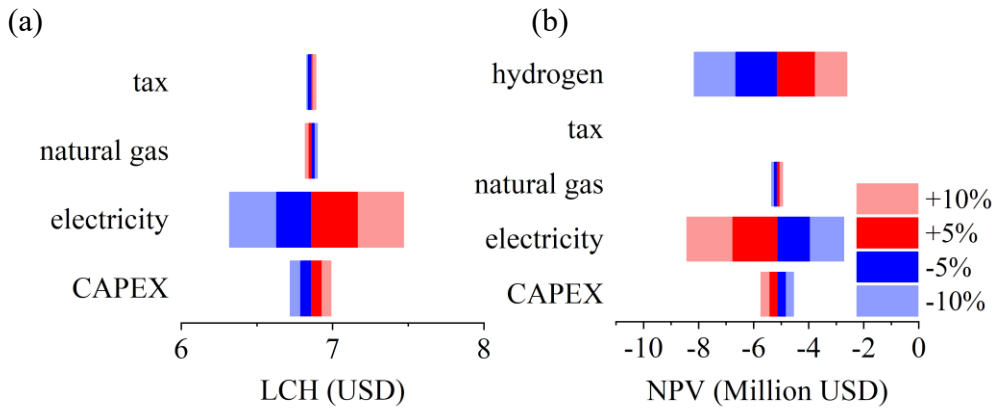


Figure 60 - Sensitivity analysis results for plants located in China: LCH (a) and NPV (b) in today scenario, 500 t/year, grid coupling

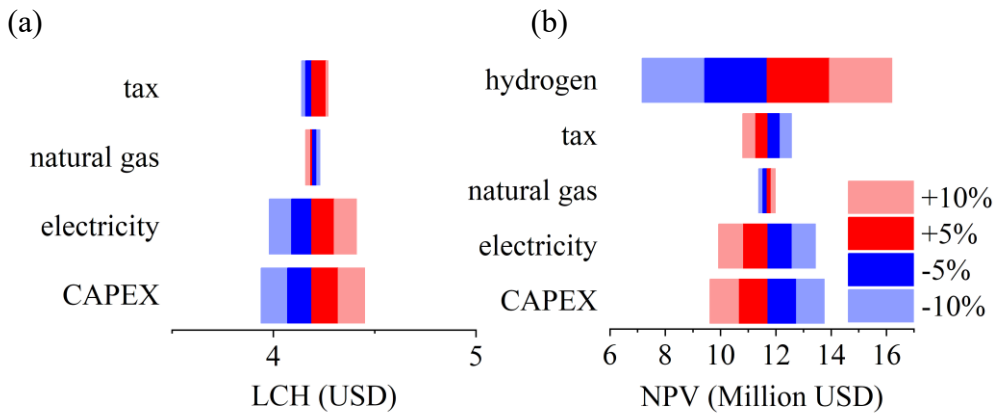


Figure 61 - Sensitivity analysis results for plants located in China: LCH (a) and NPV (b) in today scenario, 1000 t/year, renewable coupling

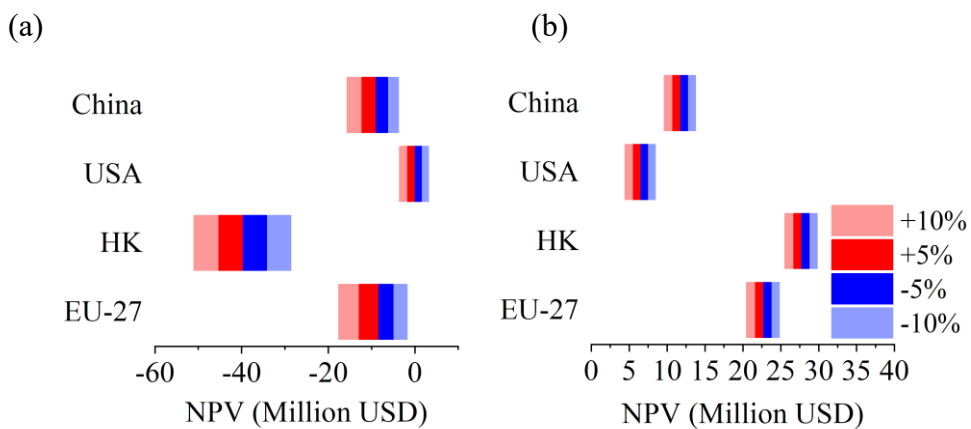


Figure 62 - NPV comparison of the effect of capital cost for different location, considering today scenario, 1000 t/year plant size grid coupling (a) and renewable coupling (b).

For renewable coupled plants, the order of impact of the parameters changes consistently with the bigger plant powers due to lower CF, and the lower electricity cost. The capital cost has the maximum effect on the LCH, then follows electricity cost, taxes, and natural gas price, see Figure 61 (a). For renewable coupled plant, The NPV behavior follows the same hierarchy of LCH with the addition of hydrogen selling price, which has the most important effects on the NPV, Figure 61 (b).

Lastly, I compared the effect of the single parameters on the plant in different locations. Parameters such as taxation or grid electricity prices affect the LCH and NPV differently according to the location. Other parameters, such as capital cost and renewable electricity cost are having the same effect for all the possible plant locations since they have been set constant worldwide. For example, I compared the NPV for the big size plant in grid coupled setup for the four locations, as reasonable the range of the variation depends on the country's electricity price and its weight on the final economic balance, see Figure 62 (a). The biggest sensitivity is registered in HK, since it has the highest electricity price, while the smallest sensitivity is registered in the USA because they have the lowest electricity price. While in Figure 62 (b) I show the effect of capital cost, that is the same for all cases, but in different range of price, because I have not linked it to the location.

## 7 Conclusions

In this work was presented an organic analysis of the membraneless electrolyzer technology, from the physical and thermodynamic side to the economic one. For the thermodynamic part data and notions taken from the literature have been used as foundations for the development of the model. With that I evaluated purity of the outlet H<sub>2</sub> and the efficiency of the electrolyzer. As result, I compared and choose between FT and FB, that considering the operational range, flexibility, and purity led to the selection of FT design for the prototyping and economic analysis.

Then, a prototyping process was performed, and the prototype used for the experiment was 3D-printed after several evolution in the design from the first concept. The experimental experiences have proved that the theoretical model developed match the experimental results almost perfectly, in the ohmic dominated region of the polarization curve. To take into account the fluid-dynamic effect of the bubble's behavior, that makes the voltage diverges, a more detailed model should be implemented. And, to make consistent measures on hydrogen production rate and purity, a direct coupling with a gas chromatographer, a flowmeter, and the possibility to operate for several days are suggested.

For the electrolysis plant, capital cost and operative cost were estimated for the many cases and scenarios analyzed, considering stack cost, plant size, power sources, location, and carbon tax level. The analysis was performed in four location with different characteristics: China, USA, HK, and EU-27. Each of them with its economic and market properties. The results were very promising for the technology, with LCH below  $2 \frac{\text{USD}}{\text{kgH}_2}$ , that is the main benchmark for the competition with the steam methane reforming hydrogen. In general renewables coupled configurations have shown profitable outputs worldwide, while grid coupling was financially sustainable only in the USA. The analysis of the implementation of carbon tax has also improved the economic output of the electrolysis plant.

Then looking at the single impact of the various components on the final LCH, I found out, that the main contribution is due to electricity, but taxation and BoP have a considerable weight too.

A sensitivity analysis has shown the most impacting parameter on the plant cost performance, and so, the way in which the research and the optimization should be directed. For large renewable coupled plant, on the reduction of electricity cost and capital cost, not for the stack part, but mostly in BoP and other collateral area, while for grid coupled plant the reduction of electricity cost component, by mean of a higher efficiency.

In conclusion this technology could be highly profitable already today in some configurations and the prototyping and the developed model have gained experimental validation, surely suitable for further analysis with prototypes and pilot plants.

## 8 List of symbols and parameters

Table 8 - Symbols

Variable	Description	Unit
$ASR_{\Omega}$	Area specific resistance	$\Omega \text{ cm}^2$
$B_n$	Net cash flow in the year $n$	USD
$c$	Channel of the electrolyzer	-
$c_n$	Operating cost of the plant in the year $n$	USD
$C_{\text{tax}}$	Corporate tax rate	-
$D_{\text{tube}}$	Diameter of the tubes of the hydraulic circuit	m
$d$	Debt percentage of the investment	-
$d_i$	Debt interest	-
$e$	Equity percentage of the investment	-
$e_r$	Equity rate of return	-
$E_0$	Reversible voltage	V
$f$	Gas volume fraction of the electrolyte	-
$F$	Faraday's constant	C/mol
$f_{\text{dist}}$	Loss factor for distributed losses	-
$g$	Gravitational acceleration	$\text{m/s}^2$
$h$	Electrode gap	cm
$H_{\text{dev}}$	Hydraulic head of the electrolyzer cell	m
$H_{\text{dist}}$	Hydraulic head of distributed losses	m
$H_k$	Henry coefficient of the $k$ gas in the electrolyte	1/Pa
$H_k^0$	Henry coefficient of the gas $k$ in pure water	1/Pa
$H_{\text{minor}}$	Hydraulic head of minor or concentrated losses	m

$H_{\text{tot}}$	Hydraulic head of the circuit	m
$HHV_{H_2}$	Higher heating value of hydrogen	J/kg
$i$	Discount rate	-
$I$	Initial investment	USD
$j$	Current density	A/cm <sup>2</sup>
$j_0$	Exchange current density	A/cm <sup>2</sup>
$k_{\text{conc}}$	Loss factor for concentrated losses	-
$K_k$	Setchenov constant	-
$L_{\text{tube}}$	Hydraulic circuit pipes length	m
LCH	Levelized cost of hydrogen	USD/kg <sub>H<sub>2</sub></sub>
$\dot{m}_{\text{ely}}$	Electrolyte flow rate	kg/s
$\dot{m}_{H_2}$	Total mass of hydrogen produced in one year	kg
$\mathcal{M}_{H_2}$	Molecular mass of hydrogen molecule	kg/kmol
$n$	Is the year index	year
$\dot{n}_{H_2, \text{gas}, \text{out}, c}$	Molar flow rate of hydrogen in c exit channel	mol/s
$\dot{n}_k$	Molar flow rate of gas k produced by the electrochemical reaction	mol/s
$\dot{n}_{O_2, \text{gas}, \text{out}, c}$	Molar flow rate of oxygen in c exit channel	mol/s
$N_{\text{minor}}$	Number of concentrated losses	-
NPV	Net present value	USD
$p$	Pressure of the system	Pa
$p_k$	Partial pressure of the k gas	Pa
$p_{\text{vap}}$	Water vapor pressure	Pa
$P_{\text{cell}}$	Electrolyzer power	W
$P_{\text{pump}}$	Pump power to circulate the electrolyte	W

$\text{purity}_{\text{H}_2,c}$	Hydrogen purity of the c exit channel	-
$\text{purity}_{\text{O}_2,c}$	Oxygen purity of the c exit channel	-
$R$	Ideal gas constant	J/(K mol)
$t$	Thickness of the electrode	cm
$t^*$	Break-even year	year
$T$	Temperature	K
$T_R$	Critical temperature	K
$v$	Electrolyte velocity in the pipes	m/s
$V_{\text{cell}}$	Voltage of the cell	V
$w$	Weight percentage of the salt in the electrolyte solution	-
WACC	Weighted average cost of capital	-
$x_{0,k}$	Molar concentration of dissolved gas in pure water	-
$x_{e,k}$	Molar concentration of dissolved gas k in the electrolyte	-
$y_k$	Molar fraction of the gas	-
$z_k$	Number of free electrons in the chemical reaction	-
$\alpha$	Transfer coefficient of the reaction	-
$\Delta g_{\text{rxn}}$	Gibbs free energy of the reaction	J/(K mol)
$\eta_{\text{act}}$	Activation overvoltage	V
$\eta_{\text{conc}}$	Concentration or diffusive overvoltage	V
$\eta_{\text{HHV}}$	Higher heating value efficiency	-
$\eta_{\text{faradic}}$	Faradic efficiency of the chemical reaction	-
$\eta_{\text{pump}}$	Hydraulic efficiency of the pump	-
$\eta_{\text{ohmic}}$	Ohmic overvoltage	V
$\rho_0$	Resistivity of the pure electrolyte	$\Omega$ cm

$\rho_{\text{elect}}$	Resistivity of the electrode	$\Omega \text{ cm}$
$\rho_{\text{ely}}$	Resistivity of the electrolyte	$\Omega \text{ cm}$

Table 9 - Parameters

<b>Empirical parameter</b>	<b>Value</b>	<b>Reference</b>
$A_{1,H_2}$	-4.73284	[20]
$B_{1,H_2}$	6.08954	[20]
$C_{1,H_2}$	6.06066	[20]
$A_{1,O_2}$	-9.44833	[20]
$B_{1,O_2}$	4.43822	[20]
$C_{1,O_2}$	11.42005	[20]
$A_2$	16.3872	[21]
$B_2$	3885.7	[21]
$C_2$	230.17	[21]
$K_{O_2}$	3.66	[8]
$K_{H_2}$	3.14	[8]

## 9 Appendix A

Matlab code for the evaluation of outlet gas purities and molar flow rates, the code reported below is developed for the evaluation of the parameters at different temperature. For the runs at different current densities and at different and flow rate, the code is similar, but with little changes in the loops setting.

```
clear all
close all
clc
%% DATA Henry
Tc=647.096;           %[K]
AA=16.3872;          %Antoine eq
BA=3885.7;           %Antoine eq
CA=230.17;           %Antoine eq
AH2=-4.73284         %Henry eq H2
BH2=6.08954;        %Henry eq H2
CH2=6.06066;        %Henry eq H2
AO2=-9.44833;       %Henry eq O2
BO2=4.43822;        %Henry eq O2
CO2=11.42005;       %Henry eq O2
KK_O2=3.66;         %corrective coefficient for the presence of KOH in the solution
KK_H2=3.14;         %corrective coefficient for the presence of KOH in the solution
%% DATA loop
P0_H2=2/3*101325;   %[Pa] Initial partial pressure of H2
P0_O2=1/3*101325;   %[Pa] Initial partial pressure of O2
n_ely=3.140*0.5;    %[mol/s] Electrolyte flowrate ( 2 chambers 50% each)
R=8.134;            %[J/mol/K]
toll=5e-8;          %admitted tolerance to end the loop
Area=7;             %[cm^2]
Faradic_eff=0.90;   %faradic efficiency
F=96485;            %Faraday's constant
%% Temperature and current density loop
tic
TT= [20 40 60 80];   %[°C]
current_density=0.04:0.02:4; %[A/cm^2]
fid=fopen('purity_current.txt','w');
col= ['b' 'r' 'y' 'g'];
for jj=1: length (TT) %Temperature loop
    clear x1_O2 x1_H2 P1_O2 P1_H2 x2_O2 x2_H2 P2_O2 P2_H2
    clear n1_O2g n1_H2g n1_O2l n1_H2l n2_O2g n2_H2g n2_O2l n2_H2l
    for nn=1: length (current_density) %Current density loop
        cur_dens=current_density(nn);
        %% Henry evaluation
        Antoine=@(T)1000*exp (AA-BA/(T+CA)); % [T in °C]
        T_celsius=TT (jj);
        Psat=Antoine(T_celsius);
        %% Henry eq.
        HenryO2=@(Tr) (exp (AO2/Tr+(BO2*((1-Tr)^0.355))/Tr+CO2*((Tr)^-0.41)*exp((1-Tr))))*Psat;
        HenryH2=@(Tr) (exp (AH2/Tr+(BH2*((1-Tr)^0.355))/Tr+CH2*((Tr)^-0.41)*exp((1-Tr))))*Psat;
```

```

T_kelvin=T_celsius+273.15;
Tr=T_kelvin/Tc;
H_O2=HenryO2(Tr)*10*KK_O2*0.3; %correction according to the concentration of KOH
H_H2=HenryH2(Tr)*10*KK_H2*0.3; %correction according to the concentration of KOH

%% Parameters initialization
Molar_vol=R*T_kelvin/101325*1000; % [L/mol]
nH2=cur_dens*Area*Faradic_eff/2/F; % [mol/s] H2 produced by the reaction
x0_old_O2=1/3*101325/H_O2; % [mol/mol] solubility O2
x0_old_H2=2/3*101325/H_H2; % [mol/mol] solubility H2
n_H2l_lim=x0_old_H2*n_ely*2; % [mol/s] H2 flowrate liquid phase limiting
n_O2l_lim=x0_old_O2*n_ely*2; % [mol/s] O2 flowrate liquid phase limiting
n0_H2g(nn)=nH2; % [mol/s] start H2 flowrate gas phase
n0_O2g(nn)=0.5*nH2; % [mol/s] start O2 flowrate gas phase
n0_O2l(nn)=x0_old_O2*n_ely*2; % [mol/s] start O2 flowrate liquid phase
n0_H2l(nn)=x0_old_H2*n_ely*2; % [mol/s] start H2 flowrate liquid phase
Vol_flow_H2=(nH2)*Molar_vol; % [L/s] total volumetric flow gas H2 flow (from
reaction)
Vol_flow_O2=(0.5*nH2)*Molar_vol; % [L/s] total volumetric flow gas O2 flow (from
reaction)

k=1; % counter of iterations
dmass2=1;
dmass1=1;
clear n_ref_H2 n_ref_O2
n_ref_H2(k)=n0_H2l(nn);
n_ref_O2(k)=n0_O2l(nn);
%% Molar flow rates computation
while dmass2>toll & dmass1>toll

    n2_H2l(nn)=n0_H2l(nn);
    n2_O2l(nn)=n0_O2l(nn);

    x1_O2(nn)=n0_O2l(nn)*0.5/(n_ely+H_O2*Vol_flow_H2/R/T_kelvin);
    P1_O2(nn)=H_O2*x1_O2(nn);
    P1_H2(nn)=101325-P1_O2(nn);
    x1_H2(nn)=P1_H2(nn)/H_H2;
    n1_H2l(nn)=x1_H2(nn)*n_ely;
    n1_O2l(nn)=x1_O2(nn)*n_ely;
    n1_O2g(nn)=P1_O2(nn)*Vol_flow_H2/R/T_kelvin;
    n1_H2g(nn)=n0_H2g(nn)+n0_H2l(nn)-n1_H2l(nn);

    x2_H2(nn)=n0_H2l(nn)*0.5/(n_ely+H_H2*Vol_flow_O2/R/T_kelvin);
    P2_H2(nn)=H_H2*x2_H2(nn);
    P2_O2(nn)=101325-P2_H2(nn);
    x2_O2(nn)=P2_O2(nn)/H_O2;
    n2_O2l(nn)=x2_O2(nn)*n_ely;
    n2_H2l(nn)=x2_H2(nn)*n_ely;
    n2_H2g(nn)=P2_H2(nn)*Vol_flow_O2/R/T_kelvin;
    n2_O2g(nn)=n0_O2g(nn)+n0_O2l(nn)-n2_O2l(nn);

```

```

n0_H2l(nn)=n1_H2l(end)+n2_H2l(end);           %[mol/s] new start H2 flowrate liquid phase
n0_O2l(nn)=n1_O2l(end)+n2_O2l(end);           %[mol/s] new start O2 flowrate liquid phase
n0_H2g(nn)=nH2+n0_H2l(nn)-n_H2l_lim;
n0_O2g(nn)=0.5*nH2+n0_O2l(nn)-n_O2l_lim;
Vol_flow_H2=(nH2+n0_H2l(nn)-n_H2l_lim)*Molar_vol;           %[L/s] total volumetric
                                                             flow gas H2 flow (from
                                                             reaction)

Vol_flow_O2=(0.5*nH2+n0_O2l(nn)-n_O2l_lim)*Molar_vol;           %[L/s] total volumetric
                                                             flow gas O2 flow (from
                                                             reaction)

dmass1=abs(n_ref_H2(k)-n0_H2l(nn))/abs(n_ref_H2(k));
dmass2=abs(n_ref_O2(k)-n0_O2l(nn))/abs(n_ref_O2(k));
    n_ref_H2(k+1)=n0_H2l(nn);
    n_ref_O2(k+1)=n0_O2l(nn);
k=k+1;
end
purityH2(nn)=n1_H2g(end)/(n1_H2g(end)+n1_O2g(end));
purityO2(nn)=n2_O2g(end)/(n2_O2g(end)+n2_H2g(end));
%% Mass balance
%O2 mass balance
delta_O2=n0_O2g+n0_O2l-n1_O2g(end)-n1_O2l(end)-n2_O2g(end)-n2_O2l(end);
err_rel1(jj)=abs(delta_O2)/abs(n0_O2g+n0_O2l);
%H2 mass balance
delta_H2=n0_H2g+n0_H2l-n1_H2g(end)-n1_H2l(end)-n2_H2g(end)-n2_H2l(end);
err_rel2(jj)=abs(delta_H2)/abs(n0_H2g+n0_H2l);
H2_capt(nn)=n1_H2g(end);
end
%% Plot
figure(1)
set(gca,'FontSize',20)
set(gca,'LineWidth',1)
    plot(current_density,purityH2*100,'LineWidth',2,'displayname',['\it T=\rm' num2str(TT(jj))
    '\textcircled{C}'], 'Color', col(jj))
set(gca,'fontname','Times New Roman')
xlabel('\it j \rm(A/cm^2)')
ylabel('purity H_2')
ytickformat('percentage')
legend boxoff
hold on
box on
%% Data saving
purity=[current_density; purityH2; H2_capt];
fprintf(fid,'%1s','Temp=',num2str(TT(jj)),'\textcircled{C}');
fprintf(fid,'\r\n');
fprintf(fid,'%1s\r\n','Current_density Purity H2_capt');
fprintf(fid,'%1.4f %16.4f %12.9f\r\n',purity);
end
legend('Location','SE')
xlim([0 4])
ylim([85 100])

```

```
saveas(figure(1),'DEFT purity over current at different T.png')  
time=toc
```

## 10 Appendix B

LCH composition for USA, EU-27, and HK cases

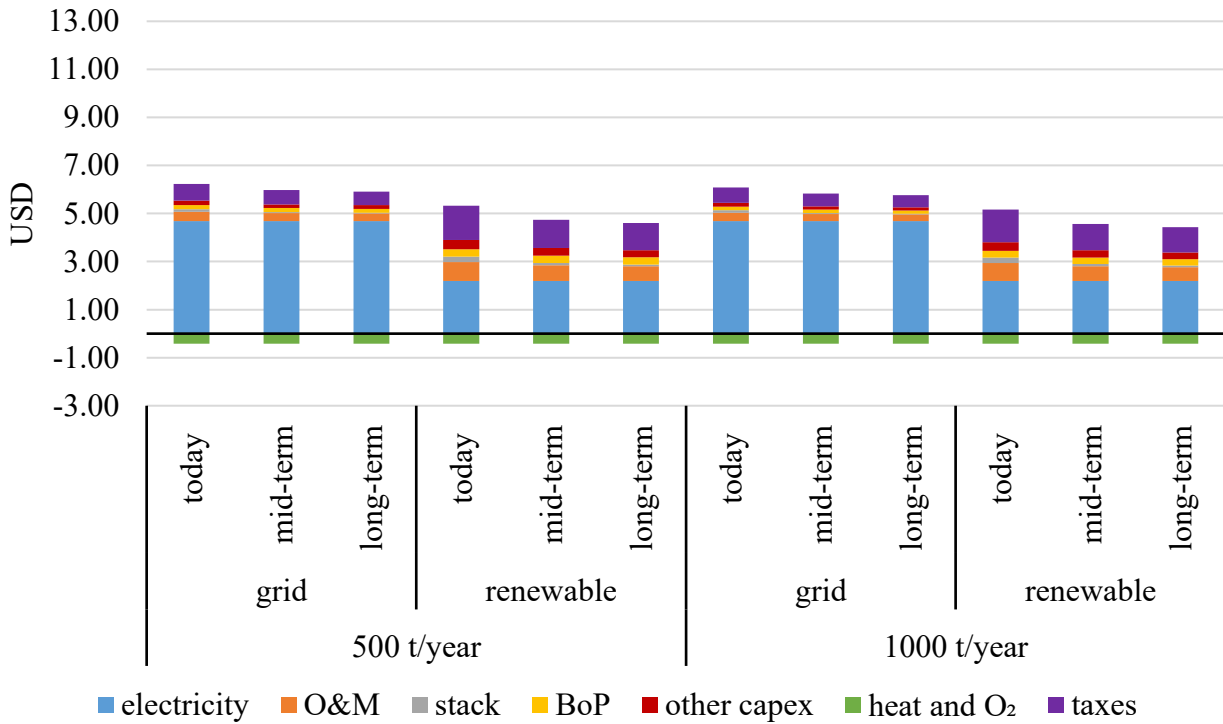


Figure 63 - LCH composition for USA case

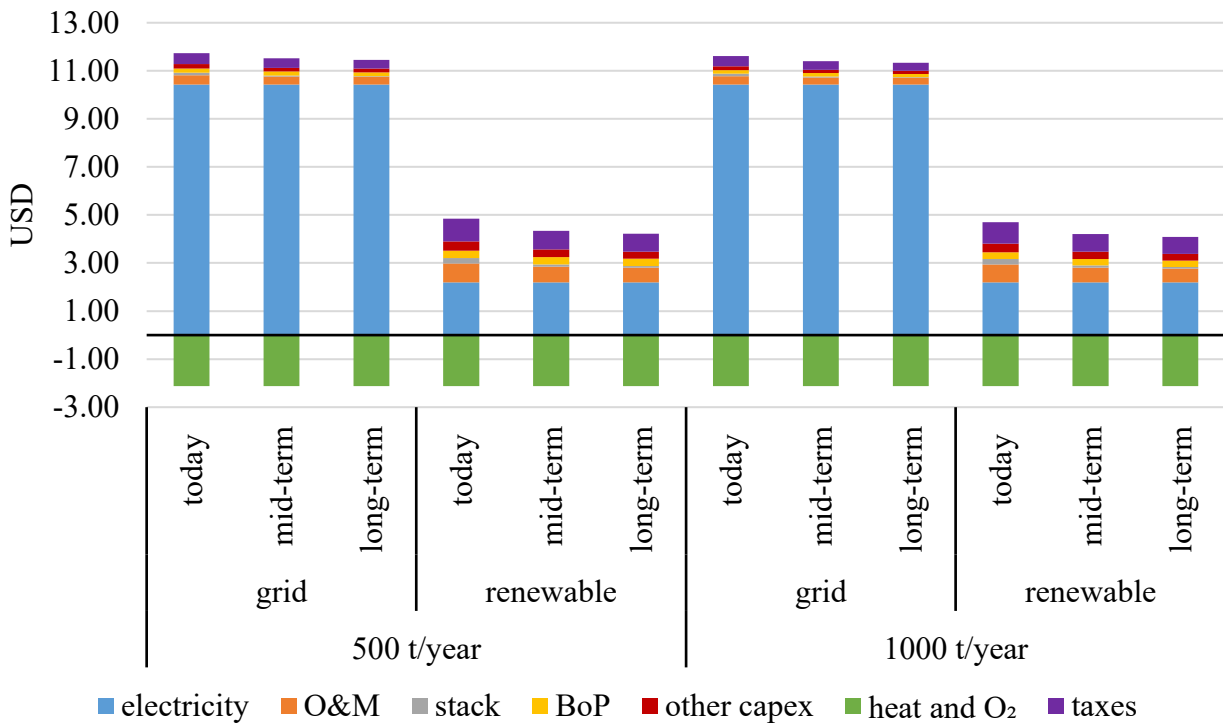


Figure 64 - LCH composition for HK case

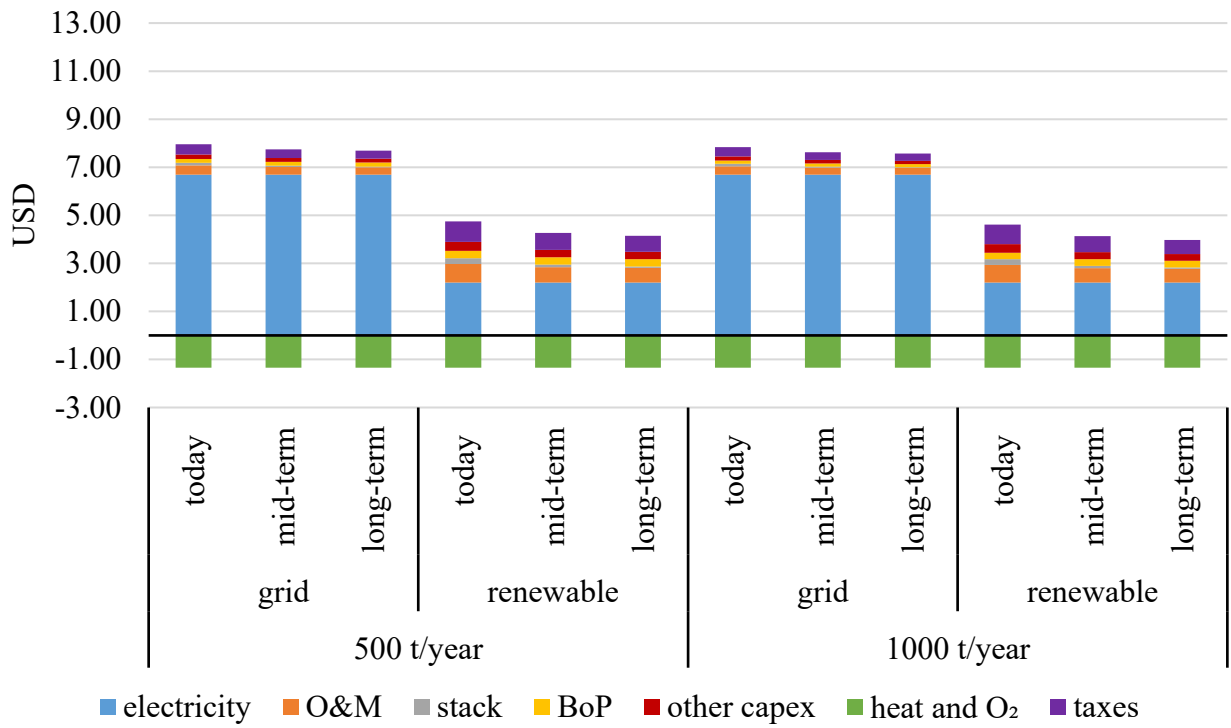


Figure 65 - LCH composition for EU-27

## 11 Appendix C

Table 10 - Experimental results without catalyst

Ni electrodes (no catalyst)							
Flow rate (mL/min)	Current (A)	j (A/cm <sup>2</sup> )	Voltage (V)				
			series 1	series 2	series 3	Mean value	Standard deviation
300 mL/min	0.05	0.069	2.8	2.9	3	2.90	0.10
	0.1	0.138	3.9	4	3.9	3.93	0.06
	0.15	0.207	4.6	5	4.8	4.80	0.20
	0.2	0.276	6.1	5.6	5.7	5.80	0.26
	0.25	0.345	8.5	7.3	7.4	7.73	0.67
	0.3	0.414	9.2	10.7	10.6	10.17	0.84
400 mL/min	0.05	0.069	2.9	3	2.9	2.93	0.06
	0.1	0.138	3.7	4	3.8	3.83	0.15
	0.15	0.207	4.6	4.9	4.9	4.80	0.17
	0.2	0.276	5.2	5.8	5.4	5.47	0.31
	0.25	0.345	6.2	6.7	6.4	6.43	0.25
	0.3	0.414	7.5	8.3	8.5	8.10	0.53
500 mL/min	0.05	0.069	2.8	2.9	2.8	2.83	0.06
	0.1	0.138	3.7	4.1	3.8	3.87	0.21
	0.15	0.207	4.4	5	4.9	4.77	0.32
	0.2	0.276	5.2	5.8	5.9	5.63	0.38
	0.25	0.345	6.2	6.8	7	6.67	0.42
	0.3	0.414	7	7.5	8.6	7.70	0.82
	0.35	0.484	7.7	8.7	9.1	8.50	0.72
	0.4	0.553	9	10	10.3	9.77	0.68
600 mL/min	0.05	0.069	2.7	3	3	2.90	0.17
	0.1	0.138	3.7	3.9	3.9	3.83	0.12
	0.15	0.207	4.5	4.9	4.7	4.70	0.20
	0.2	0.276	5.2	5.8	5.4	5.47	0.31
	0.25	0.345	5.9	6.7	6.4	6.33	0.40
	0.3	0.414	6.7	7.6	7	7.10	0.46
	0.35	0.484	7.5	8.3	7.7	7.83	0.42
	0.4	0.553	8.6	9.2	8.6	8.80	0.35
	0.45	0.622	9.5	9.5	9.4	9.47	0.06
	0.5	0.691	10.2	10.5	10.1	10.27	0.21
700 mL/min	0.05	0.069	2.7	2.9	3	2.87	0.15
	0.1	0.138	3.6	3.7	3.8	3.70	0.10
	0.15	0.207	4.4	4.5	4.6	4.50	0.10
	0.2	0.276	5.1	5.3	5.2	5.20	0.10
	0.25	0.345	5.9	6.1	5.9	5.97	0.12
	0.3	0.414	6.7	6.8	6.7	6.73	0.06

	0.35	0.484	7.6	7.6	7.4	7.53	0.12
	0.4	0.553	8.3	8.8	8.4	8.50	0.26
	0.45	0.622	10	9.9	9.3	9.73	0.38
	0.5	0.691	10.3	10.6	9.8	10.23	0.40
	0.55	0.760	11.5	11.3	10.8	11.20	0.36
800 mL/min	0.05	0.069	2.8	2.9	2.8	2.83	0.06
	0.1	0.138	3.7	3.8	3.7	3.73	0.06
	0.15	0.207	4.5	4.5	4.5	4.50	0.00
	0.2	0.276	5.3	5.2	5	5.17	0.15
	0.25	0.345	6.2	6.1	5.9	6.07	0.15
	0.3	0.414	6.9	6.8	6.7	6.80	0.10
	0.35	0.484	7.6	7.5	7.5	7.53	0.06
	0.4	0.553	8.6	8.4	8.4	8.47	0.12
	0.45	0.622	9.4	9.5	9.1	9.33	0.21
	0.5	0.691	9.9	10.4	10.3	10.20	0.26
	0.55	0.760	11.1	11.2	11.3	11.20	0.10
	0.6	0.829	13	12.6	12.9	12.83	0.21
0.65	0.898	14.9	14	13.8	14.23	0.59	
900 mL/min	0.05	0.069	2.9	2.9	3.1	2.97	0.12
	0.1	0.138	3.6	3.8	3.8	3.73	0.12
	0.15	0.207	4.6	4.7	4.6	4.63	0.06
	0.2	0.276	5.5	5.6	5.3	5.47	0.15
	0.25	0.345	6.4	6.2	6.1	6.23	0.15
	0.3	0.414	7.2	7	6.8	7.00	0.20
	0.35	0.484	7.7	7.6	7.5	7.60	0.10
	0.4	0.553	8.5	8.4	8.3	8.40	0.10
	0.45	0.622	9.2	9.1	9.1	9.13	0.06
	0.5	0.691	9.8	9.8	9.9	9.83	0.06
	0.55	0.760	10.6	10.8	10.9	10.77	0.15
	0.6	0.829	11.4	11.5	11.7	11.53	0.15
1000 mL/min	0.05	0.069	3	3	2.9	2.97	0.06
	0.1	0.138	3.8	4	4.1	3.97	0.15
	0.15	0.207	4.5	4.8	4.9	4.73	0.21
	0.2	0.276	5.4	5.6	5.7	5.57	0.15
	0.25	0.345	6.1	6.2	6	6.10	0.10
	0.3	0.414	6.9	6.9	6.6	6.80	0.17
	0.35	0.484	7.5	7.8	7.3	7.53	0.25
	0.4	0.553	8.2	8.3	8	8.17	0.15
	0.45	0.622	8.9	9	8.7	8.87	0.15
	0.5	0.691	9.8	9.6	9.5	9.63	0.15
	0.55	0.760	10.5	10.3	10.4	10.40	0.10
	0.6	0.829	11.4	11	11.2	11.20	0.20
	0.65	0.898	12	11.7	11.9	11.87	0.15
	0.7	0.967	12.7	12.4	12.6	12.57	0.15
0.75	1.036	13.9	13.1	13.3	13.43	0.42	
1100 mL/min	0.05	0.069	2.8	3	3.1	2.97	0.15
	0.1	0.138	3.8	4.1	3.8	3.90	0.17

	0.15	0.207	4.7	4.7	4.6	4.67	0.06
	0.2	0.276	5.4	5.4	5.5	5.43	0.06
	0.25	0.345	5.9	6.1	5.9	5.97	0.12
	0.3	0.414	6.6	6.7	6.5	6.60	0.10
	0.35	0.484	7.3	7.4	7.1	7.27	0.15
	0.4	0.553	8	8	7.8	7.93	0.12
	0.45	0.622	8.7	8.7	8.4	8.60	0.17
	0.5	0.691	9.5	9.5	9.2	9.40	0.17
	0.55	0.760	10.1	10.2	10	10.10	0.10
	0.6	0.829	10.8	10.9	10.7	10.80	0.10
	0.65	0.898	11.5	11.6	11.5	11.53	0.06
	0.7	0.967	12.3	12.2	12.3	12.27	0.06
	0.75	1.036	12.9	12.6	12.5	12.67	0.21
	0.8	1.105	13.7	13.5	13.3	13.50	0.20
	0.85	1.174	14.3	14	14	14.10	0.17
	0.9	1.243	15.1	14.8	14.7	14.87	0.21
	0.95	1.312	15.7	15.4	15.5	15.53	0.15
1200 mL/min	0.05	0.069	2.7	3.1	2.9	2.90	0.20
	0.1	0.138	3.8	3.9	3.8	3.83	0.06
	0.15	0.207	4.7	4.6	4.4	4.57	0.15
	0.2	0.276	5.2	5.3	5.2	5.23	0.06
	0.25	0.345	5.8	6	5.8	5.87	0.12
	0.3	0.414	6.6	6.7	6.5	6.60	0.10
	0.35	0.484	7.1	7.4	7.1	7.20	0.17
	0.4	0.553	7.9	7.9	7.8	7.87	0.06
	0.45	0.622	8.5	8.7	8.5	8.57	0.12
	0.5	0.691	9.4	9.6	9.2	9.40	0.20
	0.55	0.760	10	10.3	9.9	10.07	0.21
	0.6	0.829	10.6	10.9	10.8	10.77	0.15
	0.65	0.898	11.4	11.7	11.5	11.53	0.15
	0.7	0.967	12.2	12.3	12.3	12.27	0.06
	0.75	1.036	12.7	12.9	13	12.87	0.15
	0.8	1.105	13.4	13.8	13.7	13.63	0.21
	0.85	1.174	14.2	14.4	14.4	14.33	0.12
0.9	1.243	15	14.9	14.7	14.87	0.15	
0.95	1.312	15.7	15.6	15.3	15.53	0.21	
1	1.382	16.1	16.4	16.2	16.23	0.15	
1.05	1.451	16.7	17	16.9	16.87	0.15	

Table 11 - Experimental results with catalyst

Ni electrodes with catalyst			
Flow rate	Current (A)	j (A/cm <sup>2</sup> )	Voltage (V)
			series 1
300 mL/min	0.05	0.069	2.5
	0.1	0.138	3.5
	0.15	0.207	4.6
	0.2	0.276	5.5
	0.25	0.345	6.3
	0.3	0.414	7.2
400 mL/min	0.05	0.069	2.4
	0.1	0.138	3.4
	0.15	0.207	4.1
	0.2	0.276	5
	0.25	0.345	6
	0.3	0.414	6.9
	0.35	0.484	7.9
500 mL/min	0.05	0.069	2.5
	0.1	0.138	3.2
	0.15	0.207	4.1
	0.2	0.276	5
	0.25	0.345	6.1
	0.3	0.414	6.4
	0.35	0.484	7.1
	0.4	0.553	8
	0.45	0.622	9.1
	0.5	0.691	10.3
600 mL/min	0.05	0.069	2.5
	0.1	0.138	3.2
	0.15	0.207	4
	0.2	0.276	4.9
	0.25	0.345	5.7
	0.3	0.414	6
	0.35	0.484	6.2
	0.4	0.553	8
	0.45	0.622	8.6
	0.5	0.691	9.6
	0.55	0.760	10.3
700 mL/min	0.05	0.069	2.4
	0.1	0.138	3.2
	0.15	0.207	4.1
	0.2	0.276	4.8

	0.25	0.345	5.5
	0.3	0.414	6.3
	0.35	0.484	7
	0.4	0.553	7.9
	0.45	0.622	8.6
	0.5	0.691	9.5
	0.55	0.760	10.4
800 mL/min	0.05	0.069	2.2
	0.1	0.138	3.3
	0.15	0.207	4
	0.2	0.276	4.7
	0.25	0.345	5.6
	0.3	0.414	6.5
	0.35	0.484	7.3
	0.4	0.553	8
	0.45	0.622	8.9
	0.5	0.691	9.4
	0.55	0.760	10.1
0.6	0.829	11.6	
0.65	0.898	12.5	
900 mL/min	0.05	0.069	2.3
	0.1	0.138	3.3
	0.15	0.207	4
	0.2	0.276	5
	0.25	0.345	5.7
	0.3	0.414	6.5
	0.35	0.484	7.1
	0.4	0.553	7.9
	0.45	0.622	8.8
	0.5	0.691	9.5
	0.55	0.760	10.1
	0.6	0.829	10.8
	0.65	0.898	11.9
1000 mL/min	0.05	0.069	2.2
	0.1	0.138	3.2
	0.15	0.207	4
	0.2	0.276	4.9
	0.25	0.345	5.6
	0.3	0.414	6.3
	0.35	0.484	7.2
	0.4	0.553	8
	0.45	0.622	8.8
	0.5	0.691	9.5

	0.55	0.760	10.3
	0.6	0.829	11.2
	0.65	0.898	11.9
	0.7	0.967	12.9
	0.75	1.036	14.6
1100 mL/min	0.05	0.069	2.3
	0.1	0.138	3.3
	0.15	0.207	4
	0.2	0.276	4.7
	0.25	0.345	5.5
	0.3	0.414	6.2
	0.35	0.484	6.9
	0.4	0.553	7.6
	0.45	0.622	8.4
	0.5	0.691	9.1
	0.55	0.760	9.8
	0.6	0.829	10.3
	0.65	0.898	11
	0.7	0.967	11.8
	0.75	1.036	12.8
	0.8	1.105	13.4
	0.85	1.174	13.6
0.9	1.243	15.1	
0.95	1.312	17	
1200 mL/min	0.05	0.069	2.2
	0.1	0.138	3.2
	0.15	0.207	4.1
	0.2	0.276	4.8
	0.25	0.345	5.4
	0.3	0.414	6.4
	0.35	0.484	7
	0.4	0.553	7.8
	0.45	0.622	8.6
	0.5	0.691	9
	0.55	0.760	10
	0.6	0.829	10.7
	0.65	0.898	11
	0.7	0.967	12.1
	0.75	1.036	13.1
	0.8	1.105	14
	0.85	1.174	15
0.9	1.243	15.9	
0.95	1.312	16.4	

	1	1.382	17.4
	1.05	1.451	18

Table 12 - Model results for the comparison with experimental results

Theoretical model	
j (A/cm <sup>2</sup> )	Voltage (V)
0.05	2.104
0.1	2.704
0.15	3.293
0.2	3.877
0.25	4.459
0.3	5.040
0.35	5.620
0.4	6.200
0.45	6.780
0.5	7.360
0.55	7.940
0.6	8.521
0.65	9.101
0.7	9.682
0.75	10.264
0.8	10.845
0.85	11.427
0.9	12.010
0.95	12.593
1	13.177
1.05	13.761
1.1	14.345
1.15	14.930
1.2	15.516
1.25	16.102
1.3	16.688
1.35	17.275
1.4	17.863
1.45	18.451
1.5	19.040
1.55	19.629
1.6	20.219

## 12 References

- [1] J.M. Patteri Taalas, Global warming of 1.5°C, 2019.
- [2] U.R. Timur Gül, Dave Turk, Simon Bennett, The Future of Hydrogen, Paris, 2019.  
<https://www.iea.org/reports/the-future-of-hydrogen>.
- [3] Hydrogen Generation Market Size, Share & Trends Analysis Report By Application (Coal Gasification, Steam Methane Reforming), By Systems (Merchant, Captive), By Technology, And Segment Forecasts, 2020 - 2027, San Francisco, USA, 2020. <https://doi.org/GVR-2-68038-517-5>.
- [4] W. Kuckshinrichs, T. Ketelaer, J.C. Koj, Economic analysis of improved alkaline water electrolysis, *Front. Energy Res.* 5 (2017). <https://doi.org/10.3389/fenrg.2017.00001>.
- [5] D. V. Esposito, Membraneless Electrolyzers for Low-Cost Hydrogen Production in a Renewable Energy Future, *Joule.* 1 (2017) 651–658.  
<https://doi.org/10.1016/j.joule.2017.07.003>.
- [6] S.M.H. Hashemi, P. Karnakov, P. Hadikhani, E. Chinello, et al., A versatile and membraneless electrochemical reactor for the electrolysis of water and brine, *Energy Environ. Sci.* 12 (2019) 1592–1604. <https://doi.org/10.1039/c9ee00219g>.
- [7] M.I. Gillespie, R.J. Kriek, Scalable hydrogen production from a mono-circular filter press Divergent Electrode-Flow-Through alkaline electrolysis stack, *J. Power Sources.* 397 (2018) 204–213. <https://doi.org/10.1016/j.jpowsour.2018.07.026>.
- [8] G.D. O’Neil, C.D. Christian, D.E. Brown, D. V. Esposito, Hydrogen production with a simple and scalable membraneless electrolyzer, *J. Electrochem. Soc.* 163 (2016) F3012–F3019. <https://doi.org/10.1149/2.0021611jes>.
- [9] J.T. Davis, J. Qi, X. Fan, J.C. Bui, et al., Floating membraneless PV-electrolyzer based on buoyancy-driven product separation, *Int. J. Hydrogen Energy.* 43 (2018) 1224–1238.  
<https://doi.org/10.1016/j.ijhydene.2017.11.086>.
- [10] J.C. Bui, J.T. Davis, D. V Esposito, 3D-Printed electrodes for membraneless water electrolysis, *Sustain. Energy Fuels.* 4 (2019) 213–225. <https://doi.org/10.1039/c9se00710e>.
- [11] J.T. Davis, D.E. Brown, X. Pang, D. V. Esposito, High speed video investigation of bubble dynamics and current density distributions in membraneless electrolyzers, *J. Electrochem. Soc.* 166 (2019) F312–F321. <https://doi.org/10.1149/2.0961904jes>.

- [12] M.I. Gillespie, R.J. Kriek, Hydrogen production from a rectangular horizontal filter press Divergent Electrode-Flow-Through (DEFT™) alkaline electrolysis stack, *J. Power Sources*. 372 (2017) 252–259. <https://doi.org/10.1016/j.jpowsour.2017.10.080>.
- [13] M.I. Gillespie, F. Van Der Merwe, R.J. Kriek, Performance evaluation of a membraneless divergent electrode-flow-through (DEFT) alkaline electrolyser based on optimisation of electrolytic flow and electrode gap, *J. Power Sources*. 293 (2015) 228–235. <https://doi.org/10.1016/j.jpowsour.2015.05.077>.
- [14] I. Holmes-Gentle, F. Hoffmann, C.A. Mesa, K. Hellgardt, Membrane-less photoelectrochemical cells: Product separation by hydrodynamic control, *Sustain. Energy Fuels*. 1 (2017) 1184–1198. <https://doi.org/10.1039/c7se00176b>.
- [15] M. Creamer, Proudly South African hydrogen breakthrough with Shell’s backing, *Creamer Media Eng. News*. (2020). [https://www.engineeringnews.co.za/article/proudly-south-african-world-first-hydrogen-breakthrough-with-shells-backing-2020-03-30/rep\\_id:4136](https://www.engineeringnews.co.za/article/proudly-south-african-world-first-hydrogen-breakthrough-with-shells-backing-2020-03-30/rep_id:4136).
- [16] R. O’Hayre, S.-W. Cha, W. Colella, F.B. Prinz, *Fuel Cell Fundamentals*, John Wiley & Sons, Inc, Hoboken, NJ, USA, 2016. <https://doi.org/10.1002/9781119191766>.
- [17] K. Zeng, D. Zhang, Recent progress in alkaline water electrolysis for hydrogen production and applications, *Prog. Energy Combust. Sci.* 36 (2010) 307–326. <https://doi.org/10.1016/j.pecs.2009.11.002>.
- [18] D.R. Crow, *Principles and Applications of Electrochemistry*, 4th Edition, 4th ed., Routledge, London, 2017.
- [19] R.C. Weast, *CRC Handbook of Chemistry, and Physics*, 70th ed., Boca Raton, FL, 1989.
- [20] R. Fernández-Prini, J.L. Alvarez, A.H. Harvey, Henry’s constants and vapor-liquid distribution constants for gaseous solutes in H<sub>2</sub>O and D<sub>2</sub>O at high temperatures, *J. Phys. Chem. Ref. Data*. 32 (2003) 903–916. <https://doi.org/10.1063/1.1564818>.
- [21] A. Roosta, J. Hekayati, A Simple Generic Model for Estimating Saturated Vapor Pressure, *Chem. Eng. Commun.* 203 (2016) 1020–1028. <https://doi.org/10.1080/00986445.2015.1135428>.
- [22] S.K. Shoor, R.D. Walker, K.E. Gubbins, Salting out of nonpolar gases in aqueous potassium hydroxide solutions, *J. Phys. Chem.* 73 (1969) 312–317. <https://doi.org/10.1021/j100722a006>.

- [23] P. Ruetschi, R.F. Amlie, Solubility of hydrogen in potassium hydroxide and sulfuric acid. Salting-out and hydration, *J. Phys. Chem.* 70 (1966) 718–723. <https://doi.org/10.1021/j100875a018>.
- [24] B.R. Munson, T.H. Okiishi, W.W. Huebsh, A.P. Rothmayer, *Fundamentals of Fluid Mechanics*, 7th ed., John Wiley & Sons, Inc., 2015. <https://doi.org/10.1016/B978-0-12-800944-4.00002-0>.
- [25] W. Kenton, Investopedia, (n.d.). <https://www.investopedia.com/terms/n/npv.asp>.
- [26] R. Thakre, Sensitivity Analysis and Feasibility Analysis of Renewable Energy Project, *Int. J. Eng. Innov. Technol.* 4 (2014) 230–234.
- [27] F. Cucchiella, I. D’Adamo, M. Gastaldi, Financial analysis for investment and policy decisions in the renewable energy sector, *Clean Technol. Environ. Policy.* 17 (2015) 887–904. <https://doi.org/10.1007/s10098-014-0839-z>.
- [28] R. Napoli, M. Gandiglio, A. Lanzini, M. Santarelli, Techno-economic analysis of PEMFC and SOFC micro-CHP fuel cell systems for the residential sector, *Energy Build.* 103 (2015) 131–146. <https://doi.org/10.1016/j.enbuild.2015.06.052>.
- [29] Luca Bertuccioli (E4tech), Alvin Chan (Element Energy), David Hart (E4tech), Franz Lehner (E4tech), Ben Madden (Element Energy), Eleanor Standen (Element Energy), *Development of Water Electrolysis in the European Union*, Cambrinde, United Kingdom, 2014.
- [30] M.R. Shaner, H.A. Atwater, N.S. Lewis, E.W. McFarland, A comparative technoeconomic analysis of renewable hydrogen production using solar energy, *Energy Environ. Sci.* 9 (2016) 2354–2371. <https://doi.org/10.1039/c5ee02573g>.
- [31] C.H. Elizabeth Connelly, Michael Penev, Amgad Elgowainy, Current Status of Hydrogen Liquefaction Costs, *DOE Hydrog. Fuel Cells Progr. Rec.* (2019) 10.
- [32] B. Lee, H. Chae, N.H. Choi, C. Moon, et al., Economic evaluation with sensitivity and profitability analysis for hydrogen production from water electrolysis in Korea, *Int. J. Hydrogen Energy.* 42 (2017) 6462–6471. <https://doi.org/10.1016/j.ijhydene.2016.12.153>.
- [33] A.M. Philippe Chazalon, WACC EXPERT, Wacc Expert by Financ. 3.1. (n.d.). <http://www.waccexpert.com/>.
- [34] S. Alberici, S. Boeve, P. Van Breevoort, Y. Deng, et al., Subsidies and costs of EU energy., (2014) 71. <https://ec.europa.eu/energy/sites/ener/files/documents/ECOFYS %0A2014>

Subsidies and costs of EU energy\_11\_Nov.pdf.

- [35] A. Mayyas, M. Ruth, B. Pivovar, G. Bender, et al., Manufacturing Cost Analysis for Proton Exchange Membrane Water Electrolyzers Manufacturing Cost Analysis for Proton Exchange Membrane Water Electrolyzers, Natl. Renew. Energy Lab. (2019) 65.  
<https://www.nrel.gov/docs/fy10osti/72740.pdf>.
- [36] John G Wimer; Wm Morgan Summers, Cost Estimation Methodology for NETL Assessments of Power Plant Performance Quality Guidelines for Energy Systems Studies, United States, 2011. <https://doi.org/10.2172/1489510>.
- [37] AACE International Recommended Practice No. 16R-90, Conducting Technical and Economic Evaluations – As Applied for the Process and Utility Industries, 1990.  
<https://web.aacei.org/resources/publications/recommended-practices>.
- [38] M. Ruth, A. Mayyas, M. Mann, Manufacturing Competitiveness Analysis for PEM and Alkaline Water Electrolysis Systems, Fuel Cell Semin. Energy Expo. 6-9 Novemb. 2017, Long Beach, Calif. (2017). <https://www.osti.gov/servlets/purl/1550788>.
- [39] Walter Robert Pyle, Hydrogen Purification., Home Power. (1998).  
[https://www.researchgate.net/publication/281295584\\_Hydrogen\\_Purification](https://www.researchgate.net/publication/281295584_Hydrogen_Purification).
- [40] Z.Y. Zhang, China Electricity Prices for Industrial Consumers, China Brief. (2019) 1.  
<https://www.china-briefing.com/news/china-electricity-prices-industrial-consumers/#:~:text=Currently%2C%20the%20average%20industrial%20power,Sweden%20at%20US%240.060%2FKwH>.
- [41] O.Y. Brady Tyra, Christopher Cassar, Joy Liu, Peter Wong, Electric Power Monthly, U.S. Energy Inf. Adm. (2020).  
[https://www.eia.gov/electricity/monthly/epm\\_table\\_grapher.php?t=epmt\\_5\\_6\\_a](https://www.eia.gov/electricity/monthly/epm_table_grapher.php?t=epmt_5_6_a).
- [42] HK Electric, HK Electr. Investments Ltd. (2020). <https://www.hkelectric.com/en/customer-services/billing-payment-electricity-tariffs/non-residential-tariff>.
- [43] Eurostat, Energy overview, Tables, Graphs Maps. (2019).  
<https://ec.europa.eu/eurostat/web/energy/data/main-tables>.
- [44] Y. Wang, Z. Zhu, Cost of Natural Gas in Eastern Chinese Markets: Implications for LNG Imports, IEAEE Energy Forum. (2018) 21–28.  
<https://www.iaee.org/en/publications/newsletterdl.aspx?id=747>.

- [45] Natural Gas PRICE Today, Insid. Inc. (2020).  
<https://markets.businessinsider.com/commodities/natural-gas-price>.
- [46] Hong Kong fuel prices, GlobalPetrolPrices. (2020).  
<https://www.globalpetrolprices.com/Hong-Kong/>.
- [47] C.C. Dorris, E. Lu, S. Park, F.H. Toro, High-Purity Oxygen Production Using Mixed Ionic-Electronic Conducting Sorbents, Sr. Des. Reports. (2016).  
[http://repository.upenn.edu/cbe\\_sdr](http://repository.upenn.edu/cbe_sdr)[http://repository.upenn.edu/cbe\\_sdr/78%0Ahttps://repository.upenn.edu/cbe\\_sdr/78](http://repository.upenn.edu/cbe_sdr/78%0Ahttps://repository.upenn.edu/cbe_sdr/78).
- [48] M. Waidhas, Power to Gas - an economic approach, 2015. [http://www.fze.uni-saarland.de/AKE\\_Archiv/DPG2015-AKE\\_Berlin/Vortraege/DPG2015\\_AKE9.1\\_Waidhas\\_P2G-Economics.pdf](http://www.fze.uni-saarland.de/AKE_Archiv/DPG2015-AKE_Berlin/Vortraege/DPG2015_AKE9.1_Waidhas_P2G-Economics.pdf).
- [49] A. Mehmeti, A. Angelis-Dimakis, G. Arampatzis, S. McPhail, et al., Life Cycle Assessment and Water Footprint of Hydrogen Production Methods: From Conventional to Emerging Technologies, *Environments*. 5 (2018) 24. <https://doi.org/10.3390/environments5020024>.
- [50] Carbon Tax Guide, World Bank Gr. (2017) 172. <https://doi.org/10.1596/26300>.
- [51] Brad Plumer, New U.N. Climate Report Says Put a High Price on Carbon, *New York Times*. (2018). <https://www.nytimes.com/2018/10/08/climate/carbon-tax-united-nations-report-nordhaus.html>.
- [52] S.M. Hosseini Hashemi, J.-W. Choi, D. Psaltis, M.A. Modestino, et al., Electrochemical studies of a nickel electrode for the hydrogen evolution reaction, *J. Electrochem. Soc.* 32 (2019) 827–833. [https://doi.org/10.1016/0009-2509\(84\)80082-2](https://doi.org/10.1016/0009-2509(84)80082-2).
- [53] R.J. Gilliam, J.W. Graydon, D.W. Kirk, S.J. Thorpe, A review of specific conductivities of potassium hydroxide solutions for various concentrations and temperatures, *Int. J. Hydrogen Energy*. 32 (2007) 359–364. <https://doi.org/10.1016/j.ijhydene.2006.10.062>.
- [54] M.F. Kibria, M.S. Mridha, A.H. Khan, Electrochemical studies of a nickel electrode for the hydrogen evolution reaction, *Int. J. Hydrogen Energy*. 20 (1995) 435–440.  
[https://doi.org/10.1016/0360-3199\(94\)00073-9](https://doi.org/10.1016/0360-3199(94)00073-9).
- [55] P.W.T. Lu, S. Srinivasan, Effect of Temperature on Electrode Kinetic Parameters for Hydrogen and Oxygen Evolution Reactions on Nickel Electrodes in Alkaline Solutions, *J. Electrochem. Soc.* 123 (1976) 332–336. <https://doi.org/10.1149/1.2132820>.

- [56] Antonino Curcio Jian Wang Zheng Wang Zhiqi Zhang Alessio Belotti Simona Pepe Mohammed B. Effat Zongping Shao Jongwoo Lim Francesco Ciucci, Unlocking the Potential of Mechanochemical Coupling: Boosting the Oxygen Evolution Reaction by Mating Proton Acceptors with Electron Donors, *Adv. Funct. Mater.* (2020). <https://doi.org/10.1002/adfm.202008077>.
- [57] R.D. Walker, *A Study of Gas Solubilities and Transport Properties in Fuel Cell Electrolytes*, Washington D.C., 1967. <https://ntrs.nasa.gov/archive/nasa/casi.ntrs.nasa.gov/19670018110.pdf>.
- [58] I. Uehara, Separation and Purification of Hydrogen, *Encycl. Life Support Syst. I* (2009) 268–282. <https://doi.org/10.1038/35104049>.